FURTHER DEVELOPMENTS IN ORBIT EPHEMERIS DERIVED NEUTRAL DENSITY

BY

TRAVIS LOCKE

Submitted to the graduate degree program in Aerospace Engineering and the Graduate Faculty of the University of Kansas in partial fulfillment of the requirements for the degree of Master of Science.

_____

Chairperson: Dr. Craig A. McLaughlin

_____

Dr. Ray Taghavi

_____

Dr. Dongkyu Choi

Date Defended: November 14, 2012

The Thesis Committee for Travis Locke certifies that this is the approved version of the following thesis:

FURTHER DEVELOPMENTS IN ORBIT EPHEMERIS DERIVED NEUTRAL DENSITY

_____

Chairperson: Dr. Craig A. McLaughlin

Date approved:

ABSTRACT

There are a number of non-conservative forces acting on a satellite in low Earth orbit. The one which is the most dominant and also contains the most uncertainty is atmospheric drag. Atmospheric drag is directly proportional to atmospheric density, and the existing atmospheric density models do not accurately model the variations in atmospheric density. In this research, precision orbit ephemerides (POE) are used as input measurements in an optimal orbit determination scheme in order to estimate corrections to existing atmospheric density models. These estimated corrections improve the estimates of the drag experienced by a satellite and therefore provide an improvement in orbit determination and prediction as well as a better overall understanding of the Earth's upper atmosphere.

The optimal orbit determination scheme used in this work includes using POE data as measurements in a sequential filter/smoother process using the Orbit Determination Tool Kit (ODTK) software. The POE derived density estimates are validated by comparing them with the densities derived from accelerometers on board the Challenging Minisatellite Payload (CHAMP) and the Gravity Recovery and Climate Experiment (GRACE). These accelerometer derived density data sets for both CHAMP and GRACE are available from Sean Bruinsma of the Centre National d'Etudes Spatiales (CNES). The trend in the variation of atmospheric density is compared quantitatively by calculating the cross correlation (CC) between the POE derived density values and the accelerometer derived density values while the magnitudes of the two data sets are compared by calculating the root mean square (RMS) values between the two.

There are certain high frequency density variations that are observed in the accelerometer derived density data but not in the POE derived density data or any of the baseline density models. These high frequency density variations are typically small in magnitude compared to

the overall day-night variation. However during certain time periods, such as when the satellite is near the terminator, the variations are on the same order of magnitude as the diurnal variations. These variations can also be especially prevalent during geomagnetic storms and near the polar cusps. One of the goals of this work is to see what affect these unmodeled high frequency variations have on orbit propagation. In order to see this effect, the orbits of CHAMP and GRACE are propagated during certain time periods using different sources of density data as input measurements (accelerometer, POE, HASDM, and Jacchia 1971). The resulting orbit propagations are all compared to the propagation using the accelerometer derived density data which is used as truth. The RMS and the maximum difference between the different propagations are analyzed in order to see what effect the unmodeled density variations have on orbit propagation. These results are also binned by solar and geomagnetic activity level.

The primary input into the orbit determination scheme used to produce the POE derived density estimates is a precision orbit ephemeris file. This file contains position and velocity information for the satellite based on GPS and SLR measurements. The values contained in these files are estimated values and therefore contain some level of error, typically thought to be around the 5-10 cm level. The other primary focus of this work is to evaluate the effect of adding different levels of noise (0.1 m, 0.5 m, 1 m, 10 m, and 100 m) to this raw ephemeris data file before it is input into the orbit determination scheme. The resulting POE derived density estimates for each level of noise are then compared with the accelerometer derived densities by computing the CC and RMS values between the data sets. These results are also binned by solar and geomagnetic activity level.

ACKNOWLEDGEMENTS

I would like to thank Dr. Craig A. McLaughlin for the opportunity to work on this research as well as his guidance during my time as a graduate student. I am also very appreciative of his patience through this research process. I am thankful to Dr. Ray Taghavi and Dr. Dongkyu Choi for being members of my thesis committee.

This research is based upon work funded by the Department of Defense Experimental Program to Stimulate Competitive Research (DEPSCoR) grant FA9550-10-1-0038 administered by the Air Force Office of Scientific Research at the University of Kansas, Department of Aerospace Engineering. I wish to thank Jens Ramrath for his assistance with Orbit Determination Tool Kit. David Vallado's help with data conversion and ODTK is also appreciated. Thanks to Bruce Bowman for access to HASDM densities and to Sean Bruinsma for providing accelerometer derived densities for CHAMP and GRACE.

I am thankful to my research predecessors Andrew Hiatt, Eric Fattig, Steve Mance, and Anoop Arudra for building a foundation for this research. I am also thankful to my current research colleagues, Dhaval Mysore Krishna, Travis Lechtenberg, and Piyush Mehta for their help in my research.

TABLE OF CONTENTS

NOMENCLATURE

Latin Symbol	Description	Units
A	Cross sectional area	m^2
A_p	Geomagnetic daily planetary amplitude	gamma, 10^{-9} Telsa
$\vec{a}_{drag}$	Acceleration vector due to atmospheric drag	m/s^2
a_p	Geomagnetic 3-hourly planetary amplitude	gamma, 10^{-9} Telsa
$\Delta B/B$	Estimated ballistic coefficient correction	~
BC	Ballistic coefficient	m^2/kg
C_D	Satellite drag coefficient	~
$F_{10.7}$	Daily solar radio flux measured at 10.7 cm wave-length	SFU
$\bar{F}_{10.7}$	$F_{10.7}$ running 81-day centered smoothed data set	SFU
g	Gravitational acceleration	m/s^2
Δh	Altitude change	m
K_p	Geomagnetic planetary index	~
M	Mean molecular mass	amu
m	Satellite mass	kg
N	Number of elements	~
Δp	Atmospheric pressure change	N/m^2
$\bar{P}_{filter}$	Filter covariance matrix	~
$\bar{P}_{smoother}$	Smoother covariance matrix	~
R	Universal gas constant	$J\ K^{-1}\ mol^{-1}$

$\bar{R}$	McReynold's consistency test ratio	~
$\vec{r}$	Satellite position vector	m
t	Time	s
T	Temperature	K
v_{rel}	Satellite velocity magnitude relative to Earth's atmosphere	m/s
$\vec{v}_{rel}$	Satellite velocity vector relative to Earth's atmosphere	m/s
v_x	X-component of satellite velocity	m/s
v_y	Y-component of satellite velocity	m/s
v_z	Z-component of satellite velocity	m/s
$w(t)$	Gaussian white random variable	~
$\mathbf{X}$	Satellite state vector	~
$\vec{X}_{i,filter}$	filter state estimate	~
$\vec{X}_{i,smoother}$	Smoother state estimate	~
x	X component of satellite position vector	m
x	Gauss-Markov process dynamic scalar random variable	~
x	Cross correlation series	~
y	Y component of satellite position vector	m
y	Cross correlation series	~
z	Z component of satellite position vector	m

Greek Symbol	Description	Units
α	Gauss-Markov process variable	~
ρ	Atmospheric density	kg/m^3
$\Delta\rho/\rho$	Estimated atmospheric density correction	~
$\vec{\sigma}$	Denominator for McReynold's consistency test ratio	~
σ_w^2	Variance of Gaussian white random variable	~
τ	User defined correlated half-life	minutes
Φ	Transition function	~
$\omega_\oplus$	Earth's angular velocity magnitude	rad/s
$\vec{\omega}_\oplus$	Earth's angular velocity vector	rad/s

Abbreviation/Acronym	Definition
CC	Cross Correlation
CHAMP	Challenging Minisatellite Payload
CIRA	COSPAR International Reference Atmosphere
CME	Coronal Mass Ejection
COSPAR	Committee on Space Research
CNES	Centre National d'Études Spatiales
DCA	Dynamic Calibration of the Atmosphere
DoD	Department of Defense
DORIS	Doppler Orbitography by Radio positioning Integrated on Satellite

DTM	Drag Temperature Model
EUV	Extreme Ultra-Violet
GEOSAT	Geodetic Satellite
GFO	GEOSAT Follow-On
GGMO2C	GRACE Gravity Model 2
GOCE	Gravity Field and Steady State Ocean Circulation Explorer
GPS	Global Positioning System
GRACE	Gravity Recovery And Climate Experiment
GSFC	Goddard Space Flight Center
HASDM	High Accuracy Satellite Drag Model
ICESat	Ice, Cloud, and Land Elevation Satellite
ILRS	International Laser Ranging Service
LEO	Low Earth Orbit
MSISE	Mass Spectrometer Incoherent Scatter Extending from ground to space
NASA	National Aeronautics and Space Administration
NOAA	National Oceanic and Atmospheric Administration
NRL	Naval Research Laboratory
NRLMSISE	Naval Research Laboratory Mass Spectrometer Incoherent Scatter Extending from ground to space
ODTK	Orbit Determination Tool Kit
POE	Precision Orbit Ephemerides

PSO	Precision Science Orbit
RMS	Root Mean Square
RSO	Rapid Science Orbit
SETA	Satellite Electrostatic Triaxial Accelerometer
SFU	Solar Flux Units
SLR	Satellite Laser Ranging
SP	Sequential Processing
SRP	Solar Radiation Pressure
STAR	Spatial Triaxial Accelerometer for Research
TAD	Traveling Atmospheric Disturbance
TLE	Two Line Element

LIST OF FIGURES

LIST OF TABLES

1 INTRODUCTION

1.1 Objective

The objective of this research is to estimate corrections to current atmospheric density models using Precise Orbit Ephemerides (POE) data as input into a filter/smoother orbit determination scheme for low-earth orbiting satellites. The result of these corrections allows for more accurate density estimates which lead to improved satellite drag estimates, more accurate orbit determination and prediction, and also a better overall understanding of the atmospheric density in the thermosphere and exosphere. This research primarily focuses on the effect of modeling high frequency density variations in the orbit propagation process. The effects of varying levels of noise being present in the raw POE data used to compute the atmospheric density corrections are also examined.

1.2 Motivation

There are a number of non-conservative forces acting on a satellite in low Earth orbit (LEO); atmospheric drag being the most dominant and the one in which there is the most uncertainty. This uncertainty is present because the existing atmospheric density models are not accurate due to the atmospheric density being more variable than predicted by the current density models. When these atmospheric density models are used to calculate drag forces for orbit prediction, significant errors can occur due to the errors within the models. Atmospheric drag is directly related to atmospheric density, which means the influence that the density has on the drag force becomes more pronounced at lower altitudes, larger frontal area of the satellite, and

a lower satellite mass (See Equation 1.1). Therefore, in order to better predict the effect of drag on the motion of the satellite more accurate estimation of the atmospheric density is required than is available in current atmospheric density models.

The variability of the atmospheric density in the thermosphere and exosphere is driven by the Sun in two different forms. The first way the Sun affects the variations in the atmospheric density is by direct heating of the atmosphere primarily by the extreme-ultraviolet (EUV) rays from the Sun. The second is through the emission of charged particles from the sun which interact with the magnetic field of the Earth and heat up the atmosphere. The existing density models attempt to model these variations by using an input of some type of index of the Sun's electromagnetic radiation and Earth's magnetic field. These indices are only available as global averages taken over the time span of either a day or three hours. Due to the large time scale of these measurements the current atmospheric density models fail to capture the short-term variations in the density which is necessary for accurate drag prediction. These density models therefore need some sort of correction in order to be used for high accurate orbit determination and prediction.

The corrections to existing atmospheric density models are estimated using POE data as input into filter/smoother orbit determination scheme. The results are compared to densities computed from accelerometer data on-board certain satellites. Two satellites were examined, each equipped with an on-board accelerometer. The first satellite examined is the Challenging Minisatellite Payload (CHAMP). There is an accelerometer on-board CHAMP called the Spatial Triaxial Accelerometer for Research (STAR). The STAR is used to measure the non-

conservative forces on-board CHAMP. Both Sean Bruinsma[*] from the Centre National d'Etudes Spatiales (CNES) [Ref. 1] and Eric Sutton[†] from the United States Air Force Research Laboratory [Ref. 2] have derived density data from STAR. In this same way density data is recovered from the accelerometer on-board the Gravity Recovery and And Climate Experiment (GRACE) [Ref. 3]. Since no actual 'truth' model is available for the atmospheric density, the accelerometer-derived densities are used as 'truth'. Density data from the High Altitude Satellite Drag Model (HASDM) obtained from Bruce Bowman[‡] of U.S. Air Force Space Command is also used for comparison [Ref. 4].

Incorporating these estimated density corrections into the drag equation for the satellite, better models of the drag forces upon a satellite will be created. Since the drag force is the most dominant non-conservative force for low-Earth orbiting satellites and the one which contains the most uncertainty, this will in turn lead to more accurate orbit determination and prediction. This will allow for a better prediction of the satellite's future state which can prevent possible future satellite collisions as well as improve the prediction of satellite life spans and re-entry times.

1.3 Satellite Drag

As mentioned previously atmospheric drag is the most dominant non-conservative force acting on a LEO satellite and the third most dominant overall force (depending on the altitude) after the forces due to central body (Earth's gravity) and the oblateness of the Earth (J2). Other

[*] Sean Bruinsma shared the accelerometer derived density data with Dr. Craig A. McLaughlin, Assistant Professor, University of Kansas.
[†] Eric Sutton shared the accelerometer derived density data with Dr. Craig A. McLaughlin, Assistant Professor, University of Kansas.
[‡] Bruce Bowman shared the HASDM density data with Dr. Craig A. McLaughlin, Assistant Professor, University of Kansas.

significant sources of perturbations come from solar radiation pressure (SRP), Earth albedo, and third body effects from the Moon and Sun. Satellites at higher altitudes are proportionately more affected by perturbations such as SRP and third body effects, as the effects of J2 and atmospheric drag decrease quickly with increasing altitude. The main areas of interest in regard to studying atmospheric drag are orbit determination of LEO satellites, calculation of the lifespan of satellites, and the overall study of the physical properties of the upper atmosphere [Ref. 5].

Satellite drag occurs when a satellite encounters atmospheric particles which cause a force in the direction opposite of the satellite's motion due to momentum transfer. Drag is a non-conservative force because the total mechanical energy of the satellite changes due to this interaction between the outer hull of the orbiting body and the atmospheric particles. Atmospheric drag affects the orbit of a satellite over time by reducing the semimajor axis due to a loss of energy and by lowering the eccentricy which makes the orbit more circular. Other orbital elements are also effected by atmospheric drag but are periodic in nature and do not necessarily deteriorate the orbit. LEO satellites are seeing an increasing role lately which has led to a large amount of research focusing on the modeling of the upper atmosphere and its interactions with satellites in the form of drag. While there are a few applications which require atmospheric drag such as aerobraking (used for orbit maintenance) and tethers which are used to change to orientation of a satellite, for the most part satellite drag produces undesirable results with regards to the satellite's life span. According to Reference 5 an accurate model of the effect that atmospheric perturbations have on an orbiting body requires knowledge of many fields such as molecular chemistry, thermodynamics, aerodynamics, hypersonics, meteorology, electromag-

netism, planetary science, and orbital mechanics. Thus, the study of the effect of atmospheric drag on an orbiting body is very difficult.

One method to analyze the atmospheric drag on a body is to measure the accelerations experienced by the satellite and then to isolate the acceleration due to drag which occurs in the satellite's along-track direction. The acceleration experienced by a satellite due to atmospheric drag can be described by Equation 1.1 [Ref. 5] where C_d is the drag coefficient, A is the cross-sectional area of the satellite normal to the velocity vector, m is the mass of the satellite, ρ is the atmospheric density, and v_{rel} is the velocity of the satellite relative to Earth's rotating atmosphere (See Equation 1.3).

$$\vec{a}_{drag} = -\frac{1}{2}\frac{C_d A}{m}\rho v_{rel}^2 \frac{\vec{v}_{rel}}{\left|\vec{v}_{rel}\right|} \qquad 1.1$$

This equation relates the acceleration experienced by the satellite with atmospheric properties, geometric properties of the satellite, and the relative velocity of the satellite. The equation also contains a dimensionless quantity called the drag coefficient (C_d) which describes the interaction between the atmosphere and the satellite's surface material. The drag coefficient quantifies the resistance a body has to a flow (or the effect that drag has on the satellite) and depends on the temperature and composition of the atmosphere which surrounds the body as well as the surface properties of the satellite including surface temperature, geometry, and orientation. Due to the dependence of drag coefficient on the configuration of the satellite and the variability of the atmosphere, this value is typically approximated for satellites in the upper atmosphere as 2.2 for flat plates, between 2.0 to 2.1 for spherical bodies [Ref. 5], and around 2.0 to 2.3 for non-spherical convex-shaped bodies [Ref. 6]. There are difficulties which come about

when discussing complex satellite configurations which require further improvements in satellite drag determination. The variable ρ refers to the atmospheric density which is the most difficult quantity to estimate due to its variability. There are several atmospheric density models that exist which can be used to estimate the density and will be discussed later in this chapter. *A* is the cross-sectional area of the body that is normal to the velocity vector. If the orientation and geometry of a satellite is well known then *A* may be relatively easy to determine. However if the orientation of a non-spherical satellite is not well known than the determination of the cross-sectional area could become difficult, especially in the case of a satellite whose orientation is rapidly changing (tumbling). *m* is the mass of the satellite and will only change if onboard propellants are being consumed or expelled.

The quantity m/C_dA is referred to as the ballistic coefficient (BC) which is also a measure of how much the satellite is affected by drag. A higher BC correlates with a lower drag experienced by the satellite. Although this is the traditional definition of BC, in this work the inverse of this quantity will be referred to as the ballistic coefficient. Therefore in this work BC will be defined by Equation 1.2. This definition of BC is useful because it is the definition used by Orbit Determination Tool Kit (ODTK), which is the primary software package used in this research. The definition of BC described in Equation 1.2 is also used by Bruce Bowman to construct the HASDM data. Using this definition a higher ballistic coefficient means higher drag experienced by the satellite.

$$BC = \frac{C_d A}{m} \tag{1.2}$$

The last quantity in Equation 1.1 is the relative velocity of the satellite, $\vec{v}_{rel}$. The Earth's atmosphere is not stationary in the inertial reference frame but rotates with the Earth. The rate

at which the atmosphere rotates, however, is not the same as the Earth at higher altitudes. There is a velocity profile of the rotational rate of the atmosphere beginning at the atmosphere closest to the Earth which is rotating at the same rate as the Earth. As the altitude increases the rate at which the atmosphere rotates decreases. For many applications the lag in the rotational rate of the atmosphere with respect to that of the Earth is ignored and the atmosphere at the altitude of the satellite is assumed to rotate at the same rate as the surface of the Earth. Equation 1.3 is an expression for the relative velocity of the satellite in the inertial frame which takes advantage of this approximation and is given in Reference 5. In Equation 1.3, $\vec{r}$ refers to the satellite position vector and $\vec{\omega}_{\oplus}$ is the angular velocity vector of the Earth.

$$\vec{v}_{rel} = \frac{d\vec{r}}{dt} - \vec{\omega}_{\oplus} \times \vec{r} = \left[\frac{dx}{dt} + \omega_{\oplus} y \frac{dx}{dt} - \omega_{\oplus} x \frac{dx}{dt} \right]^T \qquad 1.3$$

The above equation does not take into account that there are atmospheric winds present which can generate side and lifting forces as well as drag forces on the satellite. This assumption yields maximum observed deviations on the order of 40% which leads to a less than 5% uncertainty in the drag force [Ref. 6 and 7]. Expressions exist which superimpose winds on the rotating motion of the atmosphere to help define the relative velocity term but they are not discussed in this section. There has also been work done to establish an atmospheric wind model using a limited set of vector spherical harmonics which can be found in Reference 8. Most applications neglect the effect of atmospheric winds because there are wind parameters and/or measurements which are necessary for atmospheric wind calculations that are unavailable [Ref. 6].

As previously mentioned the largest source of error in estimating drag in Equation 1.1 for LEO satellites is the atmospheric density. This is due to the high variability of the Earth's

upper atmosphere dependent on parameters such as the molecular composition of the atmosphere, the incident solar flux, and the geomagnetic activity. Each of these parameters affects the atmosphere in a different way. The molecular make-up of the atmosphere affects the atmospheric density as stated in the ideal gas law which is given below [Ref. 5].

$$\rho = \frac{pM}{RT} \tag{1.4}$$

In Equation 1.4 ρ is the density, p is the pressure, M is the mean molecular mass, R is the universal gas constant, and T is the temperature. The incident solar flux that is in the extreme ultraviolet (EUV) range heats the atmosphere directly causing an instant change in the atmosphere. Geomagnetic activity causes charged particles to collide with the atmosphere which then results in a delayed heating of the atmosphere. Both of these effects heat up the atmosphere which results in the expansion of the atmosphere causing an increase in density at higher altitudes [Ref. 9].

There are both static and time-varying models of the atmosphere, both of which depend on two primary relationships describing how the atmospheric pressure and density change. These two relations are the ideal gas law as seen in Equation 1.4 and the hydrostatic equation seen below [Ref. 5].

$$\Delta p = -\rho g \Delta h \tag{1.5}$$

Equation 1.5 relates the change in pressure, Δp, with the change in altitude, Δh. These two expressions describing how pressure and density are related within the atmosphere are used to develop atmospheric density models. As previously mentioned, there are two general types of atmospheric density models. Static density models do not take into account how the density changes with time and are therefore both the simplest and least accurate types of models. Time-

varying atmospheric density models take into account several different time-dependant parameters which affect the atmospheric density. This aspect of time-varying models makes them more accurate than the static models but also more complex. For most orbit determination and prediction applications high accuracy is desired and therefore time-varying atmospheric density models are used.

1.4 Neutral Atmosphere

This section contains a brief overview of the atmosphere as well as more detailed characteristics of static and time-varying atmospheric density models which is derived from References 9 and 10.

1.4.1 Neutral Atmosphere Overview

The structure of the neutral atmosphere is typically divided into five layers. These layers are concentric shells with thicknesses of tens to hundreds of kilometers which are divided based on the processes that take place within each layer. The boundary between layers of the atmosphere is called a pause and is sometimes difficult to define which can cause the pause to stretch for tens of kilometers. The layer closest to the surface of the Earth is called the troposphere. This first layer ranges from the surface of the Earth up to about 12 km in altitude and its chemical composition is around 78% nitrogen, 21% oxygen, and the remaining 1% is made up of other components such as carbon dioxide, argon, and helium. The stratosphere is the layer above the troposphere. The stratosphere ranges from about 12 km up to 45 km and is characterized by the increase in temperature with altitude. This is caused by the ozone present in the stratosphere which absorbs incoming UV rays from the Sun and heat up the stratosphere. The

mesosphere is the layer which lies above the stratosphere and ranges from 45 km up to about 80-85 km. The mesosphere is characterized by decreasing temperatures with altitude and can reach a low of 180 K. This layer is rarely studied because of the difficulty in positioning scientific instruments within the mesosphere. The start of the mesosphere at 45 km is above the altitude limit that can be reached by a ground based balloon and the mesopause at 80-85 km is below the lowest satellite orbits. These three lowest layers of the Earth's atmosphere are known as the lower atmosphere and have little affect on orbit determination with the exception of disturbances from the lower atmosphere propagating up into the upper atmosphere.

The primary focus with regard to orbit determination lies in the upper two layers of the atmosphere called the thermosphere and exosphere. The thermosphere starts at the mesopause (80-85 km) and extends up to around 600 km and is the atmosphere layer where most of the LEO satellites orbit. The thermosphere is also where the dominant constituent in the atmosphere changes from nitrogen to atomic oxygen (at around 175 km). The chemical composition of the thermosphere makes it the most absorptive layer in the atmosphere. This causes an increase in temperature in the layer as UV radiation from the Sun is absorbed in the thermosphere. The exosphere is the topmost layer of the atmosphere and starts at the top of the thermosphere, or the thermopause (around 600 km). In the exosphere there are so few particle interactions and the density is so low that the molecules simply follow a ballistic trajectory influenced only by the gravitational forces. This allows the fluid in the exosphere to be treated as a collection of individual particles instead of a gas. The dominant constituent in the atmosphere changes from atomic oxygen to helium at around 600 km until an altitude of about 2500 km where the primary element in the make-up of the atmosphere is hydrogen. For more information on the neutral atmosphere and the space environment in general see References 9 and 10.

1.4.2 Static Atmospheric Model

As stated earlier static atmospheric models are simple, yet they lack a high degree of accuracy which can be necessary in some applications. The accuracy of these models is low because, as their name implies, static models of the atmosphere do not include variations of parameters that change with time and instead assume them constant. There are both latitudinal and longitudinal variations that the static models do not take into account. The latitudinal variations are those that exist because the static model assumes the altitude of the satellite constant. In reality a satellite in a circular orbit inclined at an angle with respect to the Earth's equator will experience a decrease in effective altitude as it crosses the equatorial plane due to the oblateness of the Earth. This decrease in altitude is accompanied by an increase in the observed density of the atmosphere that the satellite is passing through which consequently affects the drag on the satellite.

Longitudinal variations also exist and primarily come from the variation in local time, or the position of the Sun with respect to the surface of the Earth. This is important because the lit side of the Earth experiences a significantly denser atmosphere than the unlit side which will greatly affect the drag on a satellite. There are also other longitudinal variations which arise from the features on the surface of the Earth. Certain geographical features such as oceans, mountain ranges, and deserts along with wind and temperature differences cause the atmosphere to be unsymmetrical about the Earth's axis of rotation. This can cause variations in the density observed by a satellite and thus the drag it experiences. As can be seen there are many complexities which are avoided by using static atmospheric models but the loss in accuracy caused by the 'bad' assumptions used within them can be unacceptable in some applications.

1.4.3 Time-Varying Atmospheric Model

Although time-varying atmospheric models are more complex than static models because of the fact that they do include temporal variations that affect the atmospheric density this also allows them to obtain a higher degree of accuracy. The variations in the atmosphere are primarily caused by the sun both through direct heating and through the interaction of charged particles from the Sun with the Earth's atmosphere, however there are other variations that can also be modeled. The temporal variations that affect the atmosphere which can be modeled in time-varying atmospheric models are as follows and are outlined in References 5 and 11:

a. Day/Night (Diurnal) Variations
b. 27-Day Solar Rotation Cycle
c. 11-Year Solar Cycle
d. Cyclical Variations
e. Semiannual/Seasonal Variations
f. Rotating Atmosphere
g. Winds
h. Magnetic Storm Variations
i. Gravity Waves
j. Irregular Short-Period Variations
k. Tides

Day/Night or Diurnal Variations: This is the temporal variation which is caused by the rotation of the Earth. The sunlit portion of the Earth's atmosphere experiences a bulge and therefore a density maximum due to warming. This bulge lags behind the Sun occurring at ap-

proximately 2-2:30 P.M. local time. Likewise, there is also an atmospheric density minimum which occurs opposite the bulge at approximately 4:00 A.M. local time. The bulge occurs at different latitudes at different times of the year (seasons) depending on the declination of the Sun; occurring on the equator during the equinoxes. Thus the diurnal bulge causes the atmospheric density to depend on latitude, local time, and time of the year.

27-Day Solar Rotation Cycle: The Carrington Cycle, or 27-day solar rotation cycle, is caused by the rotation of the Sun about its axis which has an average period of approximately 27 days. There are irregular changes in the solar decimetric-wavelength radio flux output by the Sun caused by the growth and decay of active solar regions which cause atmospheric density fluctuations. These active solar regions are extremely difficult to predict with many different patterns of growth, decay, and stability. These regions also exhibit an unknown cyclical pattern because of their 27-day rotational cycle with the Sun.

11-Year Solar Cycle: The 11-year solar cycle, or sunspot cycle, refers to the 11 year cycle during which sunspots and solar flux start at minimum, go to a maximum, and then back to a minimum again. This cycle greatly influences the amount of solar radiation that reaches the Earth and causes extreme variability during solar maximum.

Cyclical Variations: There is another 11-year cycle which lags a few years behind the sunspot cycle. This cycle takes about 6 or 7 years to go from maximum to minimum and therefore the minimum does not lie directly in the middle of the two maxima. The exact cause of this variation is not known exactly but it is thought to be related to sunspot activity.

Semi-Annual/Seasonal Variations: These variations are due to the varying distance between the Earth and the Sun as well as the declination of the Sun. The variations last about six months and are typically small.

Rotating Atmosphere: As stated in Section 1.3 the atmosphere is not stationary in space but instead rotates with the Earth with a certain velocity profile with a larger velocity near the surface of the Earth due to friction. This causes additional variations in the atmospheric density with respect to time.

Winds: Winds present in the upper atmosphere cause temperature variations and therefore changes in the atmospheric density. Since the dynamics in the upper atmosphere are not entirely understood, accounting for atmospheric winds in a model is very difficult and complex.

Magnetic Storm Variations: Fluctuations in the Earth's magnetic field affect the atmosphere to some degree due to the alignment of ionized particles with the Earth's magnetic field. These fluctuations can be large or small depending on the level of geomagnetic activity. High levels of geomagnetic activity often occur during magnetic storms during which variations in the solar wind impinge the atmosphere, typically after a solar flare or coronal mass ejection.

Gravity Waves: Gravity waves transfer disturbances from the lower atmosphere to the upper atmosphere. These waves transfer energy from the lower atmosphere to the mesosphere and lower thermosphere causing atmospheric density variations due to the energy transfer. Higher up in the atmosphere the gravity waves dissipate due to viscous damping.

Irregular Short-Periodic Variations: The effects of these short-periodic variations on atmospheric density are small and are caused by transient geomagnetic disturbances, random solar flares, hydrogen currents within the atmosphere, and other very small effects.

Tides: There are both ocean and atmospheric tides caused by gravity which cause a small variation in atmospheric density. There are also solar tides which can affect the atmosphere a great deal. At altitudes above 250 km the solar diurnal tide is a dominating factor due to the absorption of EUV increasing the temperature and therefore the density of the atmosphere.

1.5 Solar and Geomagnetic Indices

The atmosphere is greatly affected by the amount of solar and geomagnetic activity that exists during a certain time period and therefore it is important to have a clear measure of that activity. The primary method in which the Sun influences the atmosphere is by direct heating by extreme ultraviolet (EUV) solar radiation. This EUV radiation gets absorbed in the upper atmosphere causing it to experience an increase in temperature and therefore an increase in density. Due to this absorption of EUV in the upper atmosphere it cannot be measured on the surface of the Earth. Therefore, a proxy index is used which measures 10.7 cm wavelength electromagnetic radiation ($F_{10.7}$) from the Sun instead of trying to directly measure EUV. The 10.7 cm wavelength radiation can be used as a proxy for EUV since both types of solar radiation have been discovered to come from the same layers in the Sun's chromosphere and corona. This is also helpful because, unlike EUV, $F_{10.7}$ is not absorbed in the atmosphere and can therefore be measured on the surface of the Earth. There are some satellites in orbit equipped with instruments capable of directly measuring EUV however the only models to incorporate these measurements thus far are the Jacchia-Bowman 2006 [Ref. 12] model and the Jacchia-Bowman 2008 [Ref. 13] model which are not examined in this work.

The $F_{10.7}$ proxy index is measured in units called Solar Flux Units (SFU), where one SFU is equal to 10^{-22} W/m^2*Hz. $F_{10.7}$ values are available from 1940 up to the present and typically range anywhere from 70 SFU up to around 300 SFU. There are different types of measurements of $F_{10.7}$ including daily values, 81-day centered running averages ($\overline{F}_{10.7}$), as well as others which all are distributed by the National Oceanic and Atmospheric Administration (NOAA) at the National Geophysical Data Center in Boulder, Colorado. These measurements were taken at 1700 UT at the Algonquin Radio Observatory in Ottawa, Ontario from 1947 until

1991 when the measurements started being taken at the Dominion Radio Astrophysical Observatory in Penticton, British Columbia [Ref. 5].

Along with solar variations there are also geomagnetic variations from both the Sun and the Earth that can affect atmospheric density in a number of different ways. Magnetic disturbances cause charged particles within the atmosphere to ionize the upper atmosphere which causes variability in the density of the upper atmosphere. The solar wind also impinges the atmosphere and interacts with the Earth's geomagnetic field causing the atmosphere to heat up. Since the geomagnetic activity during a given time period can greatly influence the atmospheric density that a satellite experiences it is important to be able to measure the geomagnetic activity level in some way in order to determine the amount of heating that is taking place in the upper atmosphere. The most commonly used measure of this is known as the planetary index (K_p) and is a quasi-logarithmic, global average of the geomagnetic activity below the auroral zones. The K_p value is obtained by combining local values of geomagnetic activity (K) which are taken once every three hours from twelve different stations around the world and then using latitude corrections to calculate the global average, K_p. This global average ranges from 0.0 (low activity) to 9.0 (high activity) and are rounded to the nearest third of an integer. Another measure of geomagnetic activity level is the planetary amplitude (a_p), also known as the 3-hourly index, which is a linear equivalent of the K_p index and is designed to minimize differences at 50° latitude. There is another measure created from averaging eight values of a_p called the daily planetary amplitude (A_p). The daily planetary amplitude value is given in gamma units where one gamma is equal to 10^{-9} Tesla or 10^{-9} kg*s/m. A_p values range from 0 to 400 with values of 10-20 being average and values over 100 being rare and corresponding to extreme geomagnetic activity. Many of the variations in A_p are related to the sun-spot and

semi-annual solar cycles and are primarily caused by solar flares, coronal holes, disappearing solar filaments, and the solar-wind environment near the Earth. There are high levels of geomagnetic activity at the auroral zones which affects the shape of the atmosphere in general and makes the density in the atmosphere dependent on latitude [Ref. 5].

Measurements of solar flux and geomagnetic planetary indices and planetary amplitudes can be found in Reference 14. Due to the extreme effect that solar and geomagnetic activity has on satellite orbits there is also a lot of work that has been done on predicting the solar and geomagnetic activity indices in the future. These forecasts are done on the order of days (short-term predictions), months (mid-term predictions), or years (long-term forecasts) and can be extremely useful in many applications [Ref. 6].

Solar and geomagnetic activity levels can also be separated into bins for ease of analysis as found in Reference 15 and as seen below in Table 1.1.

Table 1.1 – Definition of solar and geomagnetic activity bins

Solar Activity ($F_{10.7}$)	**Activity Bin**
Low	$F_{10.7} < 75$
Moderate	$75 < F_{10.7} < 150$
Elevated	$150 < F_{10.7} < 190$
High	$190 < F_{10.7}$
Geomagnetic Activity (A_p)	
Quiet	$A_p < 10$
Moderate	$10 < A_p < 50$
Active	$50 < A_p$

1.6 Atmospheric Density Models

There are a number of different atmospheric density models in use today using a number of different techniques and data sources. The information found in this section about different atmospheric density models was gathered primarily from Reference 5. There are two approaches typically used when constructing a density model. The first method is to combine conservation laws and atmospheric-constituent models into a physical model. The second method uses simplified physical concepts developed from in-situ measurements and satellite tracking data. There are also both static and time-varying density models as discussed previously. There are so many different types of models because different applications may have other requirements on accuracy and computational power. As mentioned previously time-varying atmospheric models are generally the most accurate but also require more computation time. On the other hand static models might be less computationally expensive but are less accurate. With regards to orbit determination time-varying models are typically used due to the requirement of high accuracy regardless of the high computational power.

The atmospheric density models examined in this work include Jacchia 1971 [Ref. 16], Jacchia-Roberts [Ref. 17], Committee On Space Research (COSPAR) International Reference Atmosphere (CIRA-1972) [Ref. 18], Mass Spectrometer Incoherent Scatter (MSISE 1990) [Ref. 19], and Naval Research Laboratory Mass Spectrometer Incoherent Scatter (NRLMSISE 2000) [Ref. 15]. The 'E' on the end of the two MSIS model names stands for 'Extended' referring to the fact that these two models extend from sea level up to space. Each of these models is discussed in further detail later in this section.

1.6.1 Jacchia 1971 Atmospheric Model

The Jacchia 1971 atmospheric model is an upgraded version of the Jacchia 1970 model and includes more recent and complete data. Depending on the altitude the Jacchia 1971 model numerically integrates either the barometric equation (90-100 km) or the diffusion equation (100+ km) in order to determine the atmospheric density. This is also a change from the previous year's model in which the transition between which equation to integrate occurs at an altitude of 105 km instead of 100 km. However, the technique used to calculate the temperature profile in the thermosphere for the Jacchia 1971 model uses a different altitude range due to a distinct inflection point located at an altitude of 125 km. At this point the local temperature is a function of the exospheric temperature and above the inflection point an inverse tangent function is used. Atmospheric densities at altitudes lower than 90 km are not considered in the Jacchia family of atmospheric models. There are other differences between the 1970 and the 1971 versions of the Jacchia model such as the equations used to determine various atmospheric properties at certain altitudes (molecular mass, temperature profiles, etc.). The Jacchia 1971 model also incorporates a running 81 day average for solar parameters such as geomagnetic and solar activity levels. This is done in order to average out the variations caused by the 27 day solar cycle in order to achieve a three period cycle. More detailed information about the Jacchia 1971 atmospheric model can be found in Reference 16.

1.6.2 Jacchia-Roberts Atmospheric Model

The Jacchia-Roberts model is an analytical evaluation of the Jacchia 1970 atmospheric model. This was done in order to eliminate the need for numerical integration which is computationally expensive. Between 90 and 125 km the Jacchia-Roberts model uses partial fractions

for integration and above 125 km the model uses an exponential temperature profile instead of the inverse tangent function in order to obtain a form that is integrable. With this technique the Jacchia-Roberts model closely approximates the Jacchia 1970 model without using the computationally expensive technique of numerical integration. Although the Jacchia-Roberts model is based off the Jacchia 1970 model the technique can also be applied to the Jacchia 1971 model. For additional details about the Jacchia-Roberts atmospheric model see Reference 17.

1.6.3 CIRA 1972 Atmospheric Model

The Committee on Space Research (COSPAR) first developed the COSPAR International Reference Atmosphere in 1965 (CIRA-65). This first version of the model was a new model from 30-300 km and was based on previous atmospheric models (Champion and Harris-Priester) from 120-800 km. The version of the model used in this work is the CIRA-72 model which incorporates mean values as well as information from the Jacchia 1971 model. The operational range of the CIRA-72 atmospheric model is 25-2500 km. From 25-75 km the CIRA-72 model is derived from Groves [Ref. 20] and at altitudes between 110 km and 2000 km the Jacchia 1971 model is used with an intermediate altitude model used in between (75-120 km). Further details about the CIRA-72 atmospheric model can be found in Reference 18.

1.6.4 MSISE 1990 Atmospheric Model

The Mass Spectrometer and Incoherent Scatter (MSIS) family of atmospheric models are based primarily on mass spectrometer data from satellites and incoherent radar scatter data from the surface of the Earth. The MSIS models are also derived from the Drag Temperature Models (DTM) which are based on air-glow temperatures [Ref. 21]. The MSISE-90 model is

the first MSIS model to be 'Extended' from the ground up while the previous version (MSIS-86) of the model started at 90 km and extended upward from there. The MSISE-90 model has shown successful results specifically when used to analyze a satellite with a high velocity at perigee. This type of satellite can cross several layers of atmosphere in a single integration step which can possibly lead to inaccuracies if a different atmospheric model were in use. However, the MSISE family of models typically takes more computation time than the Jacchia family of models. More information on the MSISE-90 atmospheric model can be found in Reference 19.

1.6.5 NRLMSISE 2000 Atmospheric Model

The NRLMSISE-00 atmospheric model is an updated version of the MSISE-90 model produced by the Naval Research Laboratory. This model includes satellite drag data and is used in many applications. More information the NRLMSISE-00 atmospheric model can be found in Reference 15.

1.7 Previous Work on Corrections to Atmospheric Density Models

The previous research that has been done in an attempt to make corrections to existing atmospheric models can generally be classified according to two different approaches. The first approach is called dynamic calibration of the atmosphere (DCA) which is a technique used to provide information about the variations in the atmospheric density and the statistics of those variations. The second approach is to derive atmospheric density data from the non-conservative forces measured by the accelerometers on board a satellite.

1.7.1 DCA and HASDM

Dynamic Calibration of the Atmosphere (DCA) is a technique that uses a set of calibration satellites in order to determine density corrections every three hours (note that some DCA methods determine corrections once per day). These calibration satellites are a group of LEO satellites which are used because they have better observational data and thus more accurate orbit determination results compared to an average satellite. The state vector and global density corrections are solved simultaneously for each of these satellites. The 'true' ballistic coefficient is used as an input and is the basis of changing the density from one of the atmospheric models such as Jacchia or MSISE in order to achieve a correction. More information on DCA can be found in Reference 5.

DCA techniques began being used to estimate corrections to atmospheric density models in the 1980s and continue to be an active area of research. References 4 and 22 - 31 detail some of the work done in this area using the DCA approach. The Air Force Space Command's High Accuracy Satellite Drag Model (HASDM) uses a DCA algorithm in order to estimate and predict dynamic variations in the atmospheric density for altitudes between 200 km and 800 km. This algorithm uses data based on observed drag effects from 75 LEO calibration satellites in order to solve for the neutral atmospheric density in near real time. These corrections are regularly made every three hours and have the ability to be predicted by up to three days in advance by also accounting for phases and amplitudes of diurnal and semi-diurnal variations in the atmosphere. This DCA algorithm produces a global dynamically varying density model which reduces the error of the baseline atmospheric model on which the corrections are applied [Ref. 4].

Reference 22 outlines a method which can calculate daily density values by using satellite drag data. In this technique a 6-state element vector and satellite ballistic coefficient is obtained by applying a differential orbit correction program to radar and optical observations. This orbit correction program uses special perturbations orbit integration using the modified Jacchia 1970 model which was used in HASDM development. This technique computes daily temperature and density data using computed energy dissipation rates. The temperature values were validated by comparing the values obtained using this DCA technique with the values obtained by HASDM for the year 2001. The density values were validated by comparison of the values obtained in Reference 22 with historical density data from 25 satellites over the past 30 years.

Reference 23 used historical radar observations from 13 satellites (perigees ranging from 100-200 km) in order to represent the observed semi-annual density variations in the Earth's upper atmosphere over the last 40 years. The study used a differential orbit correction program for the 13 calibration satellites, finding daily density values at perigee by relating the dissipation rates of density to energy. The study was not only able to observe the semi-annual density variation but was also able to characterize the variations due to altitude and solar activity level. The process and validation technique are similar to those used to develop HASDM.

Two Line Element (TLE) sets are used to estimate density corrections to atmospheric models in the work found in Reference 24. The TLE data sets used in this work are from 300-500 LEO satellites with a perigee of less than 600 km and whose TLE data sets are regularly updated by the U.S. Space Catalog. This TLE data is used as input as well as observed solar flux and geomagnetic activity in order to compute the corrections in this work. The research

examined a 10 month period in late 2002 and early 2003 and demonstrated the capability to observe density variations in the upper atmosphere given satellite TLE data sets in near real time.

Reference 25 also uses TLE data sets in order to create density corrections. TLE data sets are taken from a large number of inactive objects in LEO orbit and used as input to obtain corrections to existing atmospheric density models. Along with the research conducted in Reference 24 this method also uses a linear density relationship with respect to altitude. The accuracy of this work was determined by comparing the orbit determination results both with and without the estimated density corrections. According to the authors this method could be improved by incorporating real-time observations along with the TLE data sets.

Corrections for atmospheric density were computed from the NRLMSISE-00 density model in Reference 26 in order to better predict the reentry time for orbiting objects. The density corrections obtained in this work increase the accuracy of orbit reentry times for all satellites examined but the increase in accuracy was found to be more pronounced in spherical satellites. This is to be expected as a spherical satellite has a constant ballistic coefficient (BC) while the BC of a non-spherical body will change with time.

Reference 27 used a slightly different DCA approach in order to improve the method and specifically reduce residual errors in the drag calculation. This method uses successive refinements to density corrections using a series of vanishing coefficients instead of the traditional method of generating global optimal correction coefficients that are directly related to the basis function. Each successive refinement uses the previous refinement step as a starting point and this process continues until a specified error threshold is met.

A comparison of results obtained using DCA corrections to the NRLMSISE-00 model and the density corrections produced by the Russian DCA method are found in Reference 28.

This study examined two time periods which were each about four years in length (1995-2000 and 1999-2003) and used data from 477 LEO satellites for comparison. The results of the research showed that the models were valid and therefore DCA is an effective method of determining density corrections to existing atmospheric models.

As has been pointed out through several other research works the DCA method can be a useful tool in determining atmospheric density corrections, however it also has some limitations. Some of the challenges that are faced when attempting to produce density corrections to the NRLMSISE-00 atmospheric model using a DCA method are outlined in Reference 29. An issue of concern with regard to the DCA method is the use of purely statistical corrections. While corrections produced by the DCA method improve accuracy, this accuracy is dependant on how the corrections are produced and how they are applied. Also, there is a large amount of information such as the time system, input/output test cases, input parameters, subroutines and model parameters which must be utilized in order to generate the density corrections. If any of this information happens to be missing, incomplete, or corrupt then the accuracy of the method can greatly decline and significant errors are observed in the orbit determination process. Another difficulty to consider is that the corrections produced by the DCA method can only be applied to the specific time period corresponding to the orbit determination scheme which created the corrections. Also, there is the limitation on the temporal resolution of the DCA method to a long time span of 3 hours or a day due to the 3-hourly geomagnetic indices and the daily solar indices which are used as input. This long of a time span is not sufficient to capture some of the short term variations in the upper atmosphere. There is also the limitation which comes from using TLE data sets as input in many of the DCA algorithms. Since the TLE data has relatively low accuracy the density corrections produced by a DCA algorithm which incorporates

these TLE data sets will also have limited accuracy. Radar observations which can also be used as input into a DCA method are not easily accessible and still are not as accurate as using precision orbit ephemerides (POE) or satellite laser ranging (SLR).

Reference 30 describes a recent project which applies a DCA algorithm to a NASA Goddard Space Flight Center (GSFC) Precision Orbit Determination and Geodetic Parameter Estimation Program referred to as GEODYN. The goal of this research was to apply density corrections to the NRLMSISE-00 atmospheric density model with the intent of improving the orbit precision of the GEOSAT Follow-On (GFO) satellite. The MSIS-86 atmospheric density model was used for comparison with the corrected density data. This was done for a range of solar and geomagnetic activity levels and included altitudes up to 600 km and there was found to be very little discrepancy between the MSIS-86 model and the corrected densities. The authors anticipate however that if their algorithm was applied to altitudes up to 800 km then an improvement would be seen when compared to the MSIS-86 model.

Another recent project found in Reference 31 uses TLE data sets in order to determine satellite drag data and then calculate density corrections using a DCA algorithm. This study used two different calibration schemes on a batch of 50 calibration satellites during the year 2000. One of the calibration schemes incorporated altitude dependant scale factors and the other scheme made corrections to the CIRA 1972 atmospheric model temperatures which directly affects the density model. The authors claim to have reduced the error from 30% using the raw empirical density models down to 15% using the corrected density models.

1.7.2 Accelerometers

The atmospheric density for LEO satellites can also be derived from the measurement of non-conservative forces by on-board accelerometers. The on-board accelerometers can measure only the non-conservative forces acting on the satellite such as atmospheric drag, solar radiation pressure, Earth albedo, and Earth infrared pressure. Gravitational forces, which are conservative forces, are not measured by the accelerometers. The total non-conservative acceleration measured by the accelerometer can then be used in conjunction with accurate radiation force modeling in order to isolate the atmospheric drag. The drag equation can then be used to estimate the atmospheric density. This method of estimating density is much more accurate than the DCA methods discussed previously. Despite the accuracy of this method, there are few satellites that are equipped with on-board accelerometers and therefore accelerometer density data is limited. The only satellites that have on-board accelerometers with sufficient accuracy are CHAMP, GRACE-A, GRACE-B, and Gravity Field and Steady State Ocean Circulation Explorer (GOCE). The accelerometer on-board CHAMP is called the Spatial Triaxial Accelerometer for Research (STAR). Information detailing the extraction of density data from CHAMP's STAR accelerometer can be found in Reference 2 and References 32 - 34. Information detailing the extraction of density data from GRACE's on-board accelerometer can be found in Reference 3. There have been a number of satellites in the past that have had accelerometers of lesser accuracy on-board. Reference 35 discusses the Satellite Electrostatic Triaxial Accelerometer (SETA) experiment which used two satellites equipped with on-board accelerometers in order to measure atmospheric density at an altitude of 200 km for selected months during the time period of 1982-1984.

Reference 32 outlines research aimed at using the accelerometers on-board CHAMP to measure thermospheric events such as those caused by coronal mass ejections (CME) that are large enough to reach the Earth's atmosphere. This study uses the data from the on-board accelerometer to model the non-conservative forces experienced by the satellite instead of using force models. While using the accelerometer data yields more accurate results, there are a number of calibration parameters that need to be adjusted. The authors also suggest external independent verification of data using either POE or SLR data for any possible future research.

The study carried out in Reference 1 focuses on estimating atmospheric density using accelerometer data while incorporating accurate force models for the radiative forces. The study points out that the accuracy of the results varies from 1% to 20% depending on the performance and calibration of the accelerometers, the magnitude of unmodeled winds, and drag coefficient uncertainty (the configuration of CHAMP is complex and creates difficulty in drag coefficient determination). The resulting density estimates were compared with the DTM2000 semi-empirical thermosphere model and showed high accuracy, with an expected further increase in accuracy with the addition of more data points.

Reference 33 outlines the process of extracting atmospheric density data from CHAMP's STAR accelerometer measurements. The accelerometer data is first corrected for any satellite maneuvers, influential events, and instrument bias before it is processed. In order to obtain the atmospheric density a 15-plate model for the satellite was used to estimate aerodynamic coefficients such as the drag coefficient. The accuracy of the 'observed' density values is determined by the uncertainty in the calibration parameters and the aerodynamic coefficients. The accuracy was also dependant on the level of geomagnetic activity. The uncertainty level in the density data was significantly higher during times of high geomagnetic activity.

This activity increases the magnitude of the neutral winds in the upper atmosphere where the empirical wind models are not sufficient. It is suggested that the simultaneous use of accelerometer and mass spectrometer measurements would likely decrease the drag coefficient uncertainty and therefore increase the accuracy of the results.

The study discussed in Reference 34 focuses on extracting density data from the accelerometer measurements from STAR. This work outlines some of the limitations and difficulties in extracting density data from accelerometer measurements such as instrument bias, scale factors, different modeling approaches, and difficulties with density retrieval. This work used 1.2 million observations over a 21 month period and the data was binned by solar and geomagnetic activity level. The resulting atmospheric density values were then compared to numerous other atmospheric density models.

Reference 2 also discusses the procedure used to extract density data from accelerometer measurements. This work focuses on the time periods surrounding three geomagnetic storms which occurred in 2002. The accelerometer derived density data is also compared with semi-empirical atmospheric density models. The study also discusses the effects of variations such as seasonal, latitudinal, local time, and solar activity variations on the atmospheric density.

Reference 36 discusses the atmospheric density variations in the thermosphere near the polar regions using CHAMP's on-board accelerometers. This examination revealed increases in density of up to 50% above ambient located around the polar cusp region and diminishing nearer to the poles. This result is observed due to the energized solar particles being 'pushed' toward the poles by the Earth's magnetic field where the energy causes variations in the atmospheric density and temperature.

The CHAMP accelerometer has been used in a number of different studies to observe various solar and geomagnetic events and how they are related to variations in atmospheric density [References 37 - 44]. As previously mentioned CHAMP is frequently used to observe polar variations because CHAMP's accelerometer is able to capture the short term density variations while empirical density models lack the necessary temporal resolution. Also, the high inclination of CHAMP's orbit plane (nearly polar orbit) allows coverage of nearly all latitudes which is necessary when trying to determine the amplitude and span of the density variations. The observed density variations from high levels of geomagnetic activity cause density waves to propagate toward the poles.

The research conducted in Reference 3 focuses on obtaining accurate density data using the measurements from the accelerometers on-board the GRACE satellites. This work realizes that there are limitations on the current empirical atmospheric density models due to the short scale variations in atmospheric density caused by solar and geomagnetic activity. However, the accelerometer derived density data can provide in situ density measurements that can then be used to correct the existing atmospheric density models and improve their accuracy. There are a number of good reasons to use the CHAMP and GRACE satellites when conducting research on the Earth's atmosphere such as availability of accelerometer, Global Positioning System (GPS), and SLR data. However, the use of these three satellites provides poor spatial coverage when compared to the DCA technique that incorporates data from hundreds of satellites.

1.7.3 Alternative Methods

There are a number of methods that can be used to determine atmospheric density other than the use of accelerometer data or a DCA technique. One of these methods is to use GPS

and SLR measurements instead of accelerometer measurements in order to determine the non-conservative accelerations experienced by the satellite. Reference 45 outlines one such method which uses satellite orbit and tracking data to make corrections to the CIRA-72 atmospheric density model. This research uses two different data sources to provide satellite orbit and tracking measurements. The first source has a high accuracy but uses a limited number of satellites that have POE data available which restricts the spatial resolution. The second source of data is TLE data sets which have very limited accuracy and low temporal resolution but allow for high spatial resolution. The combination of these two data sets acts in a complimentary manner and yields satisfactory results. The authors of this research suggest that a calibration scheme which works in near real time should be examined as this would provide atmospheric density prediction capabilities.

Another alternative method of obtained density data is GPS accelerometry which uses GPS receiver data instead of on-board accelerometers in order to estimate the accelerations experienced by the satellite due to non-conservative forces. References 46 - 48 take advantage of this method by using precision orbit data from the CHAMP satellite in order to derive the drag forces on the satellite which are then used to determine the atmospheric density. This shows that non-conservative accelerations can be obtained indirectly from GPS satellite-to-satellite observations without the need for on-board accelerometers. The results obtained from this method were compared with those derived from CHAMP's on-board accelerometer and have a high accuracy (temporal resolution of 20 minutes in both along-track and cross-track directions) because of the precision of the gravity field models which is a product of the CHAMP and GRACE gravity missions. GPS accelerometry is most accurate in the along-track direction which is where the majority of the non-conservative forces are experienced. Although the re-

sults of this research indicate that it is a feasible method to determine atmospheric density corrections it lacks the resolution required to capture the high frequency accelerations that the satellite can experience. However, future satellite missions with GPS receiver capability will increase the number of observations that can be used in this method and therefore increase the spatial resolution. Reference 48 also discusses using the GPS accelerometry technique but estimates accelerations on the GRACE-A satellite as well as CHAMP. The results were again acceptable in the along-track direction but yielded low accuracy in the radial and cross-track directions for both satellites.

Reference 49 examines both the batch least squares and Kalman filter/smoother techniques based on the GPS data received on-board the GRACE-B satellite. This method estimates the accelerations as part of the orbit determination process using either the batch or the Kalman filter. The primary focus of this work was to determine what differences existed between batch and filter/smoother techniques. Both methods provided high accuracy with a resolution of 5 cm with dual frequency data and 10 cm with single frequency data with a high correlation between the two techniques. The major finding of this work was that the batch technique is more smooth and robust during gaps in the data while the filter/smoother technique uses less computational time and memory.

The research outlined in Reference 50 examines using SLR data along with Doppler Orbitography and Radio positioning Integrated by Satellite (DORIS) data in order to observe density variations in the upper atmosphere during time periods of high geomagnetic activity level. DORIS is another way in which highly accurate satellite state vectors can be obtained and that can be utilized in order to produce atmospheric density model corrections. When the

results were first compared to existing atmospheric models the errors were significant, however they greatly improved with the addition of more enhanced data processing.

1.8 Gauss-Markov Process

Often a process noise model is introduced into the orbit determination scheme in order to account for any unmodeled or inaccurately modeled accelerations acting on the spacecraft. The Gauss-Markov process is one such model that is used for dynamic model compensation and which obeys a Gaussian probability law (normal distribution) and has the characteristics of a Markov process. A Markov process is one in which its probability density function at any time is dependant only upon the state immediately preceding it and not any other past state. More information on the Gauss-Markov Process and how it can be utilized in orbit determination can be found in Reference 51.

1.9 Current Work on Corrections to Atmospheric Density Models

The overall goal of this research is to use high precision orbit data in order to estimate corrections to existing atmospheric density models. Data from satellite GPS receivers is used in conjunction with an optimal orbit determination process to obtain highly accurate (centimeter to meter level accuracy) precise orbit ephemeris (POE) data. This POE data is then used as input into a sequential filter/smoother optimal orbit determination scheme which estimates atmospheric density corrections to existing models. The use of POE data as input instead of TLE data sets greatly improves the accuracy of the resulting density estimates. This research will focus on time periods which span the range of solar and geomagnetic activity level as previ-

ously mentioned as well as periods of localized density increases and large moving density variations. This process is carried out for both the CHAMP and the GRACE-A satellites and the resulting estimated density corrections are compared to the density data derived from the accelerometers on-board the two satellites which is considered truth in this work.

The procedure mentioned above for using POE data as input into an optimal orbit determination scheme in order to produce atmospheric density estimates can be found in Reference 52. This work also focused on checking for consistency between the overlap periods between data sets. There are typically two overlap periods of two hours each at the beginning and end of each set (14 hour spans). Reference 53 compares the results of POE derived density estimations for CHAMP with the density data derived from CHAMP's on-board accelerometer. The research conducted in Reference 54 is focused on determining which combination of inputs into the optimal orbit determination scheme yield the best correlation with the accelerometer derived densities. There are a number of different inputs which can be varied such as the baseline density model, the correlation Gauss-Markov half-lives for the density and ballistic coefficient (discussed in the previous section), as well as the time span of the solutions. The results of this study indicated that the POE derived densities exhibit a better correlation with accelerometer derived densities than either the Jacchia-71 atmospheric model densities or HASDM densities. Reference 55 focuses on estimating density corrections during times of high solar and geomagnetic activity levels. The cross correlation (CC) values are calculated to compare how well the POE derived densities and the accelerometer derived densities correlate and the results were binned by solar and geomagnetic activity level. Reference 56 focuses on using different lengths of solution fit spans and a higher correlation half-life value for the density and ballistic coefficient and the effects these changes have on the POE derived density estimates.

This provided a quantitative answer on which combination of input parameters yielded the highest correlation between the POE derived density estimates and the accelerometer derived values, finding that in general the combination of the CIRA-1972 baseline density model with a density correlated half-life of 18 minutes and a ballistic coefficient half-life of 1.8 minutes provides the overall highest degree of correlation with the accelerometer derived density. An important aspect to this research to note is that this combination did not yield the best results for all days examined, but did so for the majority of days.

The research discussed in Reference 57 also focuses on producing POE derived density corrections but includes the GRACE and TerraSAR-X satellites along with CHAMP. For more information on the TerraSAR-X satellite please see Reference 58. This work also discusses how certain high frequency density variations caused by events such as travelling atmospheric disturbances or geomagnetic cusp features (discussed later) will likely not be captured in the POE derived density data. Similar to Reference 56, this work also examines which combination of baseline density model and density and BC correlated half-lives yields to best density estimates when compared to accelerometer derived densities. The results were similar to those found in Reference 56 for the baseline density model (CIRA-1972) and the ballistic coefficient correlated half life (1.8 minutes) however this work revealed that a density correlated half life of 180 minutes rather than 18 minutes was performed better more often. Reference 59 focuses on estimating densities during this time period for CHAMP and GRACE and then comparing the results with the accelerometer derived densities obtained from the satellite's respective on-board accelerometers. Reference 60 also focuses on estimated density corrections for CHAMP and GRACE during this time period but also looks at TerraSAR-X data. Since TerraSAR-X is not equipped with an on-board accelerometer only the results for CHAMP and GRACE can be

compared to accelerometer data, but the authors are still able to draw conclusions from the TerraSAR-X results by using the results obtained from CHAMP and GRACE.

The work outlined in Reference 61 focuses on calculating CC and RMS values between the POE derived densities for CHAMP and GRACE and their respective accelerometer derived densities. The results for the twin GRACE satellites (GRACE-A and GRACE-B) are also compared with one another. The correlation between the two GRACE satellites was very high as was expected. The results from this study showed that the POE derived densities almost always outperform the existing empirical density models that were used for comparison as well as HASDM. The authors found in this research that there is a time period from late October 2005 through January 2006 where all of the density sources examined (POE, empirical models, HASDM) showed extremely poor correlation with respect to accelerometer data. This time period of anomalous behavior is expanded on and discussed in more detail in Reference 62.

The research carried out in Reference 63 uses a similar procedure as the previously discussed papers to produce POE derived density corrections to existing models for CHAMP and GRACE. However, when comparing the results with the accelerometer derived densities a different source of data is used than before. The previous references all used the accelerometer density data derived by Sean Bruinsma while this work uses the accelerometer derived density data from Eric Sutton. The two different sources of accelerometer density data are compared for both CHAMP and GRACE and it was found that they correlate well enough to substitute one source for the other. This work also looks at two additional satellites: TerraSAR-X and ICESat. As was the case with TerraSAR-X mentioned previously there are no accelerometers on board either of these satellites. This means that there is no 'truth' density data set to use for comparison and verification of results. Instead the author compared the results with those from

CHAMP and GRACE and from this was able to see similar trends in the data and understand how the atmospheric density can change with varying altitude and orbit type.

The work outlined in Reference 64 examines the POE derived density estimates for CHAMP and GRACE and the effect on accuracy of utilizing the linear weighted blending technique to combine the density data sets during periods of overlap. The linear weighted blending technique is a mathematical tool which is used to stitch together two sets of data during a region of overlap such as measurements of the same quantity at the same time but by two different instruments. The goal of this is to achieve one continuous set of data which has a value somewhere between the two separate measurements during the overlap periods. This technique is not an average of the two values since that would result in discontinuities at the beginning and end of the overlap periods. This technique is also described in Reference 65.

Reference 65 expands on the research discussed above. The author examines the effect of using different functions of geomagnetic planetary amplitude (a_p) as input into the orbit determination scheme. The three different functions examined were the 3-hourly a_p step functions, linear interpolated a_p functions, and a_p osculating spline functions. This comparison led to the conclusion that using a_p osculating spline functions as input into the orbit determination scheme yields better results than using either the 3-hourly step functions or the linear interpolated functions. The author also expands on the work done in Reference 64 and outlines the linear weighted blending technique which is used to create continuous one week density data sets from the fourteen hour POE derived density solutions. The results showed that these one week continuous POE derived density data sets provided better correlation with the accelerometer derived densities than HASDM densities for both CHAMP and GRACE. There was also work done in Reference 65 to examine the average cross sectional area facing the Sun for both Ter-

raSAR-X and ICESat in order to better estimate the atmospheric drag, the force due to solar radiation pressure, and the force due to Earth radiation pressure.

The work outlined in Reference 66 uses POE data in order to estimate atmospheric density along the orbits of CHAMP and GRACE. This work utilizes the linear weighted blending technique outlined in References 64 and 65 in order to obtain continuous solutions over the entire mission life of CHAMP and through 2011 for GRACE. The results obtained in this work confirmed previous research showing that a combination of using the CIRA 1972 atmospheric model as a baseline density model, a ballistic coefficient half-life of 1.8 minutes and a density half-life of 180 minutes was found to be the overall combination that best matched accelerometer derived densities as measured by CC and RMS. This research also found that the POE derived densities were shown to better match the accelerometer derived densities in terms of CC and RMS than either HASDM or Jacchia 71 density models. The correlation between the performance of the density sources compared to accelerometer derived density and the beta angle of the satellite was also examined. The results showed that the CC between the density sources and accelerometer derived densities was lower when the orbit plane of the satellite was near the terminator.

1.10 Estimating Density and Ballistic Coefficient Separately

In orbit determination the atmospheric density and the ballistic coefficient are directly related to each other through the drag equation (Equation 1.1). This causes difficulty when attempting to simultaneously estimate both variables in an orbit determination scheme. The research outlined in References 67 and 68 focuses on a technique to estimate both the density and ballistic coefficient simultaneously in real-time. In previous research the error in the density

models and the ballistic coefficient both had to be absorbed by the ballistic coefficient making it difficult to separate the values. However, by setting the exponential half-lives of both the ballistic coefficient and density errors sufficiently far enough away from each other the simultaneous estimation of the atmospheric density and the ballistic coefficient is possible. The half-lives of these values are defined as the time it takes the value to decay from its original value to half of the original value and they basically determine how much of the previous state (and only the previous state since it is a Gauss-Markov process) affects the value of the current state when inputting process noise. The orbit determination software used in this research, Orbit Determination Took Kit (ODTK), allows the user to vary both the density and ballistic coefficient half-lives separately. More details on this subject will be discussed in the Methodology section of this report.

The research outlined in Reference 56 focuses on varying the initial value of the ballistic coefficient in the orbit determination scheme and analyzing the effect this has on the POE derived density estimates for CHAMP. The POE derived densities were then compared to the accelerometer derived densities from which cross correlation values were obtained. The study concluded that as long as the initial BC estimate is within ±10% of the nominal BC value the POE derived densities obtained from the orbit determination process correlate well with the accelerometer derived densities. The author suggests that future work might include using the orbit determination scheme in an iterative manner in order to find a more accurate initial estimate for the ballistic coefficient [Ref. 69]. This work also examined the differences in POE derived densities produced by an orbit determination scheme which estimated BC and one that did not estimate BC. The study concluded that although the differences between the two cases

were extremely low these differences grew with an increase in solar and geomagnetic activity level.

Reference 69 also focuses on the estimation of atmospheric density and ballistic coefficient for CHAMP. Another aspect of this research is based on determining the effect of varying the initial value of BC on the estimated density corrections but also examines the effect of using a converged value of BC for the initial value, varying the correlated half-lives of both the density and the BC, and the absorption of density errors in the estimated ballistic coefficient. The authors came to the same conclusions reached in Reference 56 with regards to varying the initial BC value and its effect on the POE derived densities. As discussed previously, the authors used the orbit determination process in an iterative manner in order to come up with a converged BC value. The POE derived densities resulting from using this converged BC value as the initial value do not correlate as well to the accelerometer derived densities as did the POE derived densities which used the nominal BC value as the initial value. The authors conclude that this may be due to bias in the accelerometer derived densities and they also conclude that further study into this matter is not necessary so long as a good enough estimate of the initial BC is available. With regards to varying the correlated half-lives of the density and BC the results showed that an increase in the BC correlated half-life caused the estimated density to increase and the BC to decrease (and vice-versa). The authors also observed that increasing the correlated half-life of the density caused the estimated density to decrease and the BC to increase (and vice-versa). This work also examined how the POE derived densities obtained from the orbit determination scheme would change based on whether or not the BC was being estimated similar to the work carried out in Reference 56. Although the differences between the two were small, the authors suggest that slightly more accurate POE derived densities are ob-

tained when the BC is also estimated. The last topic this research examined was whether or not the density errors are being absorbed by the BC estimation in the orbit determination scheme. If the density errors are being absorbed by the BC estimation than the authors would expect to see a high negative CC value between the BC and the density error, which is the difference between the POE derived density and the accelerometer derived density. Only one day which experienced high solar and geomagnetic activity levels showed any significant negative correlation between the two values. The authors suggest that more days be examined to get more insight into this topic.

The research outlined in Reference 70 continues the work of Reference 69 on seeing whether or not the density errors are absorbed by the BC estimation in the orbit determination process. This work looks at CHAMP and GRACE and also examines more days than done in previous research. The CC values between the density error (difference between POE and accelerometer derived densities) and the estimated BC were obtained for two different density correlated half-lives of 18 and 180 minutes. The authors found that there was a significant negative correlation between the density errors and the BC when the density correlated half-life was 18 minutes. This means that when the density correlated half-life is 18 minutes the BC estimation absorbs errors in atmospheric density and this is not the case (as least to this magnitude) when the density correlated half-life is 180 minutes. The authors also examined the effect of not estimating the BC value in the orbit determination scheme. Although this was done in previous research, the work carried out in Reference 70 contains more days than were previously examined as well as data for GRACE. The results obtained indicated that the POE derived densities correlate more closely with the accelerometer derived densities when the BC is

estimated but the differences were very small, which is the same conclusion reached in previous work on the subject.

1.11 Travelling Atmospheric Disturbances (TAD)

Travelling atmospheric disturbances (TADs) are atmospheric density increases which propagate from the Earth's two poles towards the equator. These disturbances are caused when large coronal mass ejections (CME) from the Sun come into contact with the Earth's atmosphere and deposit large amounts of energy into the upper atmosphere at high latitudes. TADs from opposing poles come together near the equator causing constructive interference and can even travel as far as past the opposing pole starting back toward their pole of origin though their effect is much less pronounced by that point. During the period of April 15-24, 2002 there were several CMEs emanating from the Sun which were large enough to produce TADs. Although these density increases likely occurred on both the lit and unlit side of the Earth, the TADs are much easier to observe on the dark side of the Earth. The unlit side of the Earth allows for easy separation of the disturbances from the global density values while the atmospheric heating due to the Sun makes the effect of the TADs difficult to examine. For more information on TADs see Reference 37.

1.12 Geomagnetic Cusp Features

There have also been localized increases in density in the upper atmosphere near the geomagnetic poles observed by the STAR instrument on-board CHAMP. These density increases were found to be up to 50% above ambient densities and were located around 75° geo-

magnetic latitude with a basin localized around the geomagnetic pole. The actual cause of these localized increases is not exactly known but at least a portion of the increase is thought to be attributed to Joule heating and the interaction between magnetic field lines. See Reference 36 for more information on geomagnetic cusp features.

1.13 Satellites Examined

There were two satellites examined in this research and they are CHAMP and GRACE-A. This section will include a brief overview of each of them. All of the information contained in this chapter was obtained from the International Laser Ranging Service (ILRS) website [Ref. 71 - CHAMP and Ref. 72 – GRACE].

1.13.1 CHAMP

Figure 1.1 – Artist's rendering of the CHAMP satellite in orbit [Ref. 73].

The Challenging Mini-Satellite Payload (CHAMP) was launched on July, 15 2000 by GFZ Potsdam for the purpose of geophysical research and application. One of the primary goals of the mission was to resolve long-term temporal variations in the magnetic field and gravity field within the atmosphere. For this reason the satellite had an expected life-span of five years which would allow for a sufficiently long observation time. CHAMP exceeded its expected life-span and did not re-enter the atmosphere until September 20, 2010; double the life-span that was expected. The orbit of CHAMP is circular with an eccentricity of 0.00396 and nearly polar with an inclination of 87.27 degrees which allowed great geographical and altitude coverage during its lifespan. The initial perigee of the spacecraft was 474 km while the initial mass was 400 kg. There are a number of instruments onboard CHAMP which make it a suitable satellite to use in this research. The three-axis STAR accelerometer was mentioned previously and allows the POE derived density estimates to be validated against a 'truth' data set. The satellite is also equipped with a dual-frequency GPS receiver as well as a retro-reflector array which allows for SLR, both of which lead to accurate orbit positions.

1.13.2 GRACE

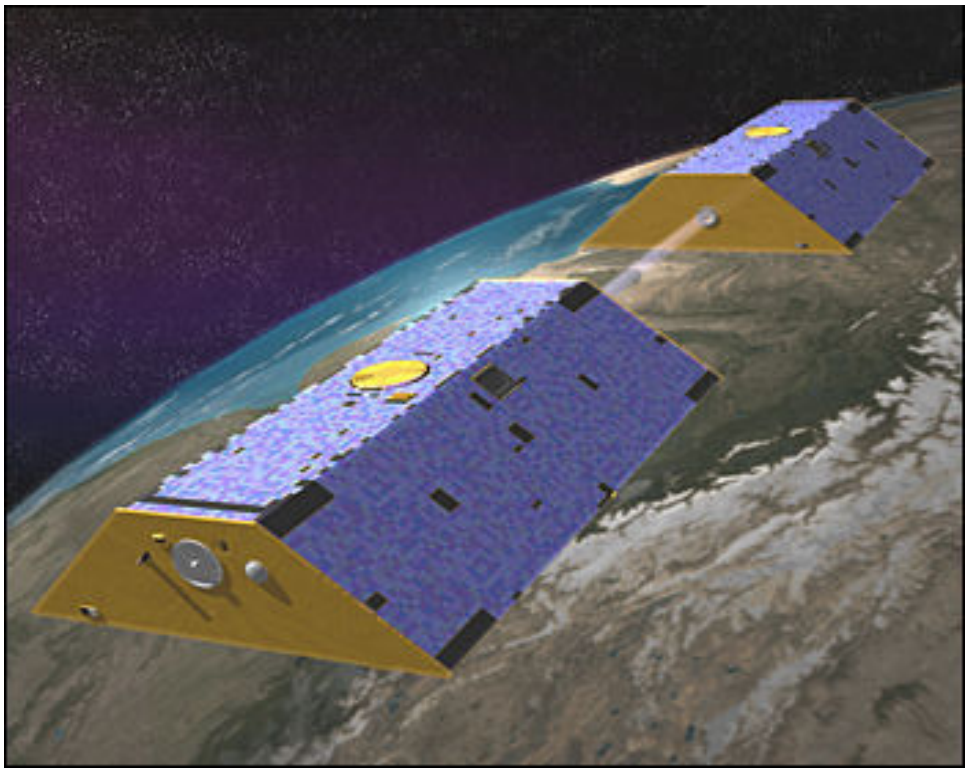

Figure 1.2 – Artist's rendering of both the GRACE satellites in orbit [Ref. 73].

The Gravity Recovery and Climate Experiment (GRACE) satellites were launched on March 17, 2002 as a cooperative effort by both NASA and GFZ with the mission of providing high resolution global estimates of the Earth's gravity field and how it varies. This mission is accomplished by measuring very small perturbations in the distance between the two satellites which occurs when one satellite passes over a portion of the Earth which is more or less dense than the whole Earth causing it to accelerate or decelerate. The initial life-span of the GRACE mission was expected to be five years but that has been exceeded and both the GRACE satellites are still in orbit. The GRACE mission consists of two identical satellites (GRACE-A and GRACE-B) flying one behind the other with a distance between them of about 220 km (only GRACE-A will be examined in this research). The orbit of the GRACE satellites is circular

with an eccentricity less than 0.005, nearly polar with an inclination of 89 degrees, and has a non-repeating ground track. The initial perigee of the satellites was 485 km while the initial mass of each of the satellites was 432 kg. The instrumentation on the GRACE satellites is similar to that of CHAMP and includes an accelerometer which allows for validation of results.

1.14 Previous Work on Examining the Effect of Density Variability

A portion of this research focuses on determining the effect that certain density variations have on the propagation of satellite orbits. There has been other research recently conducted that also focuses on the variations in the atmospheric density and the effect this can have on orbit prediction. The research conducted in Reference 74 is meant to examine how satellite orbit prediction error depends on the variability of the atmospheric density. This work primarily focuses on the importance of capturing the larger density variations with regard to horizontal wavelengths in the density profile and to determine the necessary level of knowledge of these variations for various orbit prediction applications. First, the authors used simple analytical functions (sine, step, impulse) to model density perturbations in order to isolate the effect of this one perturbation on orbit prediction. They found that the errors produced by these simple density perturbation functions when compared to a nominal constant density case were small relative to U.S. Air Force requirements (250 m error for 200 km altitude, 100 m error for 400 km altitude, and 50 m error for 800 km altitude), but not negligible. Next, the authors made a comparison between orbits propagated using NRLMSISE-00 atmospheric model and those propagated using CHAMP's accelerometer derived density data which is used as truth. The time periods analyzed were for the year 2003 (active geomagnetic) and the year 2007 (quiet geomagnetic) with specific days selected in each year to represent all levels of geomagnetic

activity. The results for the simulated two-body orbit for a 24 hour integration period showed significant differences between the two orbits for the active year of 2003 (mean difference of 1785 m, maximum difference of 6817 m) while 2007 showed smaller yet still significant differences (100 m to several hundred meters on average). In an effort to focus on reducing the effect of certain horizontal scales in the densities and therefore determining their importance, the authors smoothed the CHAMP density data over specified time intervals (6 minutes and 30 minutes). These time intervals were selected because they are integer multiples of the time interval for which data is available (45 seconds) and they are adequate to smooth out the 1000 km and 8000 km (roughly 10° and 70° latitude respectively) horizontal scales that the authors were focusing on. Orbits integrated using these smoothed CHAMP densities and those integrated using the original CHAMP densities were then compared. The results for the case averaged over 30 minutes (8000 km or approximately 70° latitude) showed orbit errors on the magnitude of 100 m while the error was reduced to being on the order to several meters for the case smoothed over 6 minutes (1000 km or approximately 10°). These results show that the effect of not including these wavelengths in orbit prediction could be significant for some applications, especially the case averaged over 30 minutes.

The work outlined in Reference 75 focuses on examining the effect of the period, amplitude, and phase of density waves on orbit propagation. The authors first developed an orbit propagation model that includes the effects of Earth's oblateness and drag, assuming a non-rotating Earth for simplicity. The model density was defined using a sinusoidal wave as a function of amplitude, phase, and period. This model was compared to that developed in the first part of Reference 74 and found to have similar results. The authors then varied the characteristics of the density wave (amplitude, phase, and number of cycles or wavelength). By varying

the cycles of the density wave it was seen that the longer wavelength density waves produce much larger variation when compared to a nominal constant density case, which means that the longer the wavelength the more easily detectable the variation in orbit trajectory. The variation of the amplitude revealed, as expected, that the amplitude variation has a linear relationship with the difference in the orbit trajectory. By varying the phase of the density wave the authors found that the difference in phase can have a large effect on the resulting orbit. This result emphasizes the importance of accurately determining the location of the crest of the density waves on orbit propagation. Overall the results showed that the estimation of orbit position is highly sensitive to assumptions made about the density wave. The second portion of this research focuses on comparing the orbit propagation of CHAMP using different sources of atmospheric density data. The density data sources that were compared in this work were the Jacchia 1971 atmospheric density model, HASDM, POE derived density data, and the accelerometer derived density data which was considered truth. The results found that there existed some bias between the different sources of density data due in part to their estimation of the uncertain ballistic coefficient (and the fact that the density data values are estimated). Therefore, in an attempt to remove any possible bias, all density data sets were shifted such that all the data sets had the same overall mean density for a particular time period as the accelerometer derived data. The results for these comparisons were also binned by solar and geomagnetic activity level. The authors found that HASDM produces the best results (compared to accelerometer data) in all solar and geomagnetic activity bins before the bias is removed. Once the bias is removed, the POE data outperforms HASDM and the baseline Jacchia 1971 model when the geomagnetic activity is quiet or moderate, while HASDM still performs the best for active geomagnetic activity levels. It is important to note that the author believes there are better ways to attempt to

remove the bias within the density data sets such as multiplication of a ratio of the estimated ballistic coefficient (as opposed to addition/subtraction). The author believes this method would produce more accurate results particularly for data sets during high geomagnetic activity, so it's likely that the accuracy of the POE data during active geomagnetic activity would be improved using a different method.

Reference 76 examines the high frequency density variations that are present in the accelerometer derived density data but do not show up in the empirical density models or in the POE derived density data. These high frequency density variations appear in all data sets but are especially prevalent during geomagnetic stores, near the polar cusps, and when the satellite orbit plane is near the terminator. This work examines the effects of these high frequency density variations by propagating the orbits of CHAMP and GRACE through a 24 hour time period (extracted from the seven day data sets developed using the linear weighted blending technique outlined in References 64 and 65) using different sources of density data as input measurements. The different density data sources examined are the POE derived densities, HASDM, and Jacchia 71 density model. All of these are compared to an orbit propagation using the accelerometer derived densities in order to see their relative accuracy. The results of Reference 76 are presented later in this work in Chapter 3.

2 METHODOLOGY

This section outlines the methods and procedures used in this research to obtain estimated density corrections to existing atmospheric models through an optimal orbit determination process. This OD process uses position and velocity vectors of satellites (CHAMP and GRACE-A in this case) derived from Precision Orbit Ephemerides (POE) as input in order to obtain density values as well as values for ballistic coefficient along the path of the satellite. These estimated density corrections are then compared to density values derived from the accelerometers on-board the two satellites. There are certain atmospheric phenomena which cause high frequency density variations often on the same order as the diurnal variations. The high frequency variations caused by these phenomena (such as the orbit plane being near the terminator, or the existence of a TAD or geomagnetic cusp) are not captured in the existing atmospheric models or in the POE derived densities [Ref. 36]. Since these variations are not observed in the POE derived density estimates, examining the effect that not modeling the variations has on the accuracy of orbit propagation could be useful. In order to see this effect an orbit propagator was constructed which uses a number of different density sources as input measurements. The results of these orbit propagations are then compared to the results obtained using the accelerometer derived density values in order to see the effect that the un-modeled high frequency density variations have on the orbit determination process. The effect of adding noise to the raw ephemeris file that is input into the Orbit Determination Tool Kit (ODTK) scheme is also examined in this research and the process in which to do so is also included in this section.

2.1 Precision Orbit Ephemerides

Precision Orbit Ephemerides (POE) are sets of position and velocity data for several satellites over a period of time that were generated using high fidelity numerical techniques. These data sets are available for CHAMP and GRACE (as well as other satellites) from the GFZ German Research Centre for Geosciences website (http://isdc.gfz-potsdam.de/). The currently available POE data for CHAMP and GRACE are in the form of either Precision Science Orbits (PSOs) or Rapid Science Orbits (RSOs). The accuracy of RSOs is around 5-10 cm when compared to satellite laser ranging data (SLR) [Ref. 77 - 80]. More detailed information on the accuracy of RSOs as well as the processing of RSO data can be found in References 77 - 80. PSO data is only available between the years of 2003 and 2005 and is not available at all for GRACE, which is why only RSOs (14 hour fit span) are used for this research.

2.2 Optimal Orbit Determination

An optimal orbit determination scheme is used in this research in order to estimate corrections to existing atmospheric density models. The information contained in this section includes a brief summary of the optimal orbit determination process and was primarily gathered from References 5, 6, and 51.

An orbit determination process is one that uses accurate measurements in order to estimate the orbit of a satellite in relations to its central body. In the case of this research the focus is on artificial Earth-orbiting satellites which are much smaller than the body they orbit. This causes the non-gravitational forces acting on the satellite (such as atmospheric drag, solar radiation pressure, and Earth albedo) to be significant. Higher order gravitational effects of the Earth must also be included.

The state of a dynamic system is a set of parameters that are required to predict the future state of the system. In the case of orbit determination there are six required parameters which are often expressed either in Cartesian using the three components each of the position and velocity vectors: x, y, z, v_x, v_y, v_z, or in Keplerian using the six classical orbital elements. For improvement in the accuracy of the orbit determination results more than six parameters can be used such as dynamic and measurement model parameters. For a general orbit determination problem, the state at any time, *t*, is denoted as $\mathbf{X}(t)$. The orbit determination problem can be stated as the following: If at an initial time, t_0, the state of a satellite, $\mathbf{X}_0(t)$, following a ballistic trajectory is known then the governing differential equations of motion can be integrated to give the state of the satellite at any other time, *t*. In the case of this work, however, the initial satellite state, $\mathbf{X}_0(t)$, as well as the dynamical models are not precisely known and therefore errors exist in the orbit determination results. The error between the predicted satellite state produced from orbit determination process and the actual state of the satellite grows larger with time. However, the orbit determination results are improved by making actual measurements of the state of the satellite whenever possible, though these measurements are not perfect as they are subject to both systematic and random errors. The updated measurements are typically in the form of range, range-rate, azimuth, elevation, as well as other observable parameters. Some of these quantities are nonlinear functions of the desired state variables and are used only to determine more useful state variables [Ref. 51]. In addition to the errors associated with the orbit determination process discussed previously, there are also errors introduced into the process due to computational procedure, numerical integration, and truncation.

The orbit determination scheme used for this work includes using POE data as input measurements in a sequential Kalman filter/smoother process which utilizes Gauss-Markov

processes. The type of filter used for this research is the extended Kalman filter which differs from the basic Kalman filter in that the state estimate of the satellite is updated at each time step when an observation is available, which increases the accuracy of the process.

The use of the word 'optimal' in the term 'optimal orbit determination' also needs some discussion. The 'best' estimate does not have a single definition but instead depends on the application. In orbit determination 'optimal' is used in a statistical sense. Several factors must be considered when deciding which orbit determination scheme/approach is 'optimal'. Some methods offer a higher level of accuracy at the expense of computational speed while others cost much less computationally but yet have poor accuracy. Other decisions must also be made such as whether to use sequential or batch methods, whether to minimize the size of orbit errors or measurement residuals, and how to model these errors. Reference 81 contains a list of eight criteria which must be met in order to consider the process 'optimal':

1. "*Sequential processing (SP) is used to account for force modeling errors and measurement information in the time order in which they are realized.*
2. *The optimal state error estimate* $\Delta\hat{X}$ *is the expectation of the state error* ΔX *given the measurement residual* Δy. *That is:* $\Delta\hat{X}=E\{\Delta X|\Delta y\}$. *This is Sherman's Theorem.*
3. *Linearization of state estimate time transition and state to measurement representation is local in time, and not global.*
4. *The state estimate structure is complete.*
5. *All state estimate models and state estimate error model approximations are derived from appropriate force modeling physics, and measurement sensor performance.*

6. *All measurement models and measurement error model approximations are derived from appropriate sensor hardware definition and associated physics and measurement sensor performance.*
7. *Necessary conditions for real data:*
    - *Measurement residuals approximate Gaussian white noise.*
    - *McReynolds filter-smoother consistency test is satisfied with probability 0.99.*
8. *Sufficient conditions for simulated data: The state estimate errors agree with the state estimate error covariance function."*

The author points out that the first six requirements on the list are defined standards for optimal algorithm design and the production of a state estimate error covariance function while the last two requirements enable the validation of the process including test criteria for optimality.

2.3 Gauss-Markov Process Half-Lives

The orbit determination process used in this work utilizes Gauss-Markov processes through the use of correlated half-lives for the density and ballistic coefficient. The OD process determines corrections to estimated density and ballistic coefficient values from existing atmospheric models. For example, ρ is the estimated density from the baseline atmospheric model then the quantity $\Delta\rho/\rho$ is the correction to the baseline density estimate. Similarly, the quantity $\Delta B/B$ is the correction to the baseline ballistic coefficient value, B or BC. Both the estimated density and BC values along with the corrections are functions of the baseline atmospheric model which is specified by the user in the form of an input into ODTK. The correlated

half-lives for both the density and ballistic coefficient value must also be specified by the user. These half-lives represent the time it takes the value (either density or BC correction) to decay to half its original value in the absence of any measurements. For more detailed information on how the OD process in this work utilizes Gauss-Markov process half-lives please see References 82 and 83. A brief description of the mathematics used in this process which was gathered from these references is presented below.

Let $x = x(t_k)$ be a scalar random variable which could represent either the density or the ballistic coefficient. This variable satisfies the exponential Gauss-Markov sequence which is given by:

$$x(t_{k+1}) = \Phi(t_{k+1}, t_k)x(t_k) + \sqrt{\left\{1 - \Phi^2(t_{k+1}, t_k)\right\}} * w(t_k), k \in \{0,1,2,...\} \qquad 2.1$$

In the above equation $w(t_k)$ refers to the Gaussian white random variable which has zero mean and a variance equal to σ_w^2. The transition function, denoted Φ, is defined by the following equation:

$$\Phi(t_{k+1}, t_k) = e^{\alpha|t_{k+1} - t_k|} \qquad 2.2$$

The constant, α, in the above equation is related to the Gauss-Markov process half-life input by the user via the following equation:

$$\alpha = \ln(0.5)/\tau \qquad 2.3$$

From Equation 2.3 it can be seen that the half-life, τ, has units of time and is thus always positive and the natural log of 0.5 is negative. Therefore the constant, α, is always negative and Φ decays over time.

2.4 Filter/Smoother

The following information on the filter and smoother utilized in the orbit determination scheme in this research is primarily gathered from References 51 and 84. The filter used in this work is a sequential filter which uses precision orbit ephemerides (POE) as input measurements and then outputs estimates of a series of desired state variables such as position/velocity vectors, density and ballistic coefficient corrections, and additional pertinent variables such as station biases, additional forces and measurements, and model parameters. At each time step throughout the orbit determination process the output state from the filter along with the measurements at the current time step are both used as input in order to estimate the state at the next time step. This characteristic of the filter makes it sequential, meaning that the filter processes the data forward in time.

The smoother process works backwards, meaning it takes the last output state from the filter and processes the data sequentially backwards to the beginning, or initialization, state of the filter. The smoother uses as input the stored state output from the filter along with the covariance estimate at each time step and any previous output data from the smoother. The initial measurements used in the filtering process are ignored during the smoother run. The output of the state from the smoother is more accurate and has a smaller covariance than the filter output as the smoother takes advantage of all observations, even if indirectly, order to come up with a solution.

2.4.1 McReynolds Filter-Smoother Consistency Test

The estimated states from the filter/smoother can be validated by using the McReynolds filter-smoother consistency test. The basis of this test is to compare the solutions obtained from the filter and those obtained from the smoother. To do this, a dimensionless variable $\vec{R}$ is cre-

ated which is a ratio of the difference between the filter and smoother output states ($\vec{X}$) compared to the square root of the difference between the covariance matrices ($\vec{P}$) gathered from both the smoother and filter. The test states that if the dimensionless variable $\vec{R}$ is less than or equal to 3 for at least 99% of the values (where both a filter and smoother solution exist) then the McReynolds filter-smoother consistency test is said to be satisfied. A brief summary of the test is outlined in Equations 2.4 and 2.5 below. More detailed information on this test can be found in Reference 81.

$$\vec{R} = \left| \frac{\vec{X}_{i,filter} - \vec{X}_{i,smoother}}{\vec{\sigma}_i} \right| \leq 3 \qquad 2.4$$

$$\vec{\sigma}_i = \sqrt{\vec{P}_{i,filter} - \vec{P}_{i,smoother}} \qquad 2.5$$

2.5 Estimating Atmospheric Density Using Orbit Determination

The atmospheric density is estimated in this work using an orbit determination process which is optimal as defined previously. The sequential filtering scheme described above estimates corrections to some existing, or baseline, atmospheric density model as well as ballistic coefficient values. The filter also computes residuals, performs consistency tests for position and velocity, generates state variables, and estimates other state parameters that may be of interest. The smoother is then applied to the filter output using the last filter solution as an initialization state and runs through the filtered data backwards towards the filter initialization. The smoother increases the accuracy of the filter estimates by taking into account all of the available filter output. The entire filter/smoother technique outputs an estimated atmospheric

density and ballistic coefficient corrections as well as covariance matrices which are determined by the physics models used in the orbit determination scheme. The force models included in the orbit determination process which are used to integrate the equations of motion for the satellite include the 90x90 GRACE Gravity Model 2 (GGMO2C), solar radiation pressure, Earth infrared, albedo radiation, solid Earth and ocean tides, luni-solar point masses, and general relativity. Reference 67 outlines a technique used in order to estimate density as part of an orbit determination process while Reference 68 shows that both the atmospheric density and the ballistic coefficient can be simultaneously observed in an OD process.

As previously stated the atmospheric density corrections obtained from the OD scheme are estimated corrections to a baseline atmospheric density model. ODTK (Version 6) has five available atmospheric density models which can be used and they are Jacchia 1971, Jacchia-Roberts, CIRA 1972, MSISE-1990, and NRLMSISE-2000. Previous research has shown that using the CIRA 1972 baseline atmospheric density model generally results in the highest correlation between the estimated density corrections and the accelerometer derived densities and therefore this is the atmospheric model used in this research [Ref. 56 and 57]. There are two different types of corrections that are applied to this baseline atmospheric model. The first correction is global in nature and is based on the historical solar flux measurement of $F_{10.7}$ as well as geomagnetic activity level in the form of planetary geomagnetic amplitude (a_p) over several solar cycles. These corrections are propagated using an exponential Gauss-Markov process from the height of perigee of the satellite through the orbit. The user is able to specify the half-life of the Gauss-Markov process that is used in this sequence which determines how much the previous data affects the corrections. Research has been done [Ref. 56 and 57] in order to see which combination of density and ballistic coefficient Gauss-Markov half-lives yielded density

estimates closest to those gathered from the on-board accelerometers, similar to the research conducted on the different baseline density models. From this research it was found that a Gauss-Markov half-life of 180 minutes for density and 1.8 minutes for ballistic coefficient yielded the best results and therefore these values are used in this research [Ref. 56 and 57]. The second type of correction is applied at each time step and accounts for each sequential observation of the satellite as well as incorporating current atmospheric conditions. These dynamic corrections are estimated as each observation is acquired which is possible because of the sequential nature of the process. Similar to the first type of corrections, the second type also uses exponential Gauss-Markov processes for the modeling errors taking into account the user-defined density and ballistic coefficient half-lives.

The filter must be initiated with some nominal value for the ballistic coefficient, or inverse of the ballistic coefficient as it has been defined in this work. Yearly averages for the inverse ballistic coefficient for CHAMP are found in Reference 85 and are as follows: 0.00444 m^2/kg for the years 2002 and 2003 and 0.00436 m^2/kg for the years 2004 and 2005. For later years the yearly average inverse ballistic coefficient value was extrapolated in Reference 56 based on satellite mass data and was found to be 0.00426 m^2/kg for the year 2006 and later. This nominal value changes for CHAMP due to the changing mass of the satellite from station keeping maneuvers as well as the decaying orbit of CHAMP. The value used for inverse ballistic coefficient for GRACE was 0.00687 m^2/kg for all years, as found in Reference 85. This value for GRACE does not change between years like that of CHAMP due to the lack of station keeping maneuvers performed by GRACE.

2.6 Validation of Estimated Density

In order to examine the accuracy of the POE derived densities they are compared to the density values obtained from the accelerometers on-board CHAMP and GRACE. The densities obtained from the accelerometers are used as truth in this work because they are the most accurate source of density data available. These accelerometer derived density values were obtained from Sean Bruinsma at the Centre National d'Etudes Spatiales (CNES). These values were averaged over ten second time intervals and were derived along the entire path of CHAMP and GRACE [Ref. 33 and 34]. HASDM density data is also compared with accelerometer derived density data so that the correlation between the HASDM data and accelerometer data can be compared with the correlation between the POE data and the accelerometer data.

2.6.1 Cross Correlation and Root Mean Square

In order to compare the POE derived densities (or HASDM densities) with the accelerometer derived densities the use of the cross correlation (CC) value and the root mean square (RMS) value are utilized. The zero delay cross correlation coefficient is a non-dimensional number somewhere between negative one and positive one and is meant to quantify how closely two data sets correlate with one another. A value of one indicates a perfect correlation between the two, a value of zero indicates that there is no correlation between the two, and a value of negative one indicates that there is a perfect inverse correlation between the two data sets. Consider two sets of data: $x(i)$ and $y(i)$, where i = 0,1,2, …., N. N is the number of data points in the set while $\bar{x}$ and $\bar{y}$ are the mean values of the two data sets. The following expression, found in Reference 86, can be used to calculate the CC value between the two data sets:

$$CC = \frac{\sum_{i=1}^{N}\left[\left(x(i)-\bar{x}\right)\left(y(i)-\bar{y}\right)\right]}{\sqrt{\sum_{i=1}^{N}\left(x(i)-\bar{x}\right)^2}\sqrt{\sum_{i=1}^{N}\left(y(i)-\bar{y}\right)^2}} \qquad 2.6$$

While the CC value is very helpful in quantifying the correlation between two data sets there is nothing in the equation that takes into account the magnitude of the two data sets. Two different data sets might have a very different magnitude but if the two sets vary in a similar manner to one another they will still have a high CC value between them. For this reason the RMS value is also examined between the two data sets in order to gain information about the magnitude of the data relative to each other. The RMS value has units, unlike the CC value, which correspond to the units of the data being analyzed. In this work two different density data sets are analyzed therefore the RMS value with have units of density (mass/length^3). The RMS value between two data sets can be calculated using the following expression:

$$RMS = \sum_{i=1}^{N}\sqrt{\frac{\left(x(i)-y(i)\right)}{N}} \qquad 2.7$$

In order to calculate either the RMS or the CC value between two data sets they must have the same number of elements and coinciding time stamps. In order to accomplish this both the POE derived densities and the HASDM densities are interpolated to match the time stamps of the accelerometer density data. Hermite interpolation is used instead of linear interpolation because previous research has indicated that Hermite interpolation is superior [Ref. 56]. Interpolation of the POE derived densities and HASDM densities is done instead of interpolating the accelerometer derived densities because in this work the accelerometer data is considered truth.

2.7 Solar and Geomagnetic Activity Level Bins

The results of this work are binned based on the solar activity level and the geomagnetic activity level in order to see the effect this has on the POE derived density estimates. For CHAMP a total of 100 days were examined and they were chosen in such a way as to be representative of the entire life-span of CHAMP. These days were selected such that they would span almost the entire mission life of CHAMP, include different periods of the solar cycle, and catch the satellite at different positions in its orbit around Earth. These bins were classified using the daily solar flux value ($F_{10.7}$) and the daily planetary geomagnetic amplitude (A_p) and are based on the work done in Reference 15. The examined days were also chosen such that their distribution would be representative in terms of solar and geomagnetic activity level to what the satellite experienced through its mission life. Table 2.1, taken from Reference 57 below shows the distribution of days in which CHAMP experienced each of the activity bins.

Table 2.1 – Distribution of CHAMP mission life in each solar/geomagnetic activity bin [Ref. 57].

Activity Bin	Definition of Bin	CHAMP Mission Life
Low Solar	$F_{10.7} < 75$	20.8 %
Moderate Solar	$75 \leq F_{10.7} < 150$	57.8 %
Elevated Solar	$150 \leq F_{10.7} < 190$	12.0 %
High Solar	$190 \leq F_{10.7}$	9.5 %
Quiet Geomagnetic	$A_P \leq 10$	63.7 %
Moderate Geomagnetic	$10 < A_P < 50$	33.5 %
Active Geomagnetic	$50 \leq A_P$	2.8 %

The 100 days that were examined in this work are shown below in Tables 2.2 and 2.3 and are shown binned in their respective solar and geomagnetic activity bins.

Table 2.2 – Days examined for CHAMP binned by solar activity level [Ref. 64].

Activity Level Bin	**CHAMP Mission Life**		
Low Solar F10.7 < 75	October 27, 2005	February 13, 2007	September 12, 2007
	May 14, 2006	March 9, 13, 16, 17, 2007	November 18, 2007
	July 11, 14, 2006	April 11, 23, 2007	March 3, 9, 2008
	September 25, 2006	June 20, 2007	May 8, 2008
	December 20, 2006	August 7, 2007	June 4, 2008
Moderate Solar $75 \leq$ F10.7 < 150	October 1, 2002	December 15, 19, 2003	November 15, 20, 2004
	January 17, 23, 2003	January 7, 8, 2004	December 14, 2004
	February 13, 24, 2003	February 8, 12, 20, 2004	January 6, 2005
	April 5, 7, 2003	March 7, 10, 2004	February 8, 2005
	May 17, 2003	April 2, 9, 14, 2004	March 7, 30, 2005
	June 24, 2003	May 8, 27, 2004	May 10, 2005
	July 8, 17, 2003	June 12, 2004	July 9, 15, 2005
	August 5, 2003	July 5, 15, 24, 25, 2004	September 20, 2005
	September 6, 24, 2003	August 5, 8, 2004	December 7, 2005
	October 5, 19, 2003	September 10, 17, 2004	April 3, 2006
	November 7, 9, 2003	October 8, 13, 2004	November 15, 2006
Elevated Solar $150 \leq$ F10.7 < 190	June 6, 2001	June 9, 2002	April 2, 2003
	August 8, 2001	October 4, 27, 2002	October 23, 2003
	March 18, 28, 2002	January 7, 13, 2003	July 20, 23, 2004
High Solar F10.7 $\geq$ 190	June 14, 24, 2001	February 5, 21, 2002	July 30, 2003
	September 26, 29, 2001	April 17, 2002	October 29, 2003

Table 2.3 – Days examined for CHAMP binned by geomagnetic activity level [Ref. 65].

Activity Level Bin	**CHAMP Mission Life**		
Quiet Geomagnetic $Ap \leq 10$	June 6, 14, 24, 2001	January 8, 2004	September 20, 2005
	August 8, 2001	February 8, 20, 2004	October 27, 2005
	February 21, 2002	March 7, 2004	December 7, 2005
	March 28, 2002	April 2, 14, 2004	April 3, 2006
	June 9, 2002	May 8, 27, 2004	May 14, 2006
	July 30, 2002	June 12, 2004	July 11, 2006
	January 13, 17, 2003	July 5, 15, 20, 2004	September 25, 2006
	February 13, 24, 2003	August 5, 8, 2004	November 15, 2006
	April 7, 2003	September 10, 2004	March 9, 17, 2007
	May 17, 2003	October 8, 2004	April 11, 2007
	July 8, 2003	November 15, 2004	June 20, 2007
	August 5, 2003	December 14, 2004	September 12, 2007
	September 6, 2003	January 6, 2005	November 18, 2007
	October 5, 23, 2003	March 30, 2005	March 3, 2008
	November 7, 2003	May 10, 2005	May 8, 2008
	December 19, 2003	July 15, 2005	June 4, 2008
Moderate Geomagnetic $10<Ap<50$	September 26, 29, 2001	November 9, 2003	February 8, 2005
	February 5, 2002	December 15, 2003	March 7, 2005
	March 18, 2002	January 7, 2004	July 9, 2005
	October 27, 2002	February 12, 2004	July 14, 2006
	January 23, 2003	March 10, 2004	December 20, 2006
	April 2, 5, 2003	April 9, 2004	February 13, 2007
	June 24, 2003	July 24, 2004	March 13, 16, 2007
	July 17, 2003	September 17, 2004	April 23, 2007
	September 24, 2003	October 13, 2004	August 7, 2007
	October 19, 2003	November 20, 2004	March 9, 2008
Active Geomagnetic $Ap \geq 50$	April 17, 2002	October 1, 4, 2002	July 23, 25, 2004
		October 29, 2003	

For GRACE a total of 20 days were examined, selected in a manner similar to CHAMP. For GRACE however, data corresponding to elevated and high solar activity levels was not available and therefore these bins are not included. The days examined for GRACE can be found in Table 2.4 binned in their respective solar and geomagnetic activity level bins.

Table 2.4 – Days examined for GRACE binned by solar and geomagnetic activity level [Ref. 65].

Activity Level Bin	**GRACE Mission Life**	
Low Solar F10.7 < 75	October 27, 2005 August 4, 7, 2006	March 13, 2007 February 4, 2008
Moderate Solar 75 ≤ F10.7 < 150	November 9, 2004 March 9, 18, 2005 April 7, 2005 May 10, 13, 2005 August 2, 2005 September 11, 20, 2005	November 17, 2005 December 7, 2005 January 21, 26, 2006 February 3, 2006 April 28, 2007
Quiet Geomagnetic Ap ≤ 10	April 7, 2005 May 10, 2005 August 2, 2005 September 20, 2005 October 27, 2005	December 7, 2005 January 21, 2006 February 3, 2006 August 4, 2006 February 4, 2008
Moderate Geomagnetic 10<Ap<50	March 9, 18, 2005 May 13, 2005 January 26, 2006	August 7, 2006 March 13, 16, 2007 April 28, 2007
Active Geomagnetic Ap ≥ 50	November 9, 2004	September 11, 2005

2.8 Effect of Unmodeled High Frequency Density Variations

The orbits are propagated using density data from the following sources: accelerometer derived density, POE derived density, HASDM, and the Jacchia-71 density model. The orbit is propagated for a 24 hour period using a fourth order Runge-Kutta integration process (integrator step size of ten seconds) and includes only earth central body and oblateness (J2) and atmospheric drag in the force models. The initial POE data sets are fourteen hour solution spans, but the data sets used in this work are 24 hour spans that are extracted from seven day continuous solutions. These seven day data sets are stitched together from the fourteen hour solution spans using the linear weighted blending technique which is described in References 64 and 65. The accelerometer and HASDM densities are also extracted from larger continuous data sets. A position and velocity vector is taken from the POE solutions and used to initialize the integration.

The accelerometer derived density data is considered truth and therefore the other densities (POE, HASDM, and Jacchia-71) are normalized to the same mean as the accelerometer densities. This can be done because the primary concern of this work is the effect of temporal variations on the orbit propagation and not on the bias between the different densities. The normalization is carried out via the following equation:

$$\rho_{Normalized} = \left(\frac{Mean(\rho_{Acc})}{Mean(\rho)} \right) * \rho \qquad 2.8$$

In Equation 2.8 ρ refers to either of the three density data sets other than the accelerometer densities (POE, HASDM, or Jacchia 71). The results are analyzed by calculating both the RMS and the maximum difference between the different orbit positions. The RMS values are calculated using Equation 2.9. In this equation $\left|\overrightarrow{r_{i,ACC}}\right|$ is the magnitude of the propagated

position vector using the accelerometer data and $\left|\vec{r}_i\right|$ is the magnitude of the propagated position vector using any of the other three density sources (POE, HASDM, or Jacchia 71). The summation variable n refers to the number of data points (time steps).

$$RMS = \sqrt{\frac{\sum_{i=1}^{n}\left(\left|\overrightarrow{r_{i,ACC}}\right| - \left|\vec{r}_i\right|\right)}{n}} \qquad 2.9$$

2.9 Ephemeris Noise

The raw ephemeris file, which is downloaded from the GFZ Potsdam website is first converted into a NAVSOL file format for input into the orbit determination scheme in Orbit Determination Tool Kit (ODTK). Different levels of noise are then added to the NAVSOL file before it is input into ODTK via Equation 2.10 where '*var*' is the variance associated with the desired error level and '*randn*' refers to the Matlab function which returns a pseudo-random number drawn from a normal distribution with zero mean and a standard deviation of one.

$$pos\_new = pos\_old + (\sqrt{\text{var}} * randn) \qquad 2.10$$

The orbit determination scheme is then carried out as many times as needed with the only difference between the runs being the different noise levels added to the input NAVSOL file. The initial position vector input into the orbit determination scheme as well as the orbit uncertainty values for the cross-track, in-track, and radial directions are updated in-between each run to reflect the added noise. As mentioned previously the input density and ballistic coefficient Gauss-Markov correlated half-lives are set for 180 minutes and 1.8 minutes respectively. However, no research has been done to determine which combination of correlated half-lives yields

the best performing density estimates when compared to accelerometer derived densities. The values used in this work were chosen because results were found in previous research showing that this combination of correlated half-lives generally produced the best results when the original ephemeris file (with no noise added) was used.

There were a number of checks performed during this portion of the research in order to ensure that the correct level of noise was added and also that the measurement residuals were reasonable. Firstly, in order to confirm what levels of noise were being added, the newly created noisy ephemeris files were compared to the original ephemeris file by differencing the positions (See Figure 2.1).

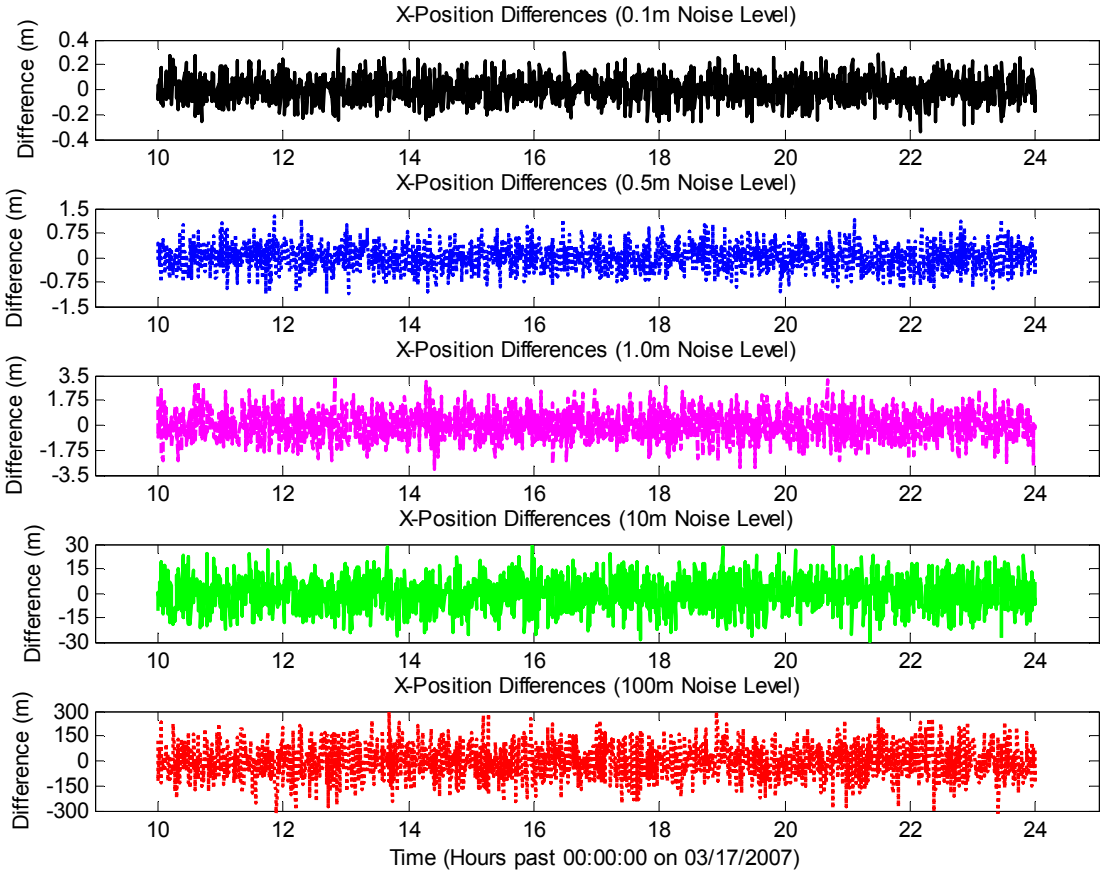

Figure 2.1 – X-position differences for CHAMP on 03/17/2007.

Only the differences between the x components of position are shown here as the y and z component differences are nearly identical with regards to magnitude. From Figure 2.1 the noise levels in the ephemeris files are as expected. RMS values were also calculated for these x position differences between the noisy ephemeris files and the original ephemeris file and can be seen in Table 2.5. These RMS values should be close to the expected noise level, which they are.

Table 2.5 – Noise levels and associated x position RMS values.

Noise Level (m)	Ephemeris RMS (m)
0.1	0.10
0.5	0.39
1	0.99
10	9.89
100	100.13

Another check that was performed to ensure the validity of this work was to examine the plot of the measurement residuals and make sure that there weren't a significant number of measurements being thrown out. Figures 2.2 - 2.4 contain the residuals plot for CHAMP during the day of March 17, 2007. Figure 2.2 is the residuals plot with the original ephemeris file with no noise added. The residuals are well within the sigma bounds. Examining Figure 2.3 it can be seen that the residuals for the 1 m noise case are larger than the no noise case, which is expected, but they are still within the sigma bounds for the most part and ODTK is disregarding a very small number of the measurements. The residuals are even larger in Figure 2.4 which shows the 100 m noise level case. This is also expected but the important aspect to notice is that the vast majority of the measurements are still within the sigma bounds. This should be the case as the sigma bounds based on measurement noise were specified as user input into ODTK.

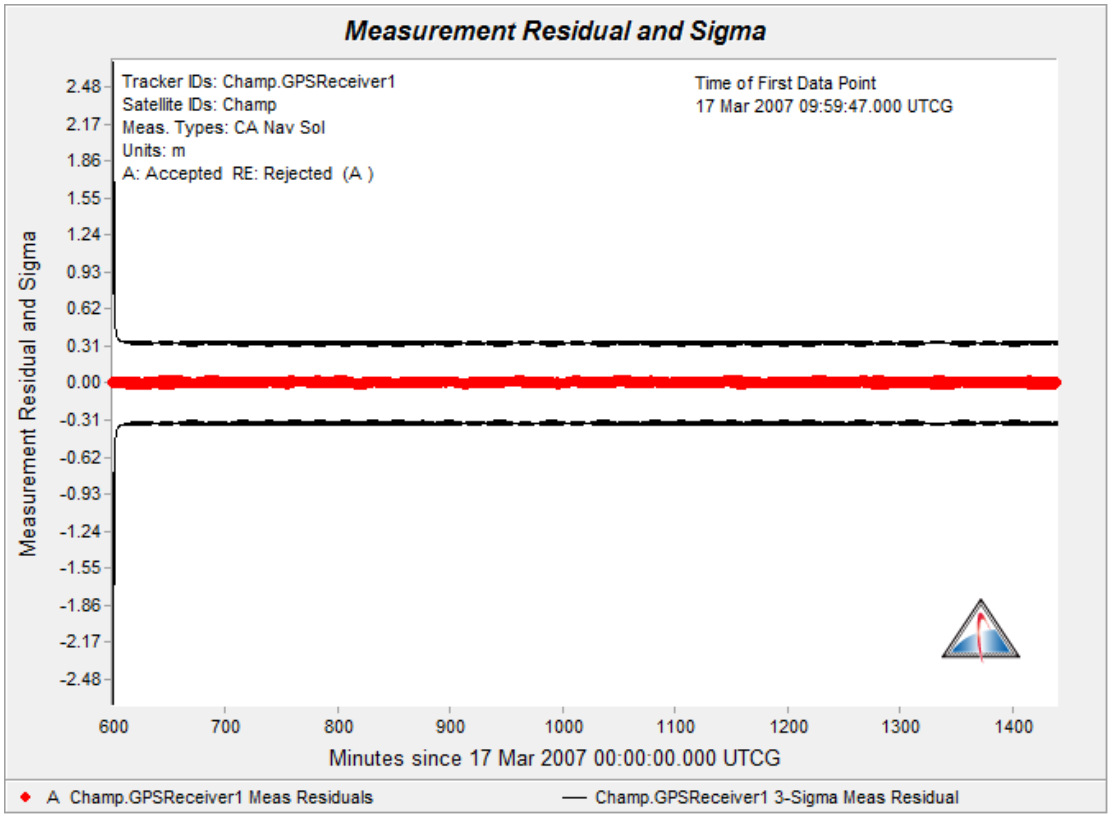

Figure 2.2 – Measurement residuals for CHAMP on 03/17/2007 (No Noise).

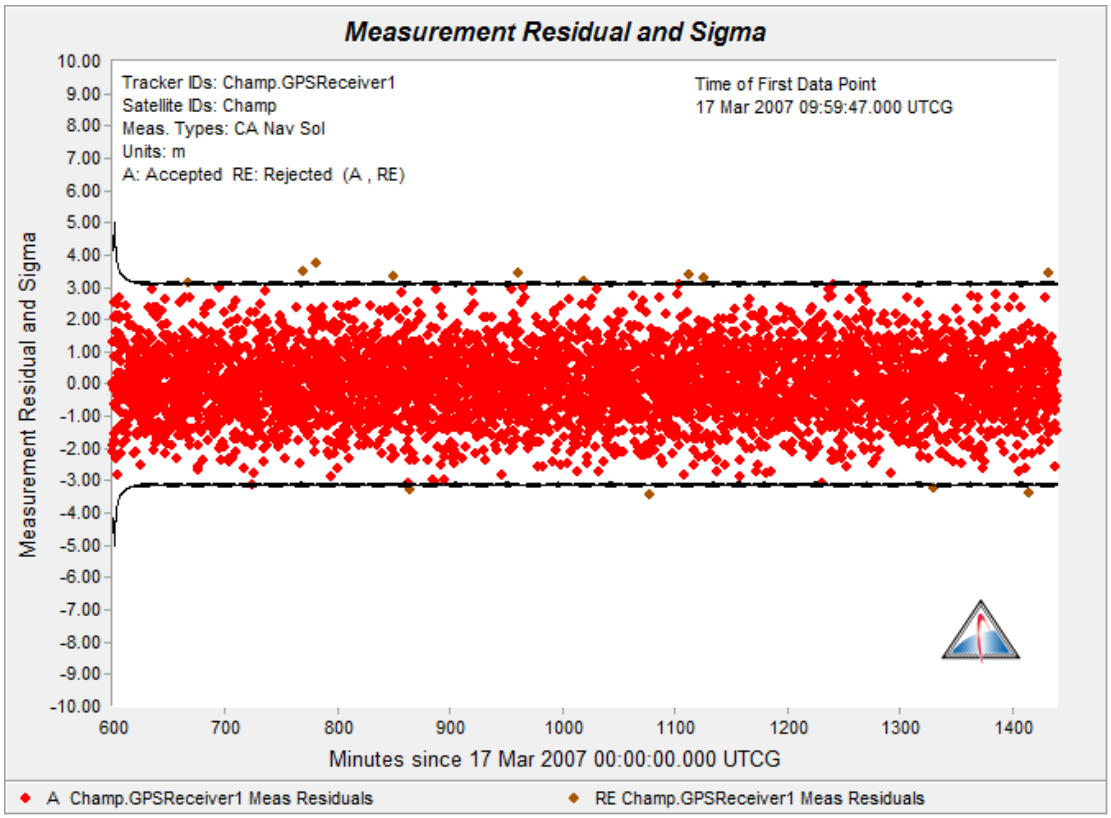

Figure 2.3 – Measurement residuals for CHAMP on 03/17/2007 (1 m Noise).

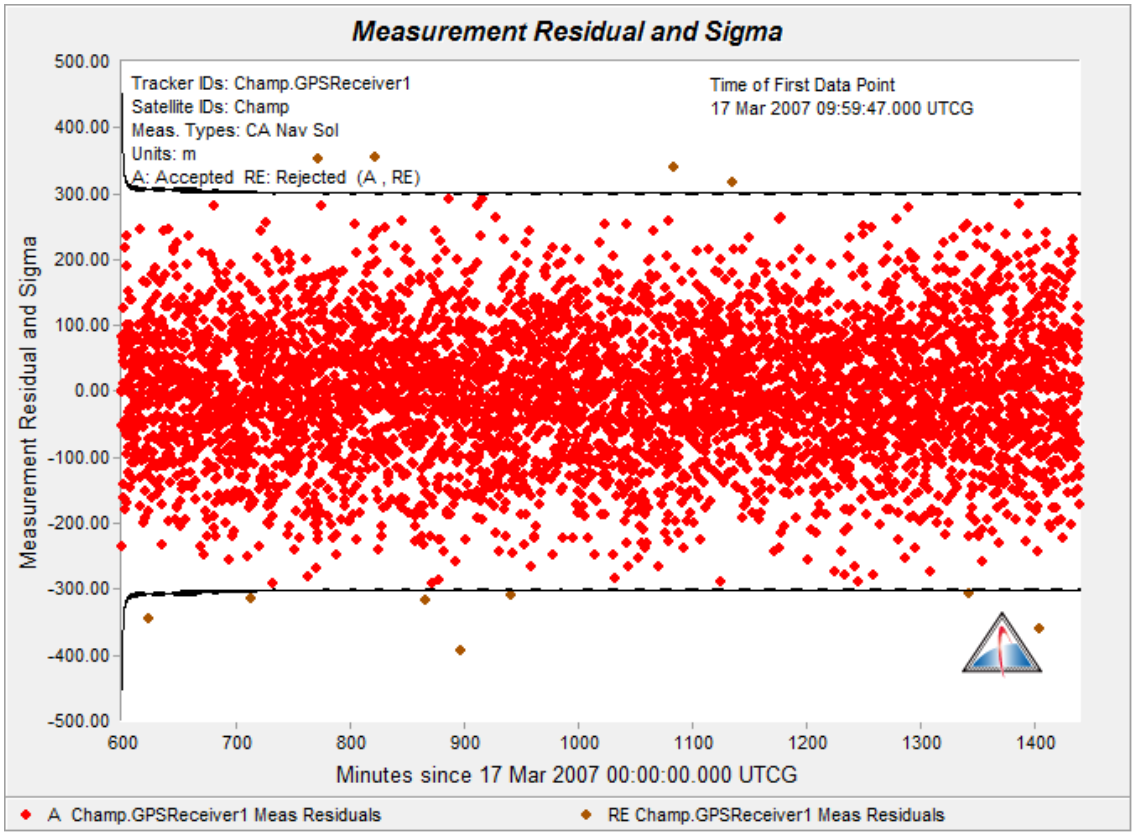

Figure 2.4 – Measurement residuals for CHAMP on 03/17/2007 (100 m Noise).

3 EFFECT OF MODELING HIGH FREQUENCY DENSITY VARIATIONS

Results have shown in the plots of the atmospheric density for both CHAMP and GRACE satellites that there are high frequency variations in the accelerometer derived density that are not seen in the Jacchia family of density models, the High Accuracy Satellite Drag Model (HASDM), or the Precise Orbit Ephemeris (POE) derived density estimates. These high frequency density variations observed in the density data derived from the on-board accelerometers are typically small in magnitude compared to the overall day-night variation. However during certain time periods, such as when the satellite is near the terminator, the variations can be on the same order of magnitude as the diurnal variations. These variations can also be especially prevalent during geomagnetic storms (travelling atmospheric disturbances) and near the polar cusps. This work will simulate the error in orbit propagation caused by these high frequency density variations and determine the significance of this error. The propagation errors are also binned by geomagnetic and solar activity levels.

3.1 Results

In order to examine the effects of the small frequency density variations on the accuracy of orbit propagation both the density values and the position error in the orbit propagation are plotted. The density values plotted are those from the raw density files, not the normalized values. This was done in order to better observe the differences in the different density sources. Also, the position error that is shown in the plots is the magnitude of the vector difference between the vector obtained from the accelerometer density and that obtained from the other source (POE, HASDM, or Jacchia 71).

Normal Day: Figure 3.1 shows the density values and propagation errors for CHAMP for a normal day. The results from examining the plot comparing the propagation errors between the density sources show that the POE derived densities provide better accuracy than HASDM or Jacchia 71. The maximum error seen in the propagation using the POE derived densities is 13 m which is not significant for most applications.

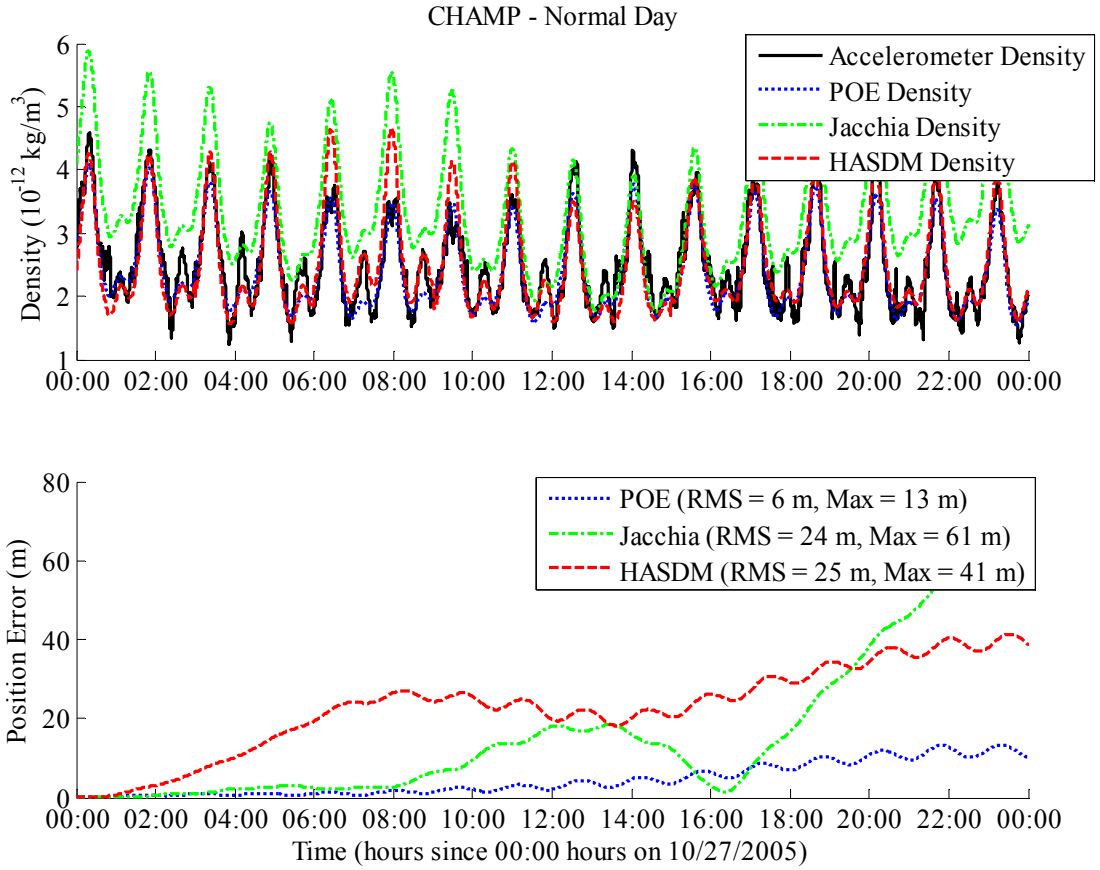

Figure 3.1 – Comparison of different density sources for CHAMP on 10/27/2005.

Orbit Plane Near the Terminator: Figure 3.2 shows the density values and propagation errors for CHAMP on a day when the orbit plane is near the terminator. During the time period when the satellite's orbit plane is near the terminator the high frequency density variations observed only in the accelerometer data can be on the same order of magnitude as the day-night

density variations caused by the satellite passing from daylight into darkness and back. This happens because the satellite never travels into full darkness or full daylight and therefore the normal density variations are of much lower magnitude. The lower overall magnitude of the density variations can be seen in Figure 3.2 where the high frequency variations are much closer to the same magnitude as the normal variations as opposed to Figure 3.1. In the lower part of the figure below the results show that the POE derived densities still provided the best propagation accuracy with a maximum error of 4 m.

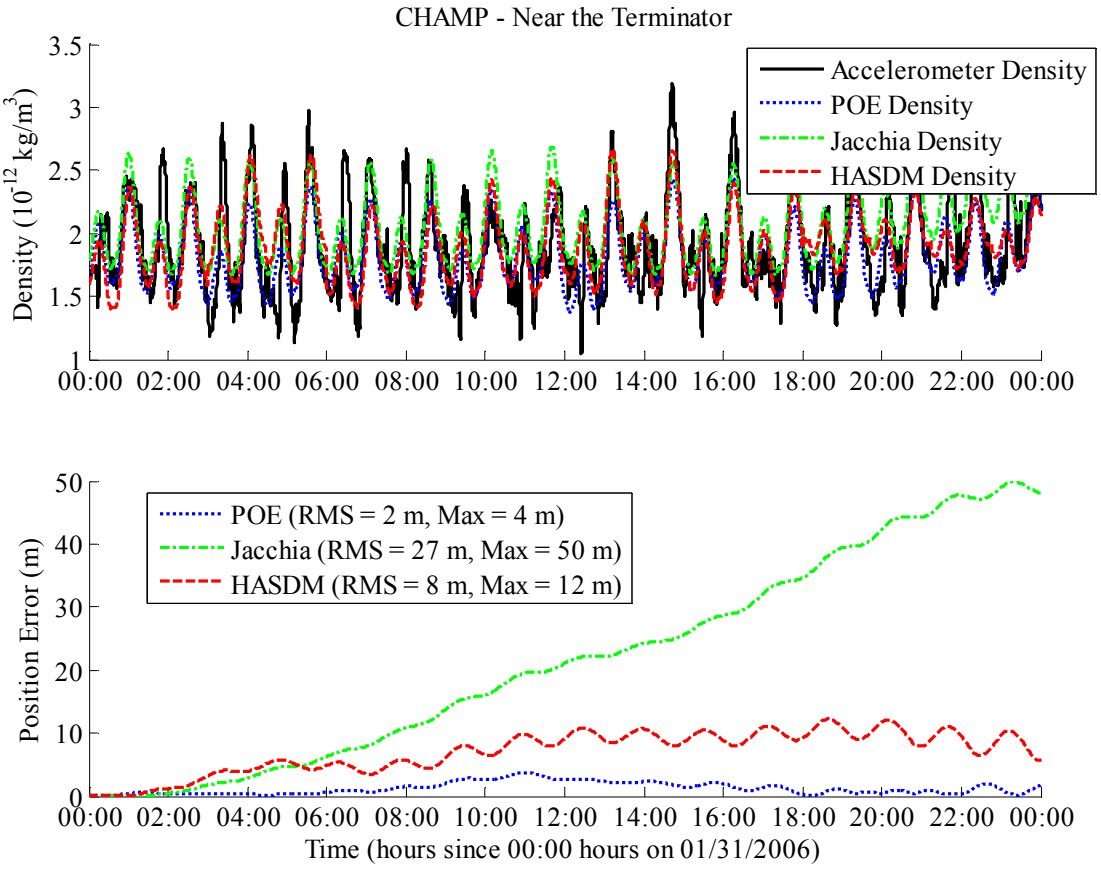

Figure 3.2– Comparison of different density sources for CHAMP on 01/31/2006.

Geomagnetic Cusp Density Enhancement: There are density enhancements occurring around the polar cusp which have been observed by the accelerometer on-board CHAMP. These density enhancements are observed as spikes in atmospheric density that occur on both sides of the magnetic pole. Figure 3.3 shows the density values and propagation errors for CHAMP on a day which geomagnetic cusp enhancements were observed. With the exception of a small spike in the accelerometer density there are no extreme differences between the density sources and the propagation errors are still low with the POE derived densities providing the most accurate propagation with a max error of 9 m.

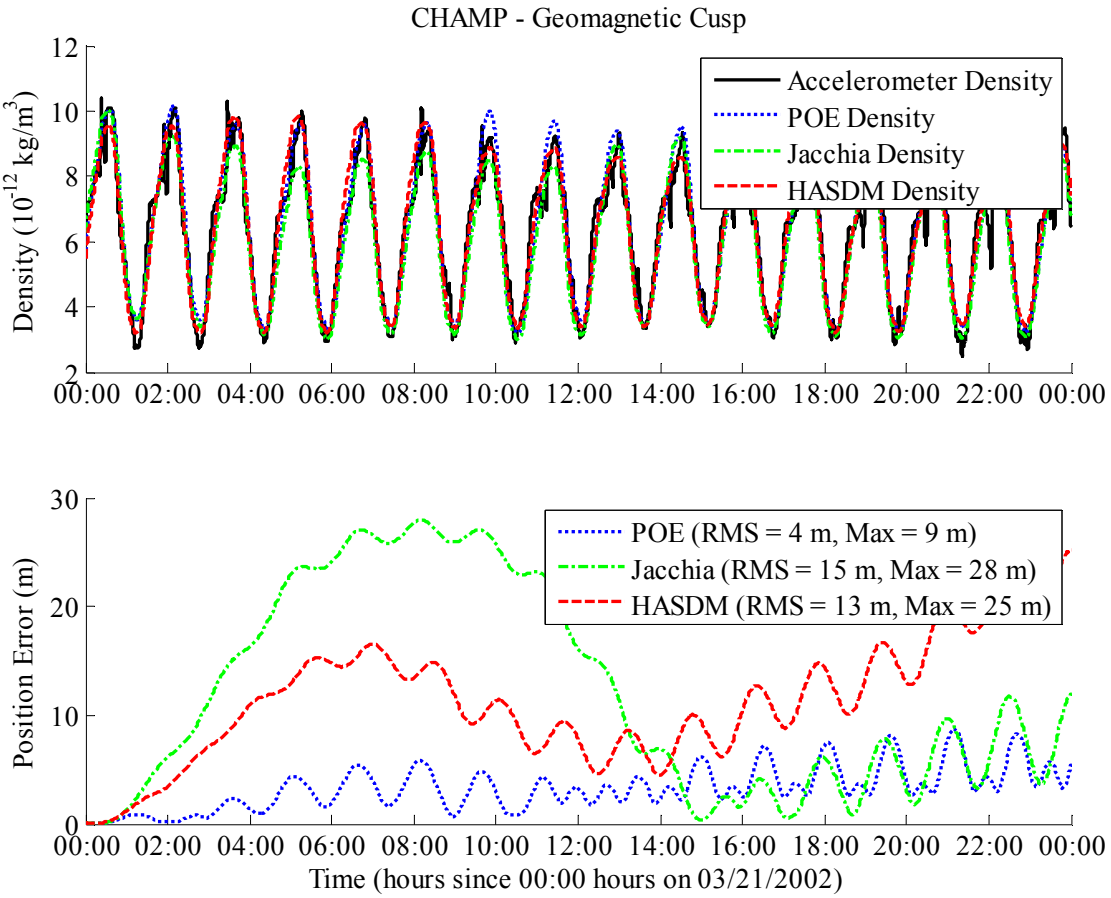

Figure 3.3– Comparison of different density sources for CHAMP on 03/21/2002.

Travelling Atmospheric Disturbance: A travelling atmospheric disturbance (TAD) is an increase in atmospheric density caused by geomagnetic activity that starts at high latitudes and propagates toward the equator. This process results in constructive interference near the equator where the two waves propagating from opposing poles interact. For more information about TAD's see Reference 37. Figure 3.4 shows the density values and propagation errors for CHAMP during a day on which a TAD was observed. The TAD occurs between 1100 and 1500 UTC on 4/19/2002 and the resulting density enhancements can be observed in the figure in the accelerometer density data. There is an interesting trend in the Jacchia 71 propagation error as it shifts direction at the time of the TAD. The results clearly show that the high frequency variations observed only in the accelerometer data do not have a major effect on orbit propagation as evident in the propagation errors still being relatively small with the POE again providing the highest accuracy and a maximum error of 22 m.

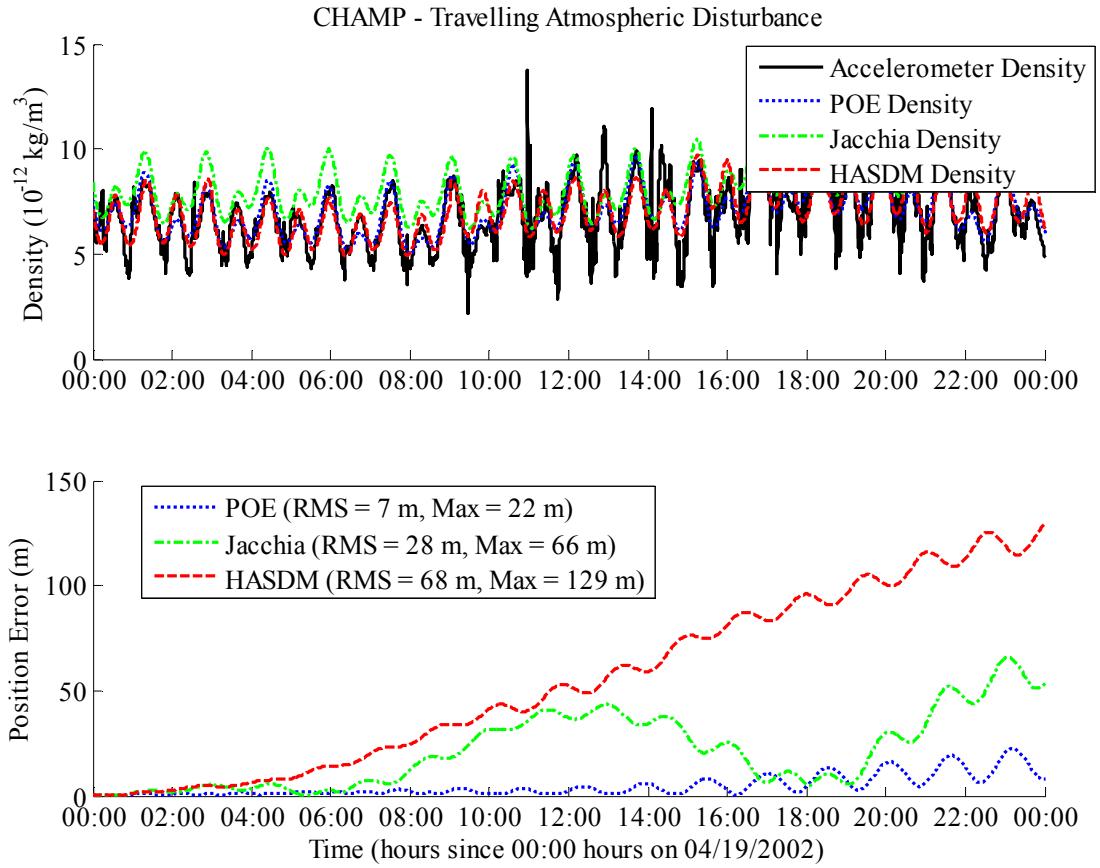

Figure 3.4– Comparison of different density sources for CHAMP on 04/19/2002.

Normal Day (GRACE): Figure 3.5 shows the density values and propagation errors for GRACE for a normal day. Since GRACE is at a higher altitude than CHAMP the resulting densities are about an order of magnitude lower than CHAMP. This also causes the orbit propagation errors to be much lower for GRACE than for CHAMP. As can be seen from the figure all of the orbit propagation errors are less than 10 m with the POE providing the highest accuracy with a maximum error of less than 1 m. The results from the top portion of the figure show that the Jacchia 71 model would have extremely high errors because of the observed bias between it and the other density sources. This is not the case because as stated earlier these propagation errors are for densities that have been normalized to the same mean and not the errors for the density values shown.

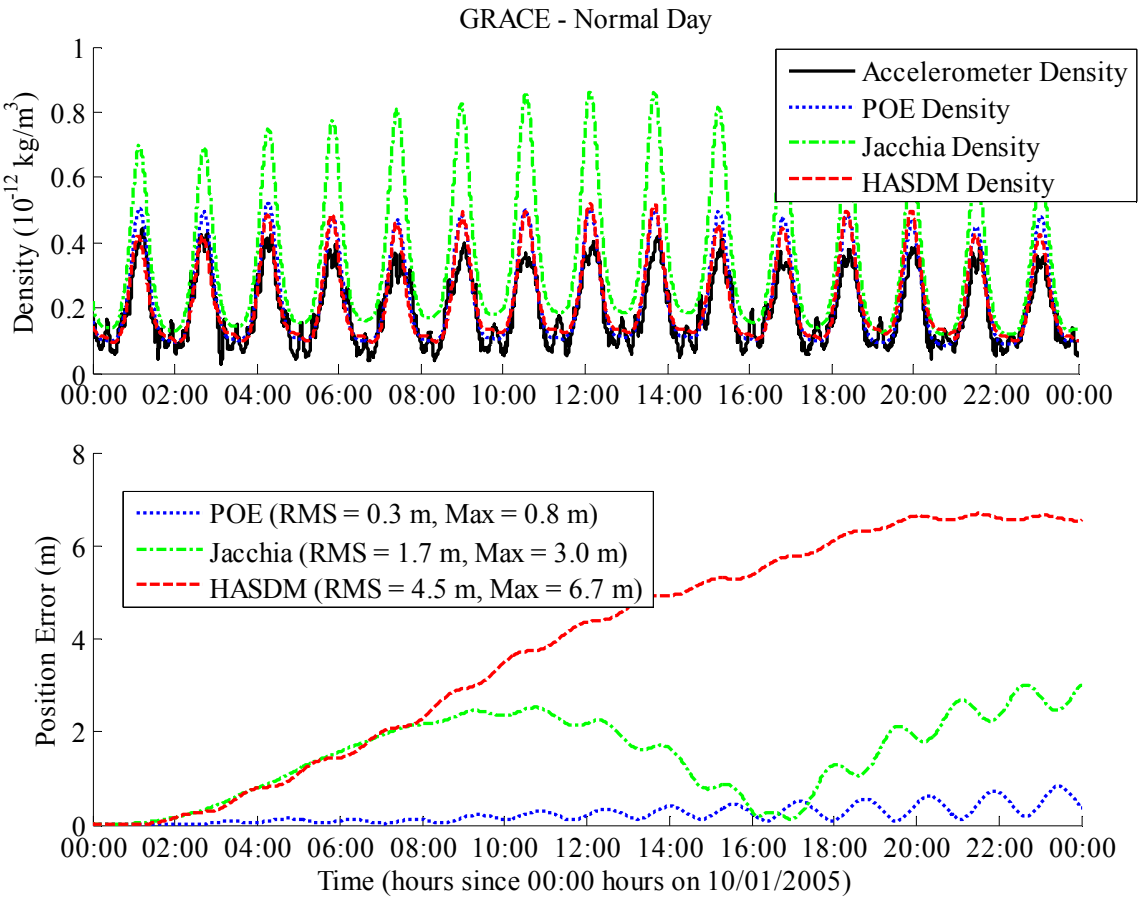

Figure 3.5– Comparison of different density sources for GRACE on 10/01/2005.

Orbit Plane near the Terminator (GRACE): Figure 3.6 shows the density values and propagation errors for GRACE on a day when the orbit plane is near the terminator. The effects of the satellite orbit plane being near the terminator are more easily seen in this example rather than Figure 3.2 due to the difference in altitude. Even though these high frequency density variations seen only in the accelerometer data are more apparent the propagation errors are still low. In the lower part of the figure below the results show that the POE derived densities and the HASDM densities performed best with maximum propagation errors of around 1 m while the maximum propagation error for the Jacchia density model had was around 19 m.

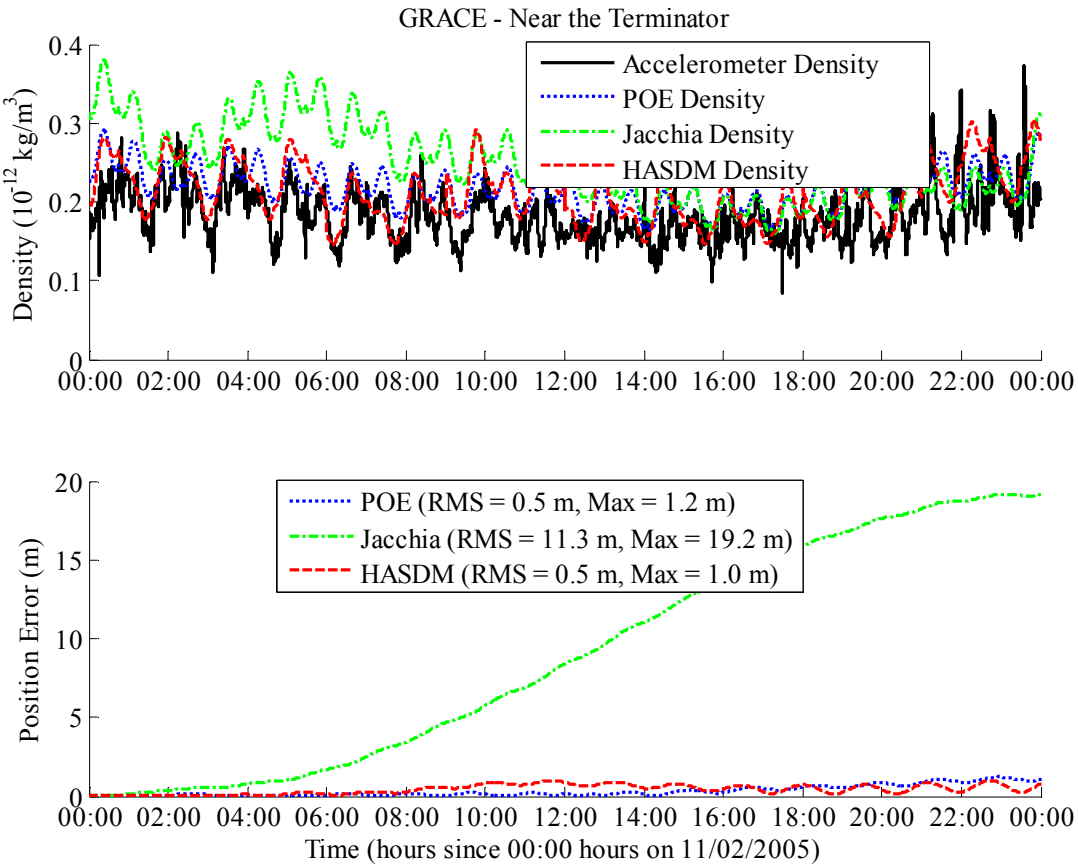

Figure 3.6– Comparison of different density sources for GRACE on 11/02/2005.

Other days are also examined from Tables 2.2 - 2.4 for CHAMP and GRACE and binned according to solar and geomagnetic activity level. The resulting RMS and maximum difference values for CHAMP are seen in Tables 3.1 -3.4.

Table 3.1 – Average RMS values (m) by solar activity level for CHAMP.

Density Source	Low Solar	Moderate Solar	Elevated Solar	High Solar
POE	6.75	6.52	7.38	11.27
Jacchia-71	39.94	54.01	79.54	87.33
HASDM	14.90	18.67	23.79	22.50

Table 3.2 – Average RMS values (m) by geomagnetic activity level for CHAMP.

Density Source	Quiet Geomagnetic	Moderate Geomagnetic	Active Geomagnetic
POE	6.15	7.79	14.58
Jacchia-71	51.26	52.83	136.52
HASDM	16.66	19.84	35.97

Table 3.3 – Average maximum difference values (m) by solar activity level for CHAMP.

Density Source	Low Solar	Moderate Solar	Elevated Solar	High Solar
POE	13.06	13.04	15.29	24.74
Jacchia-71	65.89	89.26	142.30	169.26
HASDM	26.18	31.97	44.00	42.48

Table 3.4 – Average maximum difference values (m) by geomagnetic activity level for CHAMP.

Density Source	Quiet Geomagnetic	Moderate Geomagnetic	Active Geomagnetic
POE	12.49	15.26	31.12
Jacchia-71	84.50	90.54	270.81
HASDM	29.30	34.74	68.27

The results shown in Tables 3.1-3.4 reveal that generally the RMS values and the maximum difference values increase with an increase in either solar or geomagnetic activity level which is expected. Typically the only exception to this trend is going from the low solar activity bin to the moderate solar activity bin for the propagations using POE derived density data. In this case both the RMS value and maximum difference value decrease a small amount when going from low to moderate solar activity. This is likely due to the amount of days differing in each of the bins and because geomagnetic and solar activity can't be separated. The

results also show that the propagations utilizing POE derived densities perform better than those using either Jacchia or HASDM when compared with the propagation using accelerometer derived densities in every solar and geomagnetic activity bin. Table 3.5 shows the total average RMS and maximum difference values for CHAMP.

Table 3.5 – Total average RMS and maximum difference values (m) for CHAMP.

Density Source	RMS	Maximum Difference
POE	7.12	14.44
Jacchia-71	56.79	97.58
HASDM	18.94	33.38

These total RMS and maximum difference average values also show that orbit propagations using POE derived densities as input more closely compare to those using accelerometer derived densities as input than do the other two sources of density data. Figure 3.7 shows the RMS and maximum difference values for all days analyzed for CHAMP.

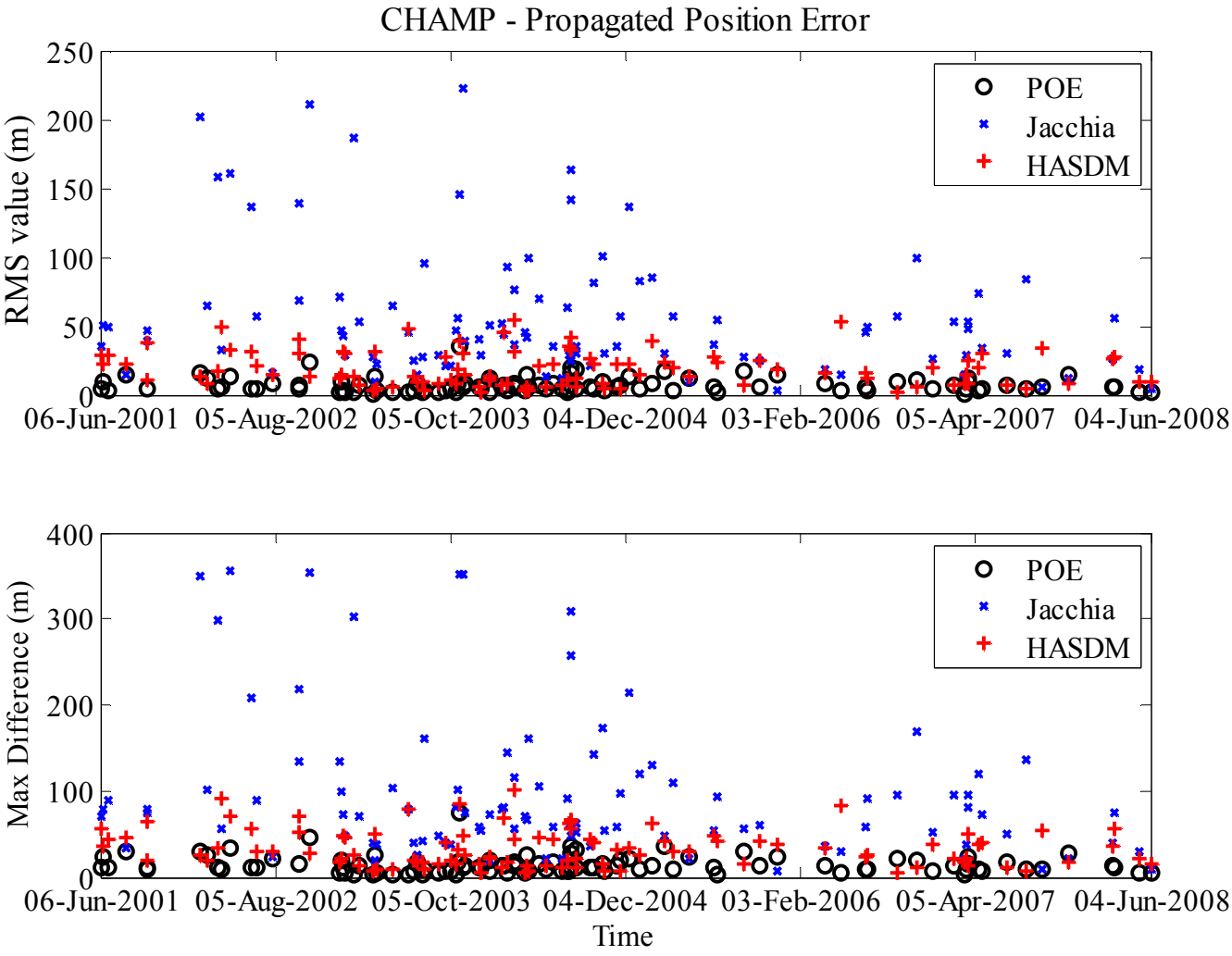

Figure 3.7– Comparison of different density sources for CHAMP (all days)

The data shown in Figure 3.7 agrees with Tables 3.1-3.5 with regards to which source of density used in orbit propagation corresponds most closely with orbit propagation using accelerometer derived densities as input. The results clearly show that the POE density data outperforms the Jacchia and HASDM density data for most of the days examined for CHAMP. The resulting RMS and maximum difference values for GRACE are seen in Tables 3.6 -3.9. As mentioned previously there is no data available for GRACE corresponding to elevated and high

solar activity levels therefore only the lower two solar activity bins are examined as can be seen from Tables 3.6 and 3.8.

Table 3.6 – Average RMS values (m) by solar activity level for GRACE

Density Source	Low Solar	Moderate Solar	Elevated Solar	High Solar
POE	2.05	2.88	NA	NA
Jacchia-71	8.73	19.93	NA	NA
HASDM	2.83	4.63	NA	NA

Table 3.7 – Average RMS values (m) by geomagnetic activity level for GRACE

Density Source	Quiet Geomagnetic	Moderate Geomagnetic	Active Geomagnetic
POE	1.65	1.23	12.28
Jacchia-71	6.06	13.97	76.97
HASDM	3.21	4.17	7.97

Table 3.8 – Average maximum difference values (m) by solar activity level for GRACE

Density Source	Low Solar	Moderate Solar	Elevated Solar	High Solar
POE	4.14	5.31	NA	NA
Jacchia-71	14.68	34.77	NA	NA
HASDM	4.90	8.40	NA	NA

Table 3.9 – Average maximum difference values (m) by geomagnetic activity level for GRACE

Density Source	Quiet Geomagnetic	Moderate Geomagnetic	Active Geomagnetic
POE	3.48	2.59	19.69
Jacchia-71	10.69	22.45	140.60
HASDM	5.85	6.59	17.03

The results seen in Tables 3.6-3.9 reveal that generally the RMS values and the maximum difference values increase with an increase in either solar or geomagnetic activity level which is expected. For GRACE the only exception to this trend is going from the quiet geomagnetic activity bin to the moderate geomagnetic activity bin for the propagations using POE derived density data. In this case both the RMS value and maximum difference value decrease a small amount when going from low to moderate solar activity. This is likely due to the amount of days differing in each of the bins and because geomagnetic and solar activity can't be separated. The results also show that the propagations utilizing POE derived densities perform better than those using either Jacchia or HASDM when compared with the propagation using accelerometer derived densities in every solar and geomagnetic activity bin except the active geomagnetic bin. Table 3.10 shows the total average RMS and maximum difference values for GRACE.

Table 3.10 – Total average RMS and maximum difference values (m) for GRACE.

Density Source	RMS	Maximum Difference
POE	2.51	4.69
Jacchia-71	15.83	27.54
HASDM	4.03	7.20

These total RMS and maximum difference average values also show that orbit propagation using POE derived densities as input more closely compare to those using accelerometer derived densities as input than do the other two sources of density data. Figure 3.8 shows the RMS and maximum difference values for all days analyzed for GRACE. The results seen from this figure indicate that in general the POE density data outperforms both Jacchia and HASDM densities when used as input in an orbit propagator and compared to accelerometer derived density data.

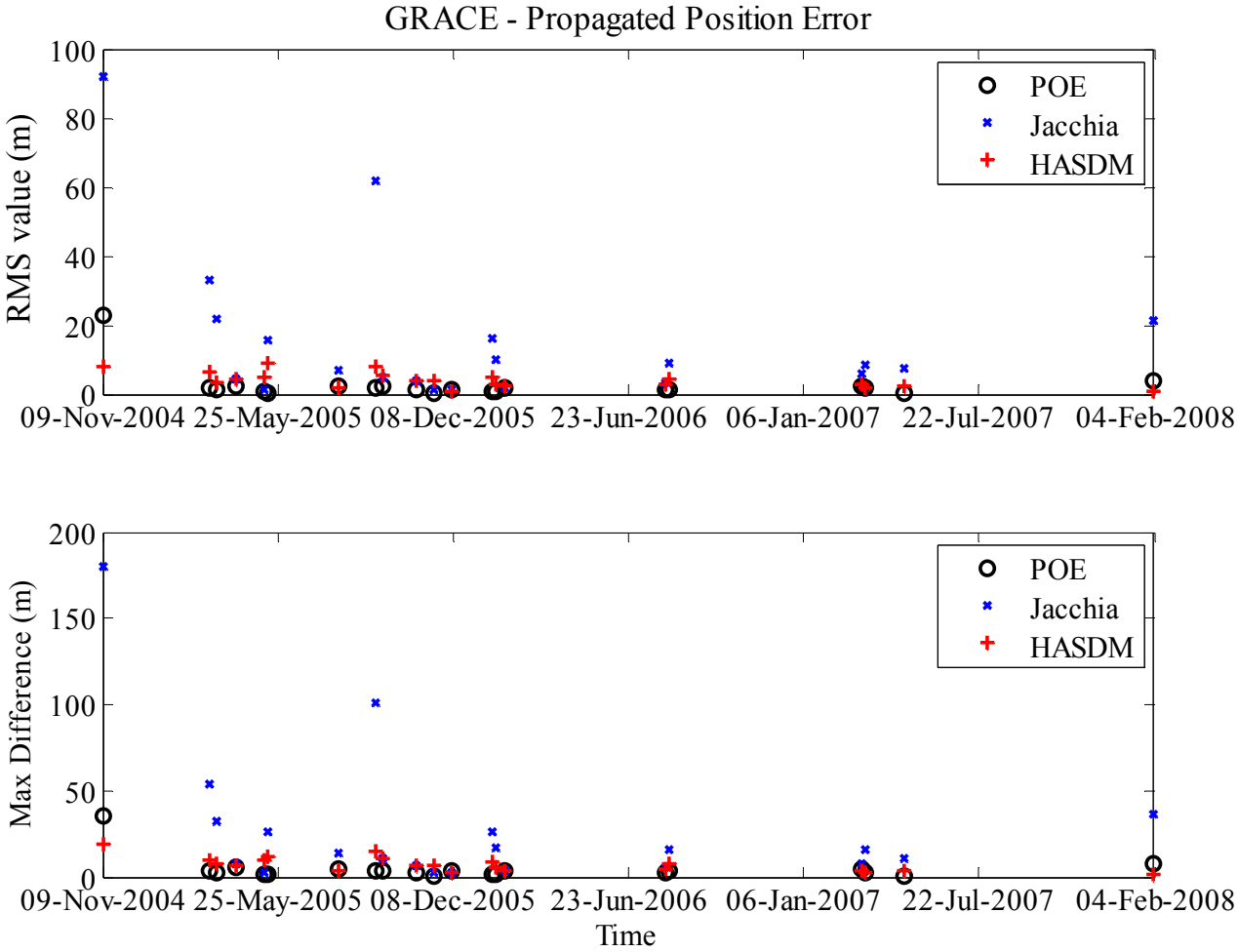

Figure 3.8– Comparison of different density sources for GRACE (all days)

3.2 Summary

The effect of high frequency atmospheric density variations on orbit propagation has been examined. These high frequency variations are observed in the accelerometer-derived density data from the CHAMP and GRACE satellite but not seen in other density sources such as Jacchia 71, HASDM, and POE-derived densities. During certain time periods (TAD, geomagnetic cusp, orbit plane near the terminator) these high frequency variations are on the same order of magnitude as the day-night variations. In order to see how these unmodeled variations might affect orbit propagation each of the density sources (Accelerometer, Jacchia 71, HASDM, and POE) was used as an input measurement into an orbit propagator for both the CHAMP and GRACE satellites. The results were then compared to those of the accelerometer data in order to see the effect. These results showed that not modeling these high frequency density variations seen in the accelerometer data is acceptable for most applications. The maximum difference between the orbits propagated using POE derived densities and those propagated using accelerometer derived densities were around 12 m to 32 m for CHAMP and ranged from around 2 m to 20 m for GRACE. The RMS between the orbits propagated using POE derived densities and those propagated using the accelerometer derived densities ranged from around 6 m to 15 m for CHAMP and from 1 m to 12 m for GRACE. Since this error is not significant for most applications not modeling high frequency variations is acceptable in most orbit analysis. Another result was that the propagation that used the POE derived densities performed much better with respect to the accelerometer data than did the other density models (Jacchia 71 and HASDM) for all cases except for GRACE during active geomagnetic time periods.

Also, the results obtained through binning the days by solar and geomagnetic activity showed that the errors generally grew with an increase in solar and geomagnetic activity as expected. For CHAMP the RMS between the POE results and the accelerometer results went from about 7 m to 11 m when going from low solar activity level to high solar activity level and from about 6 m to 15 m when going from quiet geomagnetic activity level to active geomagnetic activity level. For GRACE the RMS between the POE results and the accelerometer results went from about 2 m to 3 m when going from low solar activity level to moderate solar activity level and from about 2 m to 12 m when going from quiet geomagnetic activity level to active geomagnetic activity level. The effect of solar and geomagnetic activity level was not seen as much in the GRACE data as the CHAMP data because the propagation errors with the GRACE satellite are generally on a smaller scale than those of the CHAMP satellite.

4 EFFECTS OF EPHEMERIS NOISE ON POE-DERIVED DENSITY ESTIMATES

The primary input in the orbit determination scheme used to develop the POE-derived density estimates is a precision orbit ephemeris file. This file contains position and velocity information for the satellite based on GPS and SLR measurements. Since these files contain estimated values there will be some level of error associated with them, generally thought to be around the 5 - 10cm level [Ref. 77 - 80]. However, examining how different magnitudes of errors in the input ephemeris file can affect the POE-derived density estimates can be useful. In order to see these effects Gaussian white noise is added to the ephemeris file as it is converted into the desired format for input into the orbit propagation scheme. Different levels of noise are added in order to see how different levels of error change the POE-derived density results. The cross correlation and RMS values are calculated for each of the days shown in Tables 2.2 - 2.4 for both CHAMP and GRACE and were binned by solar and geomagnetic activity level. The white noise sigma value of the observations within ODTK is also updated with each different noise level and is set equal to the noise level itself. These noise levels can be seen in Table 4.1 below.

Table 4.1 – Noise levels, associated variances, and input ODTK orbit uncertainty sigma values.

Noise Level (m)	Variance (m^2)	Orbit Uncertainty (Radial - m)	Orbit Uncertainty (In-Track - m)	Orbit Uncertainty (Cross-Track - m)
0.1	0.01	0.25	0.3	0.2
0.5	0.25	0.5	0.6	0.4
1	1	1.1	1.2	1
10	100	11	12	10
100	10000	110	120	100

4.1 Results

When looking at the POE derived density values for a single day the results show that the error associated with each of the different noise levels when compared to the no noise control case contains some level of randomness. The lowest noise level does not appear to have the lowest error and vice versa. Figure 4.1 below shows the POE derived density estimates for each of the noise levels compared with the no noise case for the CHAMP satellite during the day of March 17, 2007, which is a day of low solar and quiet geomagnetic activity.

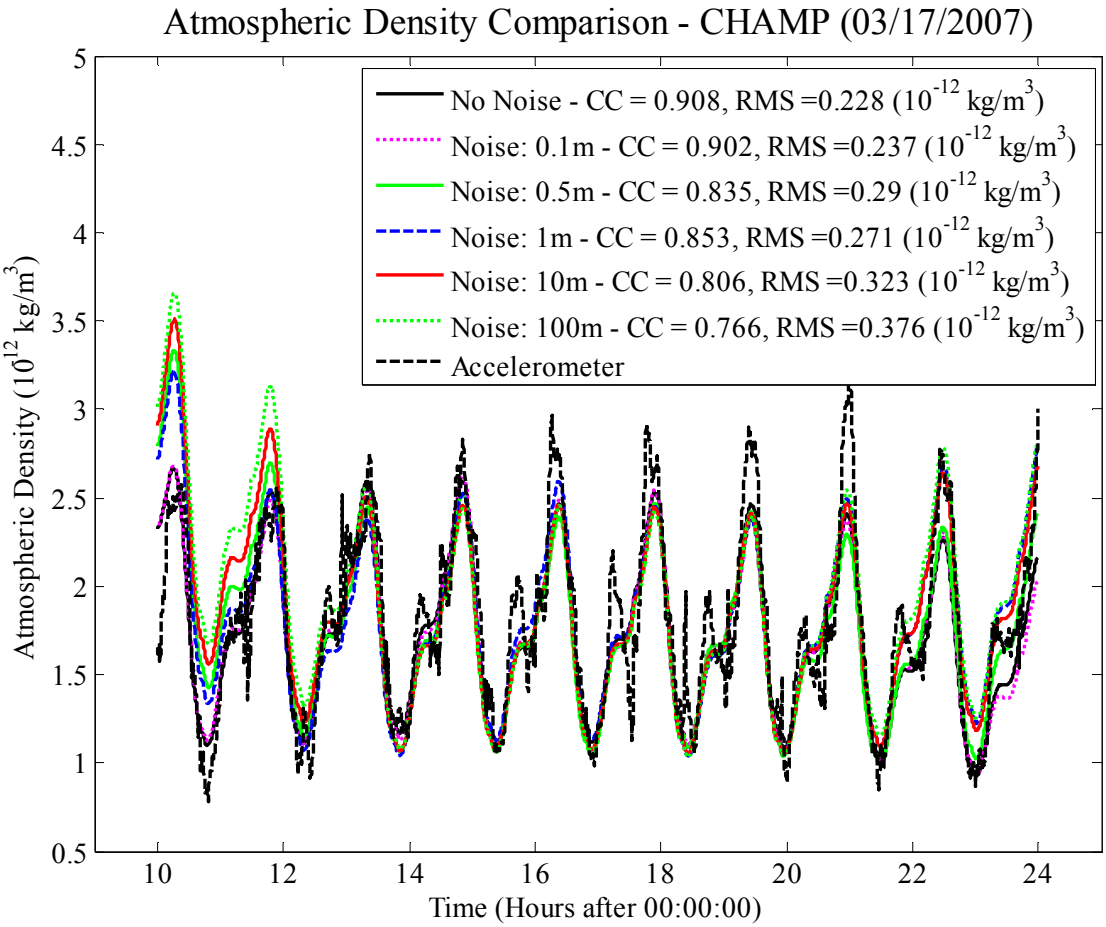

Figure 4.1 – Atmospheric Density Comparison for CHAMP on 03/17/2007.

This randomness is expected to some degree, especially in the case of the smaller noise levels, due to the method in which the noise was added to the raw ephemeris file. In general the results for this day show a trend of decreasing CC value and increasing RMS value as the noise level is increased (with the exception being between the 0.5 m and 1 m noise level cases), which is expected. Figure 4.2 shows the comparison of POE derived density estimates for the different noise levels during the day of January 23, 2003, which is a day of moderate solar and moderate geomagnetic activity.

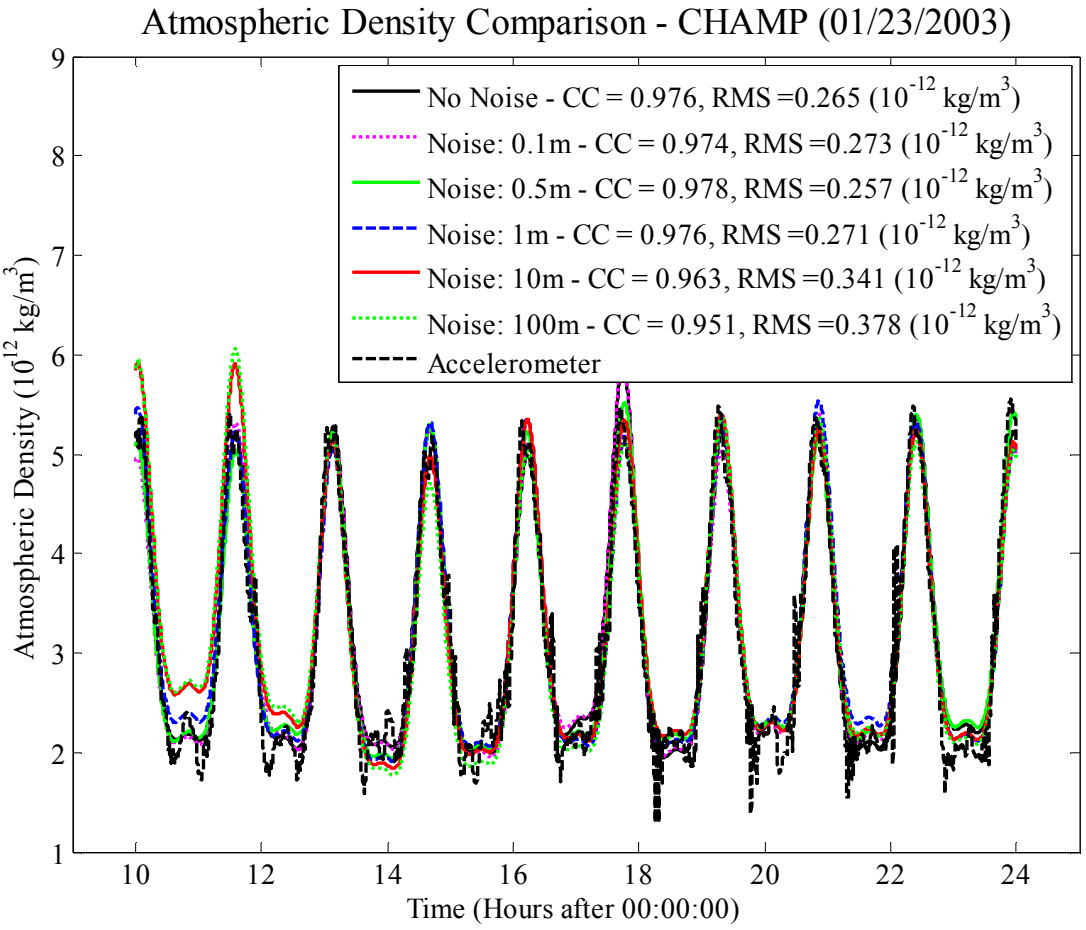

Figure 4.2 – Atmospheric Density Comparison for CHAMP on 01/23/2003.

A trend can be observed in Figure 4.2 similar to that of Figure 4.1. In general, as the noise level is increased the CC value decreases and the RMS value increases which is expected. However this is not the case every time due to the randomness of the added noise. Figure 4.3 below shows the comparison of POE derived density estimates for the different noise levels during the day of October 04, 2002, which is a day of elevated solar and active geomagnetic activity.

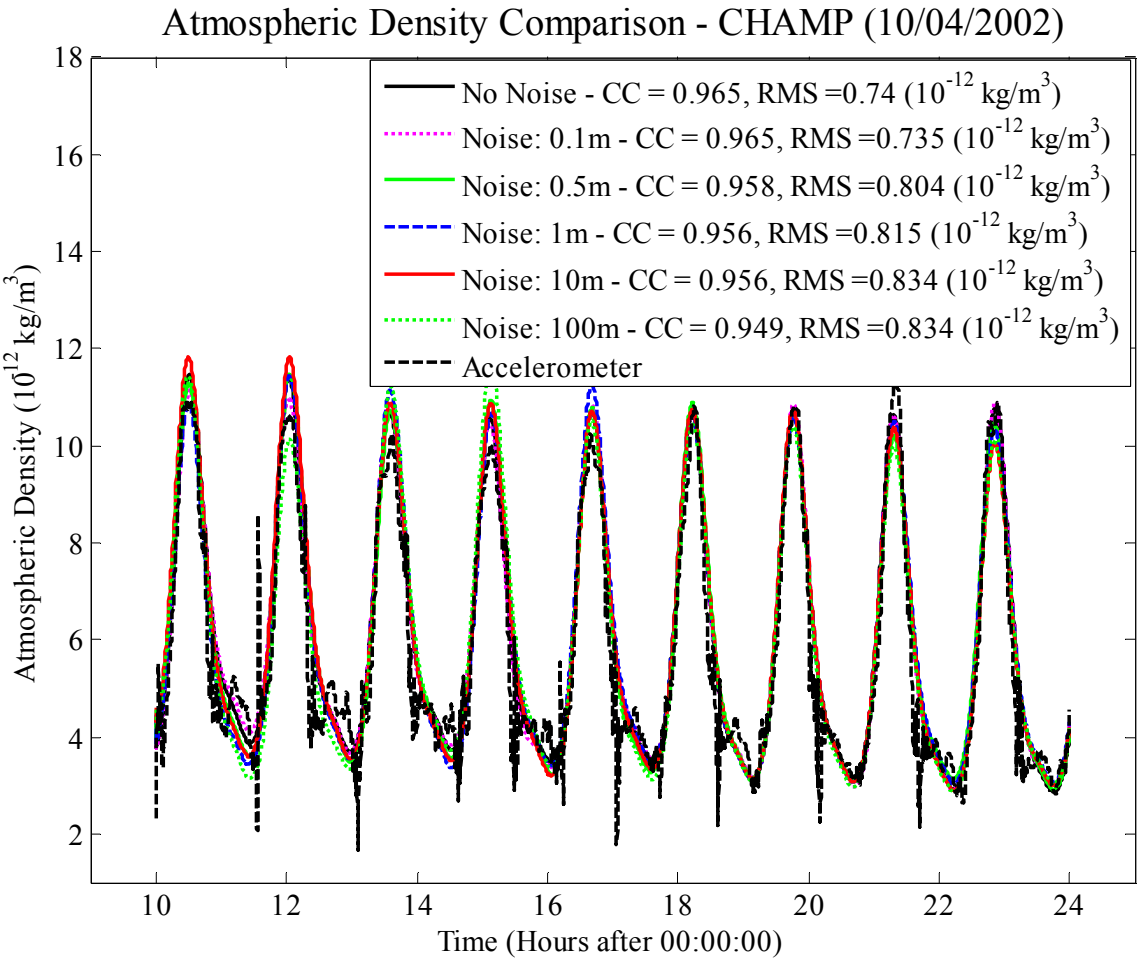

Figure 4.3 – Atmospheric Density Comparison for CHAMP on 10/04/2002.

The trend observed in Figure 4.3 is also expected: a decrease in the CC value and an increase in the RMS value as the noise level is increased. Figure 4.4 below shows the comparison of POE derived density estimates for the different noise levels during the day of April 17, 2002, which is a day of high solar and active geomagnetic activity.

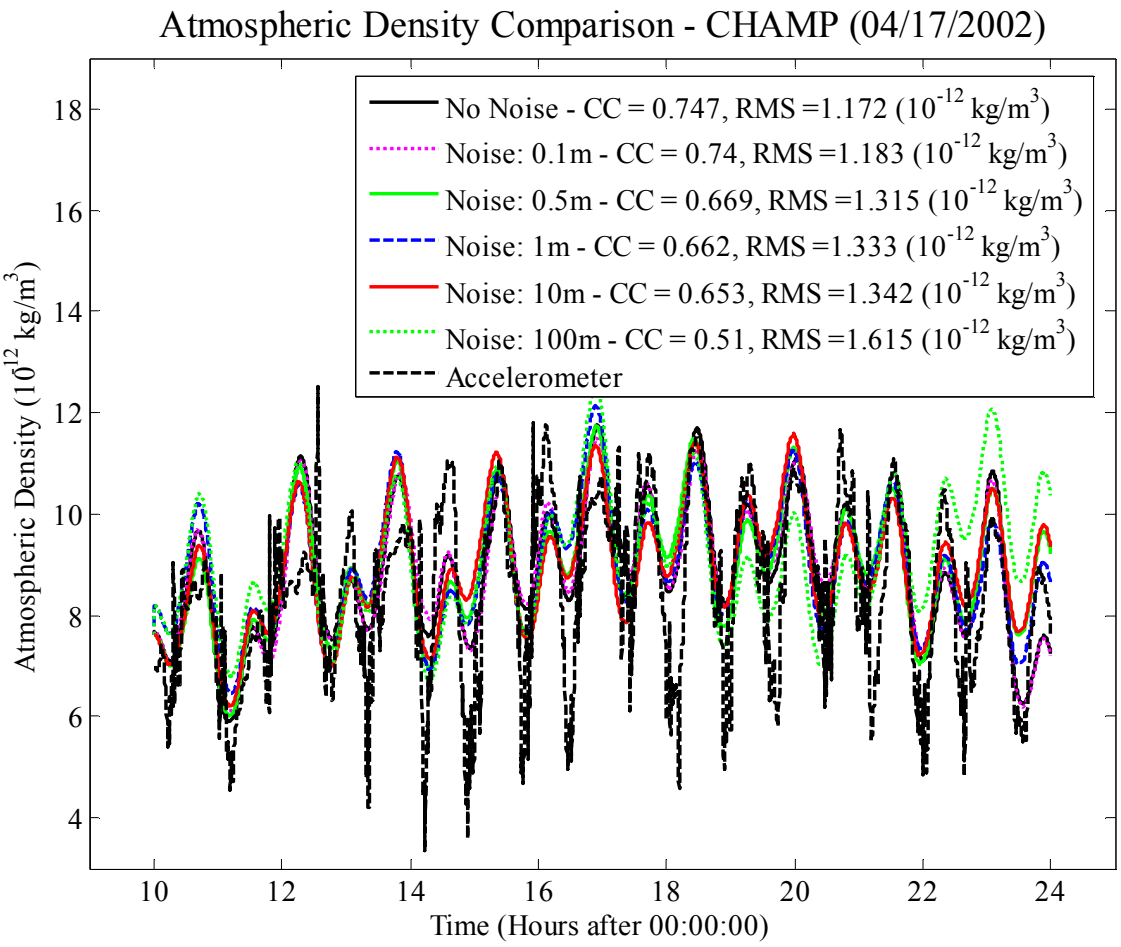

Figure 4.4 – Atmospheric Density Comparison for CHAMP on 04/17/2002.

The POE derived density estimates in Figure 4.4 show more variability between the different noise levels than the day of lower solar and geomagnetic activity shown in Figure 4.1 which is expected. However, the trend of decreasing CC value and increasing RMS value with an increase in the noise level still holds true. Figure 4.5 shows the comparison of POE derived density estimates between different noise levels for GRACE during the day of August 4, 2006, which is a day of low solar and quiet geomagnetic activity.

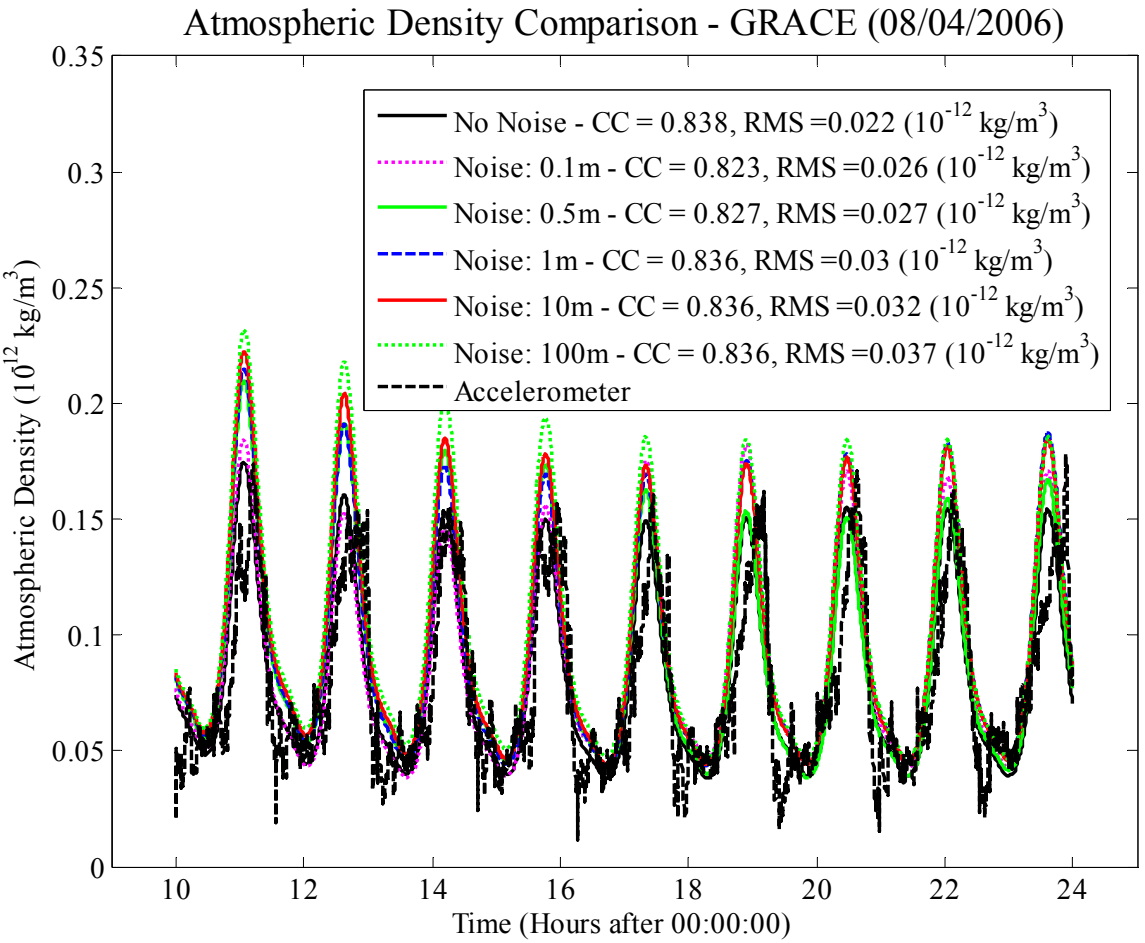

Figure 4.5 – Atmospheric Density Comparison for GRACE on 08/04/2006.

For the most part the errors between the density estimates correlate with the associated noise levels. As the noise level is increased the CC values decrease and the RMS values increase which is expected. However, this trend is not as apparent as it was in the CHAMP plots. This may be due to the lower overall magnitude of the density that the GRACE satellite experiences in comparison to CHAMP. Figure 4.6 below shows the same data except during the day of May 13, 2005, which is a day of moderate solar and moderate geomagnetic activity.

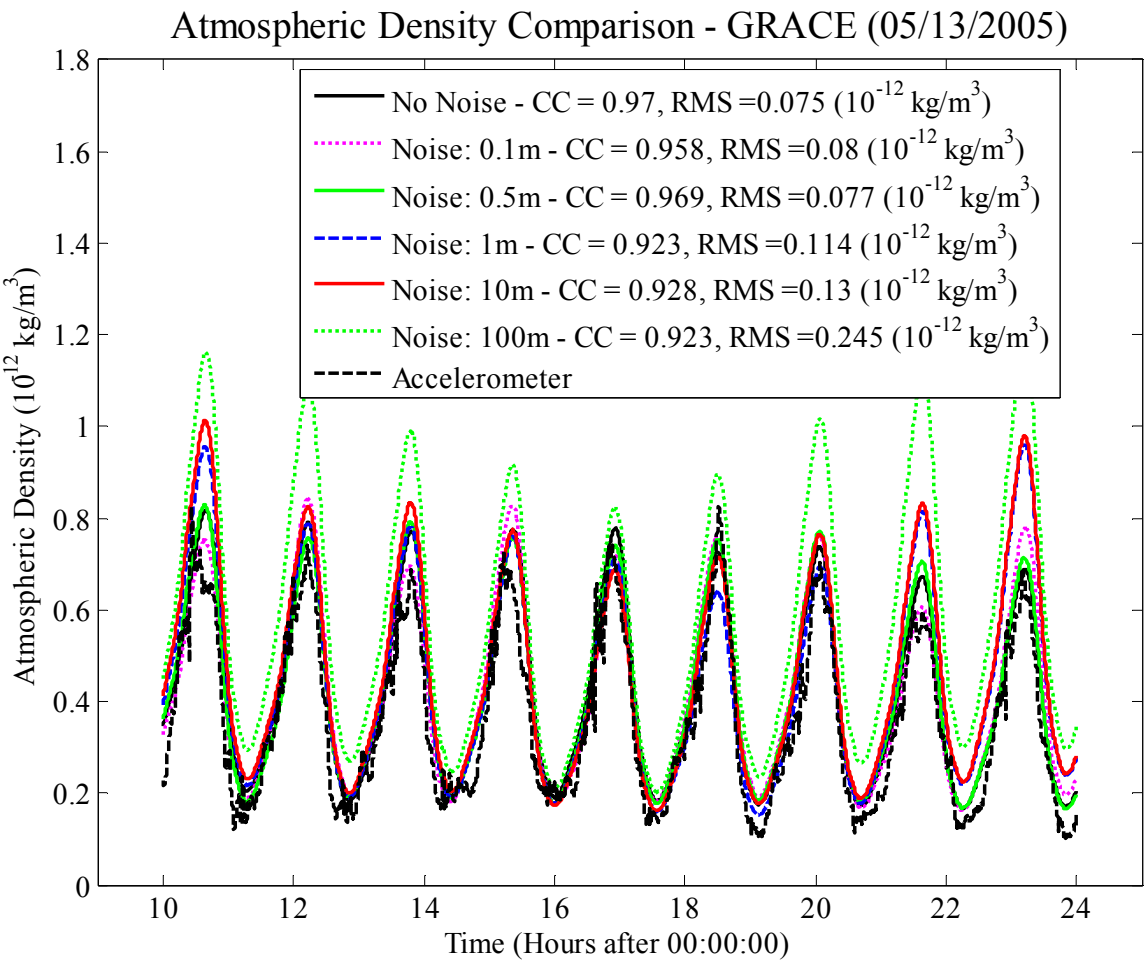

Figure 4.6 – Atmospheric Density Comparison for GRACE on 05/13/2005.

The results in Figure 4.6 also show a trend of decreasing CC value and increasing RMS value accompanying an increase in noise level. Again, this trend is not quite as clear as it was in the case of CHAMP, but is still generally observable. Figure 4.7 below shows the same data except it is during the day of November 9, 2004, which is a day of moderate solar and active geomagnetic activity.

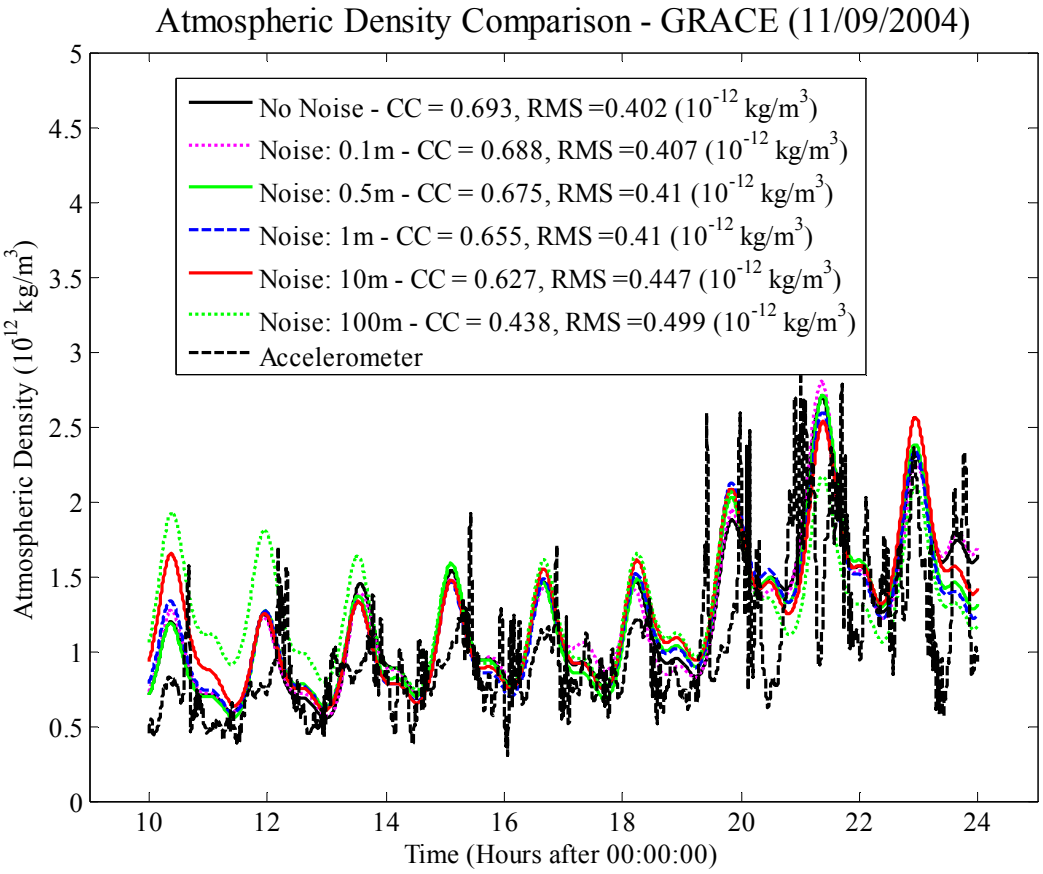

Figure 4.7 – Atmospheric Density Comparison for GRACE on 11/09/2004.

There is much more variability between the noise levels for the day of higher solar and geomagnetic activity compared to the day of lower solar and geomagnetic activity level, similar to what is seen in the CHAMP data. The trend of decreasing CC value and increasing RMS value can still be observed in Figure 4.7. Since there is a large amount of randomness in these results when looking at one particular day the CC and RMS results were binned by noise level

and solar and geomagnetic activity level in order to see what trends appear. Tables 4.2 - 4.5 below display the average CC and RMS values for all days examined for CHAMP binned by solar and geomagnetic activity level. The CC and RMS results for the Jacchia-71 density model, NRLMSISE-00 density model, and HASDM compared to accelerometer derived densities are also shown.

Table 4.2 – Average CC values for CHAMP binned by solar activity level.

Noise Level	Low Solar	Moderate Solar	Elevated Solar	High Solar
No Noise	0.900	0.921	0.947	0.889
0.1m	0.895	0.916	0.943	0.884
0.5m	0.885	0.917	0.946	0.879
1m	0.862	0.913	0.943	0.873
10m	0.851	0.911	0.943	0.875
100m	0.824	0.898	0.926	0.838
Jacchia-71	0.857	0.898	0.928	0.817
NRLMSISE-00	0.884	0.915	0.938	0.859
HASDM	0.892	0.919	0.941	0.874

Table 4.3 – Average RMS values (10^{-12} kg/m^3) for CHAMP binned by solar activity level.

Noise Level	Low Solar	Moderate Solar	Elevated Solar	High Solar
No Noise	0.304	0.357	0.481	0.838
0.1m	0.310	0.366	0.491	0.856
0.5m	0.321	0.363	0.494	0.855
1m	0.349	0.374	0.505	0.880
10m	0.374	0.379	0.505	0.874
100m	0.437	0.420	0.580	1.004
Jacchia-71	0.823	0.612	0.928	1.806
NRLMSISE-00	0.634	0.510	0.736	1.314
HASDM	0.319	0.357	0.464	0.808

Table 4.4 – Average CC values for CHAMP binned by geomagnetic activity level.

Noise Level	Quiet Geomagnetic	Moderate Geomagnetic	Active Geomagnetic
No Noise	0.937	0.891	0.857
0.1m	0.932	0.886	0.854
0.5m	0.931	0.886	0.840
1m	0.924	0.873	0.836
10m	0.920	0.873	0.836
100m	0.906	0.847	0.796
Jacchia-71	0.918	0.856	0.728
NRLMSISE-00	0.941	0.862	0.803
HASDM	0.936	0.880	0.852

Table 4.5 – Average RMS values (10^{-12} kg/m^3) for CHAMP binned by geomagnetic activity level.

Noise Level	Quiet Geomagnetic	Moderate Geomagnetic	Active Geomagnetic
No Noise	0.293	0.460	1.248
0.1m	0.301	0.472	1.254
0.5m	0.301	0.470	1.285
1m	0.313	0.493	1.305
10m	0.321	0.499	1.304
100m	0.367	0.570	1.436
Jacchia-71	0.587	0.958	2.273
NRLMSISE-00	0.506	0.726	1.589
HASDM	0.290	0.473	1.168

Table 4.6 – Total average RMS (10^{-12} kg/m^3) and CC values for CHAMP.

Noise Level	CC	RMS
No Noise	0.917	0.405
0.1m	0.913	0.414
0.5m	0.911	0.415
1m	0.903	0.431
10m	0.900	0.438
100m	0.881	0.497
Jacchia-71	0.887	0.807
NRLMSISE-00	0.905	0.643
HASDM	0.913	0.402

A number of certain trends can be seen by looking at Tables 4.2 - 4.5. Firstly, in nearly all cases the CC value decreases and the RMS value increases as the noise level is increased. This is an expected outcome since the higher the noise level is in the input ephemeris file the more uncertain the measurements are and, therefore, the more error that should be present in the estimated density values. Also in nearly all cases the CC value decreases and the RMS increases as the solar or geomagnetic activity level increases. This is not always true with all the cases (See Figure 4.2) due to the differing number of days in each of the different geomagnetic and solar activity level bins and because solar and geomagnetic activity can't be separated. The CC results for the Jacchia density model are similar to those for the 10 m or 100 m noise level POE case. However, the RMS values for the Jacchia density model are significantly higher than any of the POE noise levels. The CC results for NRLMSISE-00 are comparable to those observed for the 0.5 m or 1 m noise levels. Similar to the Jacchia RMS values, the NRLMSISE RMS values are generally higher than any of the POE noise levels. The CC and RMS results for HASDM are similar to those for the POE no noise case. Table 4.6 shows the total CC and

RMS average values for all days run for CHAMP. The trend seen in this table is as expected: the CC value decreases and the RMS value increases as the noise level is increased. This same analysis was performed for GRACE during all days examined (See Tables 4.7 – 4.10). As stated in Chapter 2.7 there were no days examined for GRACE with elevated or high solar activity levels.

Table 4.7 – Average CC values for GRACE binned by solar activity level.

Noise Level	Low Solar	Moderate Solar	Elevated Solar	High Solar
No Noise	0.711	0.900	NA	NA
0.1m	0.659	0.887	NA	NA
0.5m	0.668	0.882	NA	NA
1m	0.628	0.875	NA	NA
10m	0.610	0.878	NA	NA
100m	0.612	0.847	NA	NA
Jacchia-71	0.621	0.853	NA	NA
NRLMSISE-00	0.650	0.864	NA	NA
HASDM	0.654	0.899	NA	NA

Table 4.8 – Average RMS values (10^{-12} kg/m^3) for GRACE binned by solar activity level.

Noise Level	Low Solar	Moderate Solar	Elevated Solar	High Solar
No Noise	0.037	0.095	NA	NA
0.1m	0.043	0.100	NA	NA
0.5m	0.042	0.103	NA	NA
1m	0.049	0.107	NA	NA
10m	0.054	0.112	NA	NA
100m	0.072	0.139	NA	NA
Jacchia-71	0.099	0.179	NA	NA
NRLMSISE-00	0.074	0.126	NA	NA
HASDM	0.039	0.101	NA	NA

Table 4.9 – Average CC values for GRACE binned by geomagnetic activity level.

Noise Level	Quiet Geomagnetic	Moderate Geomagnetic	Active Geomagnetic
No Noise	0.851	0.861	0.824
0.1m	0.826	0.848	0.816
0.5m	0.829	0.834	0.806
1m	0.810	0.822	0.795
10m	0.800	0.832	0.783
100m	0.796	0.823	0.672
Jacchia-71	0.802	0.837	0.678
NRLMSISE-00	0.849	0.848	0.509
HASDM	0.833	0.873	0.773

Table 4.10 – Average RMS values (10^{-12} kg/m^3) for GRACE binned by geomagnetic activity level.

Noise Level	Quiet Geomagnetic	Moderate Geomagnetic	Active Geomagnetic
No Noise	0.051	0.070	0.270
0.1m	0.056	0.075	0.281
0.5m	0.056	0.081	0.284
1m	0.057	0.092	0.288
10m	0.059	0.093	0.311
100m	0.066	0.126	0.375
Jacchia-71	0.075	0.152	0.589
NRLMSISE-00	0.069	0.097	0.382
HASDM	0.053	0.069	0.304

Table 4.11 – Total average RMS (10^{-12} kg/m^3) and CC values for GRACE.

Noise Level	CC	RMS
No Noise	0.844	0.079
0.1m	0.823	0.084
0.5m	0.819	0.087
1m	0.803	0.092
10m	0.802	0.096
100m	0.780	0.121
Jacchia-71	0.788	0.156
NRLMSISE-00	0.815	0.113
HASDM	0.835	0.083

From examination of Tables 4.7 - 4.10 the trends are similar to those seen for CHAMP. Generally, as the noise level is increased the CC values decrease and the RMS values increase. Similarly as the solar or geomagnetic activity level increase the CC values decrease and the RMS values increase. As was the case with CHAMP this does not always hold true (See Tables 4.7 and 4.9) specifically with regards to the CC values between low and moderate solar activity within the same noise level. Again, this is due to the differing number of days in each of the bins and because geomagnetic and solar activity can't be separated. This can also be observed in the CC values in Table 4.9 between the quiet and moderate geomagnetic activity levels. Table 4.11 shows the total CC and RMS average values for all days run for GRACE. The CC results for the Jacchia density model are similar to those for the 10 m or 100 m noise level POE case. However, the RMS values for the Jacchia density model are typically higher than any of the POE noise levels. The CC results for NRLMSISE-00 are generally comparable to those observed for the 0.5 m or 1 m noise levels. The RMS results for NRLMSISE-00 are comparable

in most cases to the 100 m noise level case. The CC and RMS results for HASDM are similar to those for the POE no noise case, with the POE derived densities having slightly better results.

The POE derived densities obtained from using noisy input ephemeris data were also run through the same orbit propagator outlined in Chapter 3. The different density sources used as input into the propagator in Chapter 3 were POE, Jacchia-1971, and HASDM; all of which were compared with results obtained using the accelerometer derived densities as input. In this chapter the density sources used as input into the orbit propagator are each of the different ephemeris noise levels all compared with accelerometer results. Another difference from Chapter 3 is that these propagations are 14 hour solution spans instead of 24 hour spans because there are no one week density solutions that were obtained using the noisy ephemeris data. The orbit propagator results can be found below in Figures 4.8 – 4.14. As was the case in Chapter 3 the position error shown in the plots below is the magnitude of the vector difference between the vector obtained from the accelerometer density and that obtained from the other density source (one of the ephemeris noise levels). Figure 4.8 below shows the orbit propagation results for CHAMP with the noisy ephemeris data for the day of March 17, 2007, which is a day of low solar and quiet geomagnetic activity.

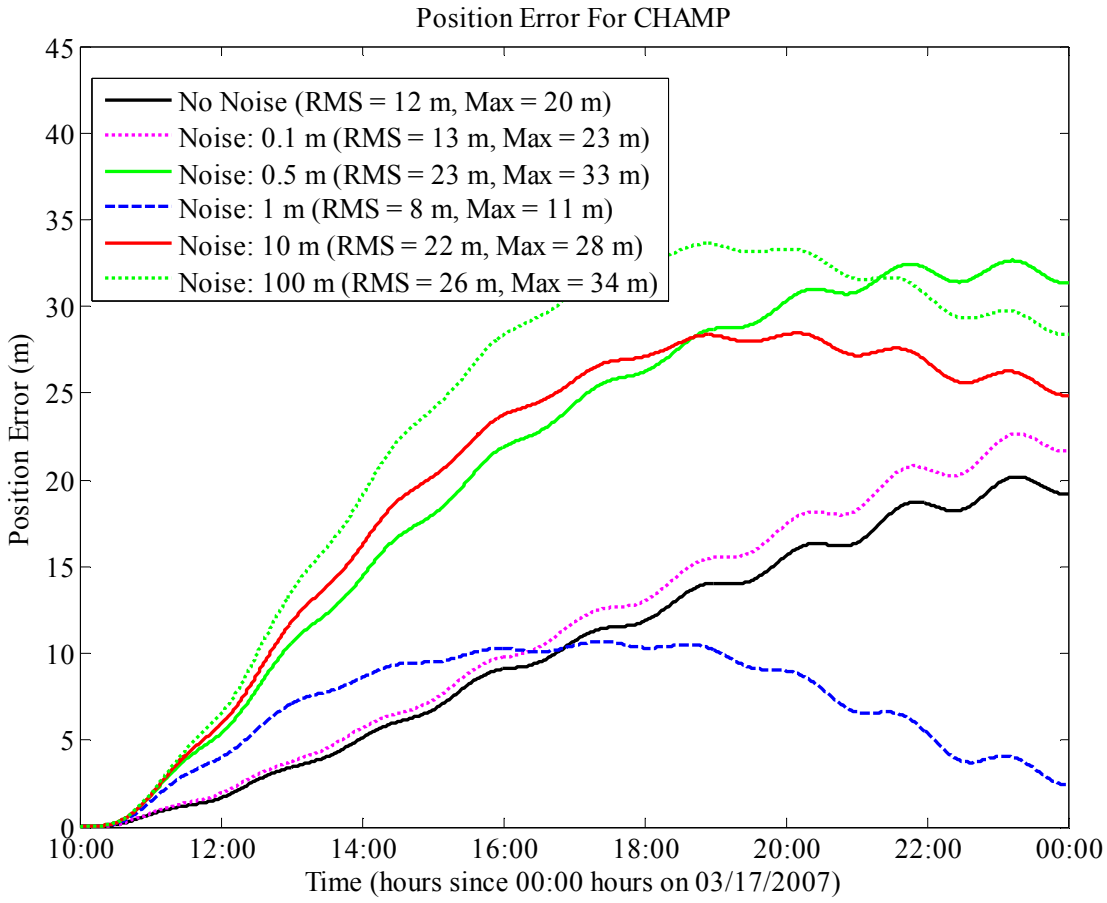

Figure 4.8 – Comparison of different ephemeris noise levels for CHAMP on 03/17/2007.

As was seen with the previous ephemeris noise results for a single day there is a level of randomness involved. While the results in Figure 4.8 show a general trend of increasing RMS and maximum error with an increase in the ephemeris noise level this is not always the case. Note that for this particular day the 1 m noise level outperforms all other noise level cases, even the smaller noise and no noise cases, which does not follow the general trend. However, some level of randomness is expected when analyzing a single day as previously discussed. Figure 4.9 below shows the orbit propagation results for CHAMP with the noisy ephemeris data for the day of January 23, 2003, which is a day of moderate solar and moderate geomagnetic activity.

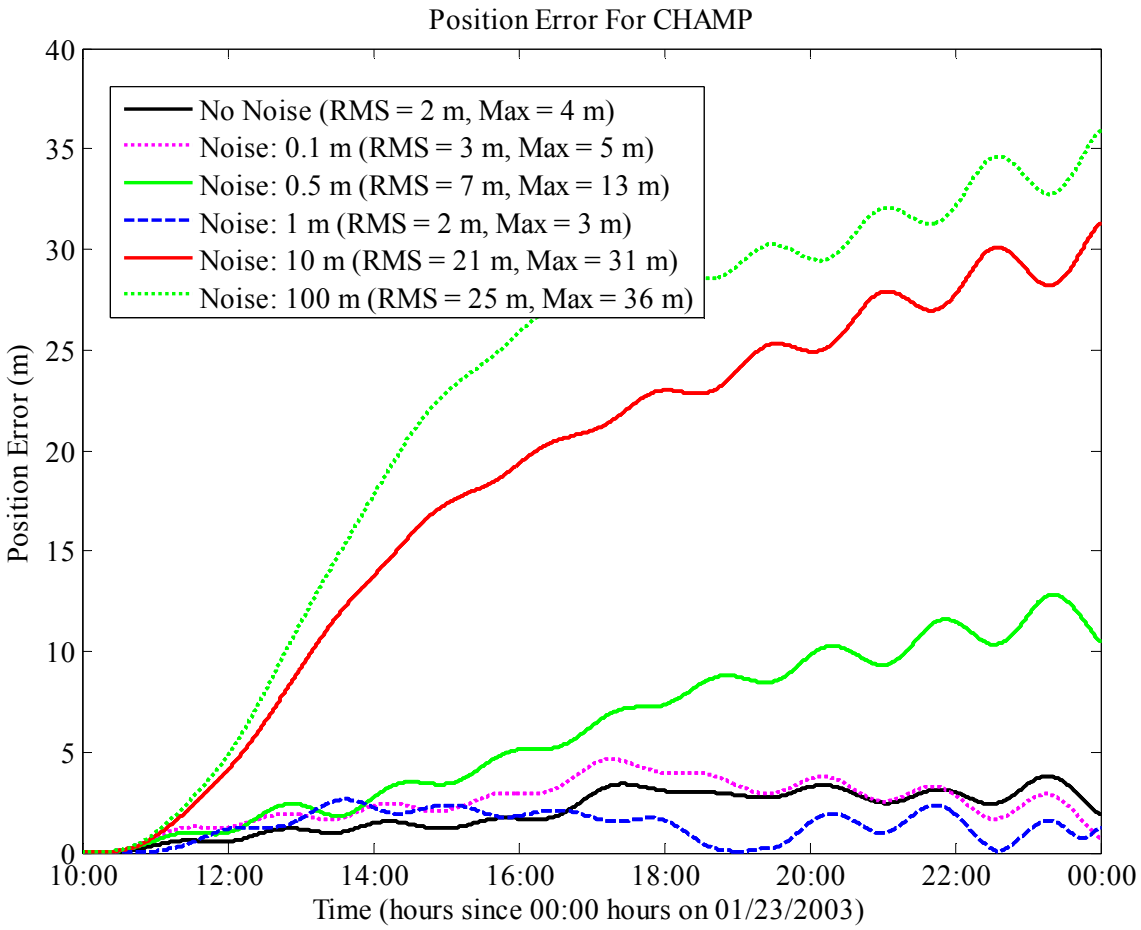

Figure 4.9 – Comparison of different ephemeris noise levels for CHAMP on 01/23/2003.

The general trend of increasing RMS and maximum error with an increase in noise level can again be observed in Figure 4.9. However, the 1 m noise level again outperforms all other noise levels. This anomaly is thought to be associated with the randomness of the noisy ephemeris data. Figure 4.10 below shows the orbit propagation results for CHAMP with the noisy ephemeris data for the day of October 04, 2002, which is a day of elevated solar and active geomagnetic activity.

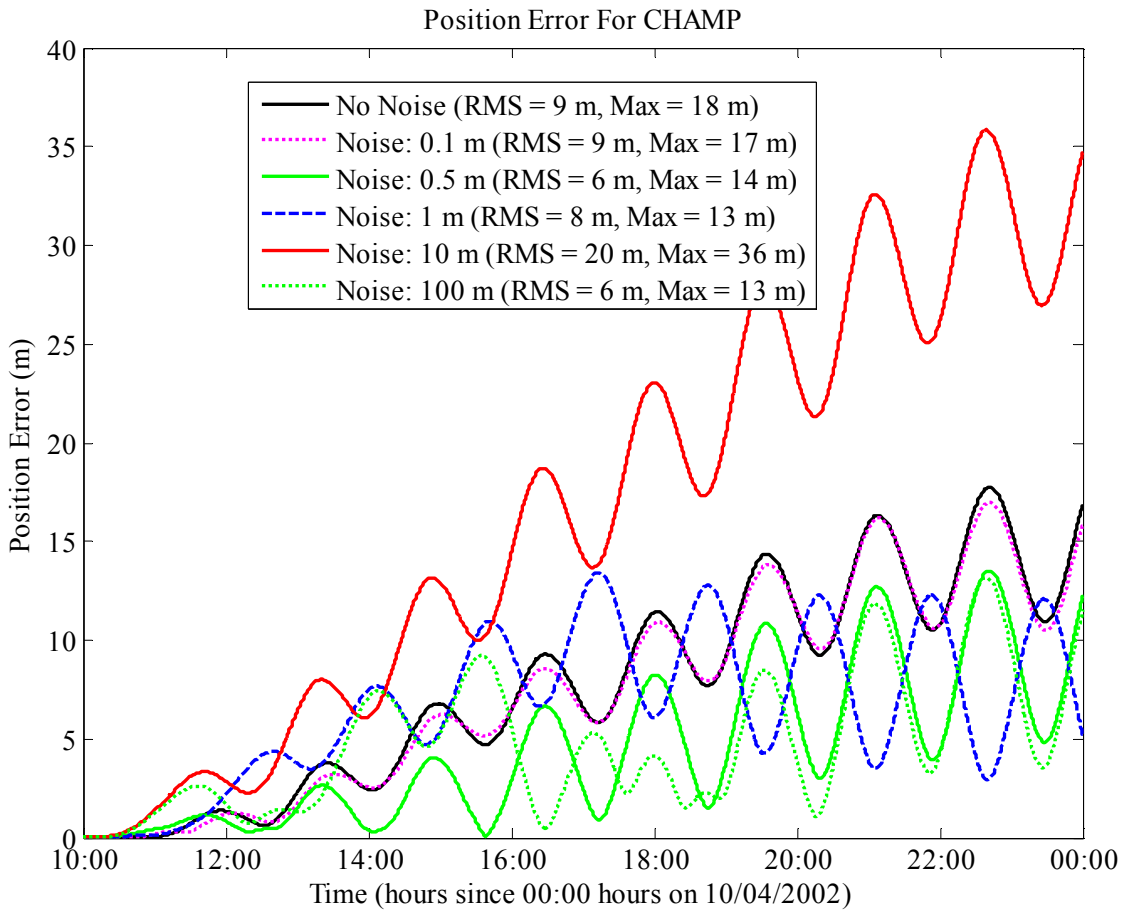

Figure 4.10 – Comparison of different ephemeris noise levels for CHAMP on 10/04/2002.

Again there is a level of randomness that can be observed in Figure 4.10. While the trend of increasing RMS and maximum error with an increase in noise level can be seen it is difficult as the 100 m noise level outperforms all other cases for this day. There is also a large amount of periodic variation in the position errors in Figure 4.10. Figure 4.11 below shows the orbit propagation results for CHAMP with the noisy ephemeris data for the day of April 17, 2002, which is a day of high solar and active geomagnetic activity.

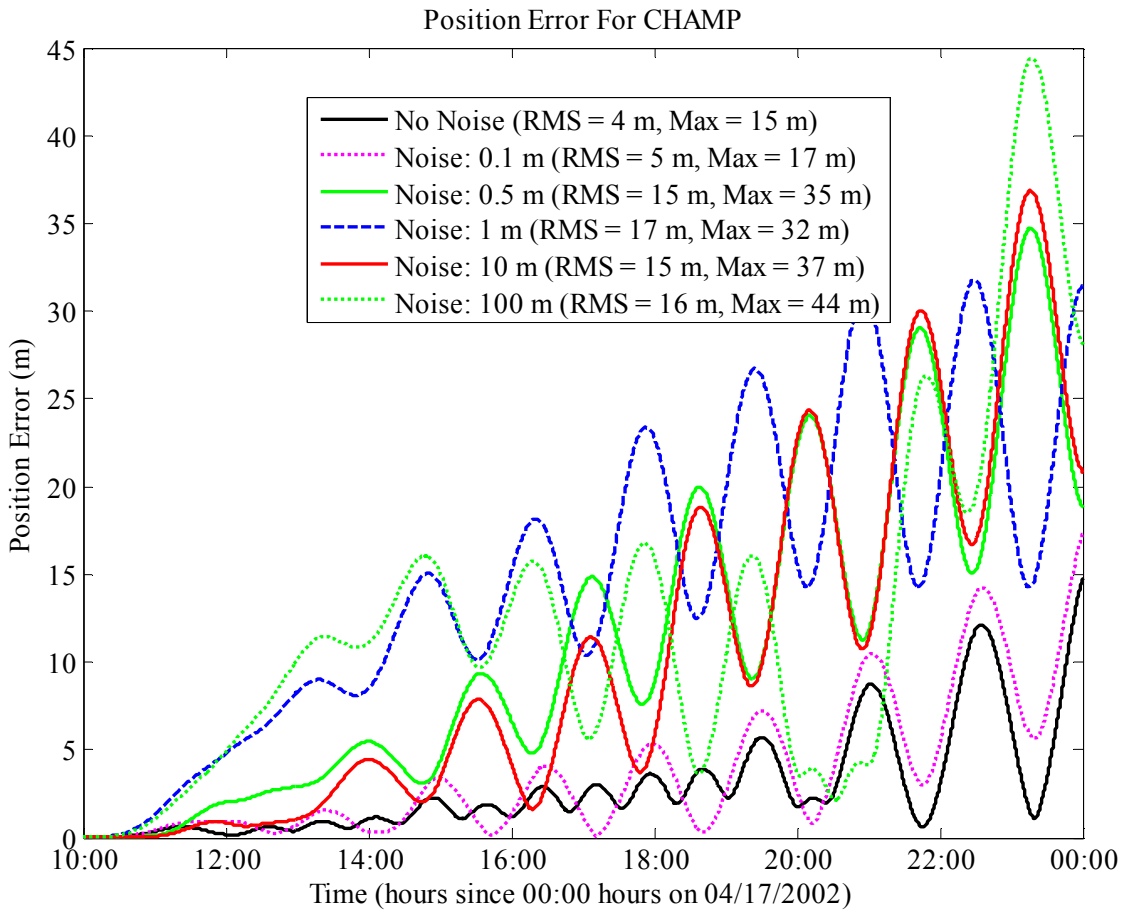

Figure 4.11 – Comparison of different ephemeris noise levels for CHAMP on 04/17/2002.

The trend of increasing RMS and maximum error values accompanying an increase in ephemeris noise can clearly be observed in Figure 4.11. There can again be seen some periodic variations in the plot of the position errors for this day. Figure 4.12 below shows the orbit propagation results for GRACE with the noisy ephemeris data for the day of August 04, 2006, which is a day of low solar and quiet geomagnetic activity.

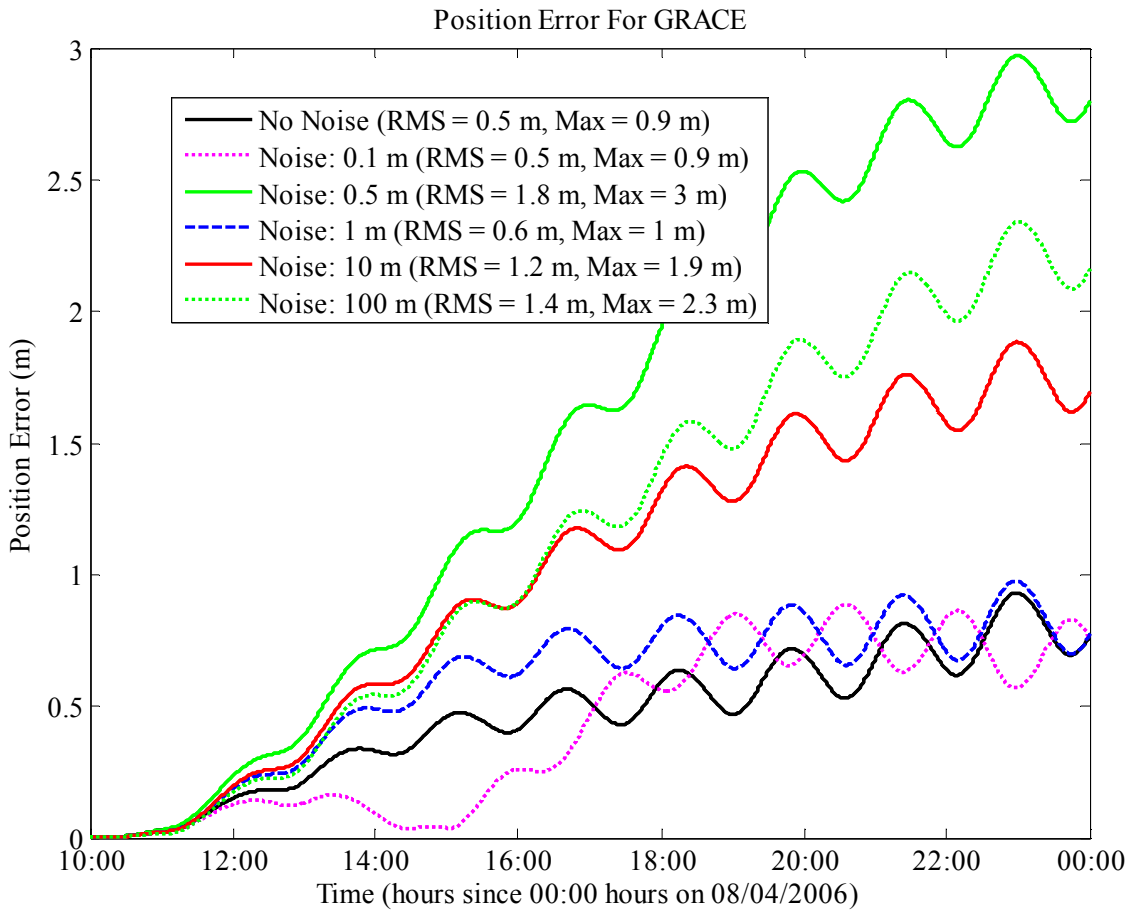

Figure 4.12 – Comparison of different ephemeris noise levels for GRACE on 08/04/2006.

The data for GRACE are similar to data for CHAMP in that there is some randomness associated with the results. A general trend can be observed of an increasing RMS and maximum error value with an increase in ephemeris noise level. However, this is not always the case as for this day the results show that the 0.5 m noise level is the worst performing case. Figure 4.13 below shows the orbit propagation results for GRACE with the noisy ephemeris data for the day of May 13, 2005, which is a day of moderate solar and moderate geomagnetic activity.

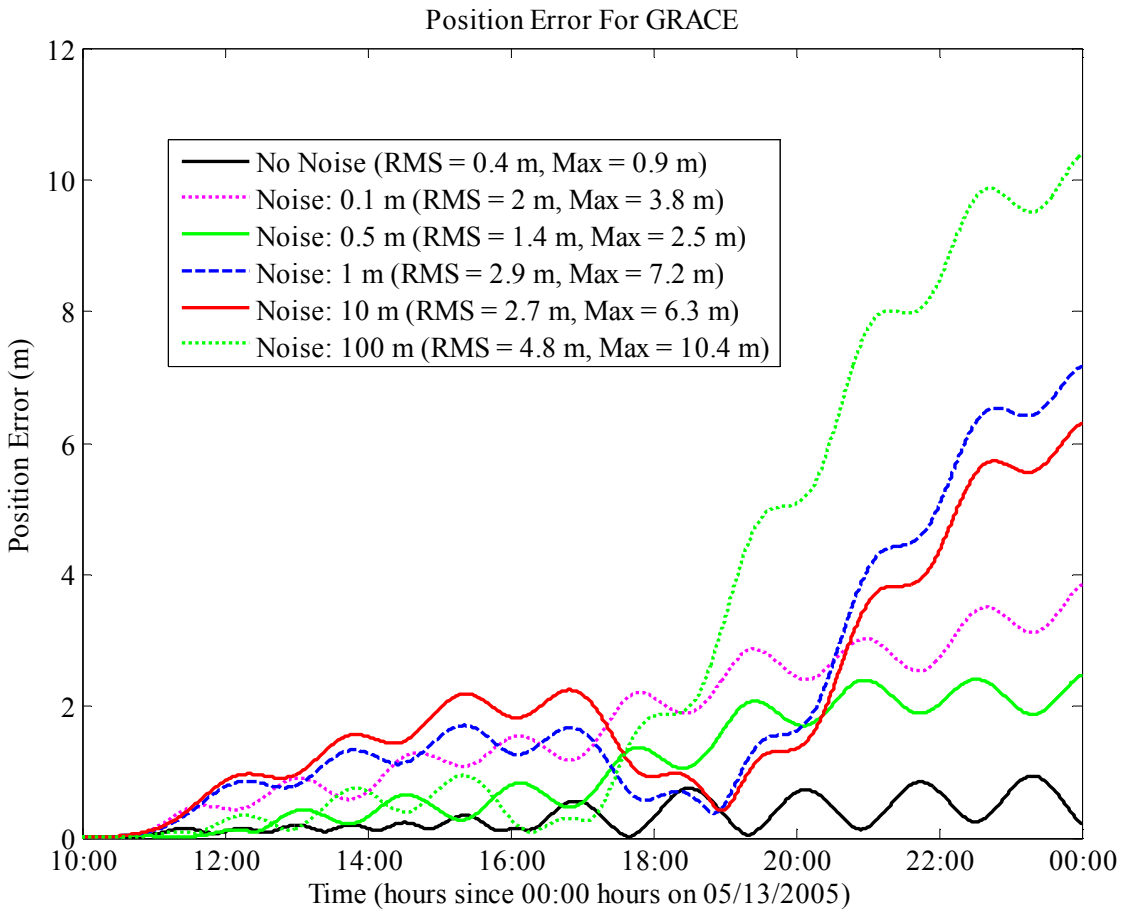

Figure 4.13 – Comparison of different ephemeris noise levels for GRACE on 05/13/2005.

The results in Figure 4.13 also generally show the expected trend of increasing RMS and maximum error with an increase in noise level. Again there is some discrepancy with this trend for this particular day such as the 0.5 m noise level case outperforming the 0.1 m noise level case and the 10 m noise level cause outperforming the 1 m noise level case. Figure 4.14 below shows the orbit propagation results for GRACE with the noisy ephemeris data for the day of November 9, 2004, which is a day of moderate solar and active geomagnetic activity.

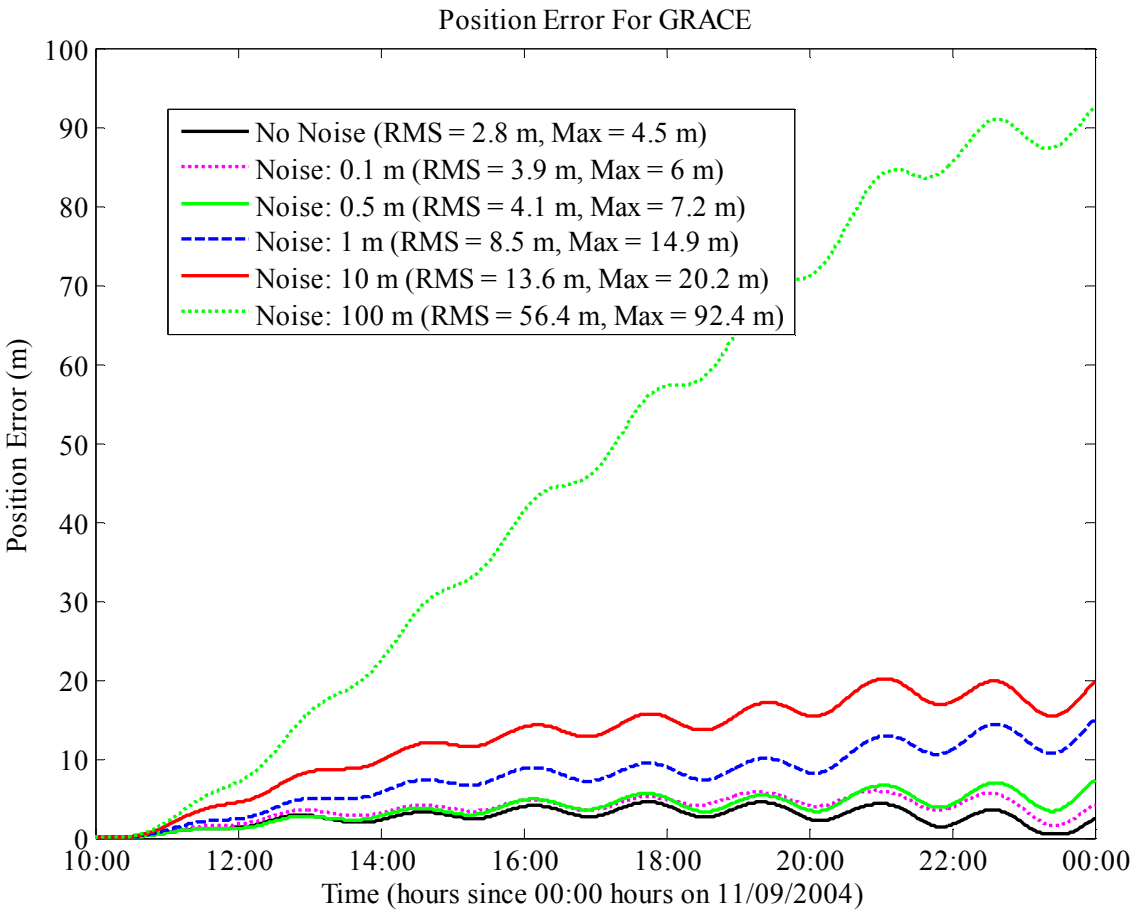

Figure 4.14 – Comparison of different ephemeris noise levels for GRACE on 11/09/2004.

The results in Figure 4.14 clearly show the trend of increasing RMS and maximum error value with an increase in ephemeris noise level. Overall, although there is a level of randomness in the results of implementing the ephemeris noise densities into the orbit propagation technique there is also an expected general trend that is seen in the data.

4.2 Summary

Different noise levels were added to the raw ephemeris file before input into the ODTK scheme in order to examine the effects of differing levels of noise present in the measurement input file. The levels of noise were verified by checking the differences between the noisy ephemeris files and the original ephemeris file with no noise before they are input into ODTK and also by computing the RMS values between these data sets. The validity of the ODTK runs was also verified by checking the measurement residuals. Both of these checks lead to the conclusion that the methodology in this portion of the research was sound. Examination of the plots of POE derived densities for each of the noise levels compared to the original no noise case for a single day revealed a certain amount of randomness in the errors associated with each of the different noise levels. This is to be expected due to the method in which the noise was added to the raw ephemeris file. When all of the days for both CHAMP and GRACE were analyzed and the CC and RMS values calculated between the POE derived densities obtained using the noisy ephemeris files and the original ephemeris files some trends can be observed. In general, as the noise level is increased the CC values decrease while the RMS values increase. This is what was expected because as the ephemeris file becomes less accurate, so too should the resultant density estimates. Another general trend that was observed was that when the solar or geomagnetic activity level increased the CC values decreased and the RMS values increased. While this trend is expected it is not true for all of the cases. This is believed to be due to the fact that there are different numbers of days in each of the bins and because geomagnetic and solar activity can't be separated. Also, the possibility exists that a day of low solar activity has a higher level of geomagnetic activity than a day of moderate solar activity which could lead to the former day containing more error in the POE derived density estimates than the latter day.

The different density data sets resulting from different levels of noise being added to the input ephemeris data were also analyzed with the orbit propagator outlined in Chapter 3. These results showed a general trend of increasing RMS and maximum error values (compared to propagation with the accelerometer densities) with an increase in ephemeris noise level which is expected. However, there was a level of randomness observed in the results as well making the trend not always hold true.

5 SUMMARY, CONCLUSIONS, AND FUTURE WORK

5.1 Summary

Atmospheric drag is not only the most dominant but also the most uncertain non-conservative force acting on a satellite in low Earth orbit. There exist variations in atmospheric density that can greatly affect the drag experienced by a satellite due to the fact that drag is directly proportional to atmospheric density. Existing atmospheric density models are not accurate enough to model these variations in atmospheric density. This work focuses on using POE data as input measurements into an optimal orbit determination scheme in order to estimate atmospheric density corrections to existing baseline density models. These density corrections improve the estimated drag experienced by a satellite and therefore improve orbit determination and prediction for satellites as well as provide a better overall understanding of the Earth's upper atmosphere.

The POE data are used as input measurement into a sequential filter/smoother process utilizing the Orbit Determination Tool Kit (ODTK) software. The POE derived density estimates are validated by comparing them with density data derived from accelerometers on-board CHAMP and GRACE. The trend in the variation of the density and the magnitude is compared by calculating the CC and RMS values respectively between the two density data sets.

Certain high frequency density variations are observed in the accelerometer derived density data, but not in the POE derived density data or any of the empirical density models. These high frequency density variations are typically small in magnitude compared to the overall day-night variation. However, when the satellite is near the terminator the variations are on the same order of magnitude as the diurnal variations. These variations can also be especially prevalent during geomagnetic storms and near the polar cusps. One of the goals of this work is

to see what affect these unmodeled high frequency variations have on orbit propagation. In order to see this effect, the orbits of CHAMP and GRACE are propagated during certain time periods using different sources of density data as input measurements (accelerometer, POE, HASDM, and Jacchia 1971). The resulting orbit propagations are all compared to the propagation using the accelerometer derived density data which are used as truth. The RMS and the maximum difference between the different propagations are analyzed in order to see what effect the unmodeled density variations have on orbit propagation. These results are also binned by solar and geomagnetic activity level.

The primary input into the orbit determination scheme used to produce the POE derived density estimates is a precision orbit ephemeris file. This file contains position and velocity information for the satellite based on GPS and SLR measurements. The values contained in these files are estimated values and therefore contain some level of error, typically thought to be around the 5-10 cm level. The other primary focus of this work is to evaluate the effect of adding different levels of noise (0.1 m, 0.5 m, 1 m, 10 m, and 100 m) to this raw ephemeris data file before it is input into the orbit determination scheme. The resulting POE derived density estimates for each level of noise are then compared with the accelerometer derived densities by computing the CC and RMS values between the data sets. These results are also binned by solar and geomagnetic activity level. The resulting density data sets are also ran through the orbit propagator previously mentioned and compared with accelerometer results.

5.2 Conclusions

Several conclusions can be drawn from the research presented in this work. Firstly, the effect of high frequency density variations present in the accelerometer derived density data but

not in the POE derived density data, HASDM, or empirical density models was analyzed. Certain time periods during which these high frequency density variations were especially prevalent were examined, including when the satellite orbit plane is near the terminator, near the polar cusps, and when encountering travelling atmospheric disturbances. In order to see these effects the orbits of CHAMP and GRACE were propagated using different density sources (POE, accelerometer, Jacchia 1971, and HASDM) as input measurements. The resulting orbit propagations were then all compared to those found using the accelerometer derived densities as input by computing the RMS and maximum difference between the propagations. The resulting RMS and maximum difference values showed that during all of these time periods the effect of not modeling the high frequency density variations did not cause significant errors in the propagation of the satellite orbits and is acceptable for most applications. This research was expanded to include many days for both CHAMP and GRACE of varying solar and geomagnetic activity levels and the resulting RMS and maximum difference values were then averaged and binned according to those levels. This analysis showed that the orbit propagations using POE derived density data performed better when compared to the propagations using the accelerometer derived densities than the other density sources (HASDM and Jacchia 1971). This was true for all cases with the exception of GRACE during active geomagnetic activity levels. Another conclusion resulting from this analysis is that the errors between the propagations using different density data sources generally grew with an increase in solar and geomagnetic activity levels, which is to be expected.

Secondly, the effect of adding different levels of noise to the raw ephemeris data on the POE derived density estimates was examined. Some randomness was seen upon comparison of the resulting density estimates using differing levels of noise in the ephemeris for a single day.

This is to be expected due to the method in which the noise was added to the raw ephemeris file, especially for the smaller noise cases. The CC and RMS values between the density estimates obtained using each of the different noise levels and the accelerometer derived density estimates were also calculated. This analysis revealed more of a trend within the results. Generally the CC value decreased and the RMS value increased as the noise level increased which was the expected result. Another observed trend was that as the solar or geomagnetic activity level increased the CC values decreased and the RMS values increased. This trend was also expected, but is not true for all of the cases examined. This is believed to be due to the differing number of days in each of the solar and geomagnetic activity level bins and because geomagnetic and solar activity can't be separated. Overall, the major conclusion from this portion of research is that an increase in the error associated with the raw ephemeris file input in the orbit determination scheme will yield an increase in error in the resultant density estimates. However, small increases in the input ephemeris file error will likely cause an increase in the error of the POE derived density estimates that is not significant for most applications.

5.3 Future Work

5.3.1 Data Decimation

Reducing the sampling rate of the raw ephemeris data may be useful to analyze. This can be done in many different ways, but the primary goal would be to see what would happen to the accuracy of the resulting POE derived density estimates if the raw input ephemeris data were much sparser. The simplest way to do this would likely be to delete certain ranges of data from the ephemeris file, such as only having data during the first third of each satellite orbit

period and deleting the rest of the data. Varying which data is available in the ephemeris file would also be useful.

5.3.2 Monte-Carlo Analysis

Due to the method in which the noise is added to the raw ephemeris file discussed in Chapter 4 the results from a Monte-Carlo type analysis of a single day would be useful to examine. Instead of running each day with one set of noisy ephemeris data a single day would be run a certain number of times, for example 100, each time having a newly created set of noisy ephemeris input data. After averaging the results the expectation would be to see a reduction in the randomness of the results for a single day and be able to be able to more clearly observe the trends.

5.3.3 Expand Days Examined

Another worthwhile project would be to expand the days examined in this research in Chapters 3 and 4 to include the entire lifespan of CHAMP and GRACE. This analysis would yield a larger sample size of data from which to draw conclusions. Binning results from the satellite's entire lifetime would likely reveal more defined trends that would not have exceptions.

REFERENCES

1. Bruinsma, S. and R. Biancale, "Total Density Retrieval with STAR," *First CHAMP Mission Results for Gravity, Magnetic and Atmospheric Studies*, eds. C. Reigber, H. Luhr, P. Schwintzer, Springer, Berlin, 2003, pp. 192-199.
2. Nerem, R. S., J. M. Forbes, E. K. Sutton, and S. Bruinsma, "Atmospheric Density Measurements Derived from CHAMP/STAR Accelerometer Data," *Advances in the Astronautical Sciences*, Vol. 116, AAS 03-621, Univelt, 2003, pp. 1879-1898.
3. Tapley, B. D., J. C. Ries, S. Bettadpur, M. Cheng, "Neutral Density Measurements from the Gravity Recovery and Climate Experiment Accelerometers," *Journal of Spacecraft and Rockets*, Vol. 44, No. 6, 2007, pp. 1220-1225.
4. Storz, M. F., B. R. Bowman, Major J. I. Branson, S. J. Casali, and W. K. Tobiska, "High Accuracy Satellite Drag Model (HASDM)," *Advances in Space Research*, Vol. 36, Issue 12, 2005, pp. 2497-2505.
5. Vallado, D. A., *Fundamentals of Astrodynamics and Applications*, Microcosm Press, El Segundo, CA, 3rd Edition, 2007.
6. Montenbruck, O. and E. Gill, *Satellite Orbits: Models, Methods, and Applications*, Springer-Verlag, Berlin, 2001.
7. King-Hele, D., *Satellite Orbits In an Atmosphere: Theory and Applications*, Blackie and Son Ltd., London, 1987.
8. Hedin, A. E., N. W. Spencer, T. L. Killeen, "Empirical Global Model of Upper Thermosphere Winds Based on Atmosphere and Dynamics Explorer Satellite Data," *Journal of Geophysical Research*, Vol. 93, No. A9, 1988, pp. 9959-9978.
9. Tribble, A. C., *The Space Environment: Implications for Spacecraft Design*, Princeton University Press, Princeton, New Jersey, 2003.
10. Knipp, D. D., *Understanding Space Weather and the Physics Behind It*, The McGraw-Hill Companies, Inc., U.S.A, 2011.
11. McLaughlin, C. A., "Upper Atmospheric Phenomena and Satellite Drag," *Advances in the Astronautical Sciences*, Vol. 123, AAS 05-315, Univelt, 2005, pp. 989-996.

12. Bowman, B. R., W. K. Tobiska, F. A. Marcos, C. Valladares, "The JB2006 empirical thermospheric density model," *Journal of Atmospheric and Solar-Terrestrial Physics*, Vol. 70, 2008, pp. 774-793, Elsevier Publications.
13. Bowman, B. R., W. K. Tobiska, F. A. Marcos, C. Y. Huang, C. S. Lin, W. J. Burke, "A New Empirical Thermospheric Density Model JB2008 Using New Solar and Geomagnetic Indices," AIAA 2008-6438, *AIAA/AAS Astrodynamics Specialist Conference*, Honolulu, HI, August 2008.
14. National Geophysical Data Center, *Solar Indices Bulletin*, Boulder, CO: National Geophysical Data Center, ftp://ftp.ngdc.noaa.gov/STP/SOLAR_DATA/SOLAR_RADIO/FLUX and ftp://ftp.ngdc.noaa.gov/STP/GEOMAGNETIC_DATA/INDICES/KP_AP/.
15. Picone, J. M., A. E. Hedin, D. P. Drob, "NRLMSISE-00 Empirical Model of the Atmosphere: Statistical Comparisons and Scientific Issues," *Journal of Geophysical Research*, Vol. 107, No. A12, 2002.
16. Jacchia, L. G., *Revised Static Models for the Thermosphere and Exosphere with Empirical Temperature Profiles*, SAO Special Report No. 332, Smithsonian Institution Astrophysical Observatory, Cambridge, MA, 1971.
17. Roberts Jr., C. E., "An Analytic Model for Upper Atmosphere Densities Based upon Jacchia's 1970 Models," *Celestial Mechanics*, Vol. 4, Issue 3-4, December 1971, pp. 368-377.
18. COSPAR Working Group IV, *COSPAR International Reference Atmosphere*, Akademie-Verlag, Berlin, 1972.
19. Hedin, A. E., "Extension of the MSIS Thermosphere Model into the Middle and Lower Atmosphere," *Journal of Geophysical Research*, Vol. 96, 1991, pp. 1159-1172.
20. Groves, G. V., "Seasonal and Latitudinal Models of Atmospheric Temperature, Pressure and Density, 25 to 100 km," AFCRL-70-0261, 1970.
21. Barlier, F., C. Berger, J.L. Falin, G. Kockarts, G. Thuillier, "A Thermospheric Model based on Satellite Drag Data", *Annales de Geophysics*. Volume 34, 1978, pp. 9-24.
22. Bowman, B., F. A. Marcos, and M. J. Kendra, "A Method for Computing Accurate Atmospheric Density Values from Satellite Drag Data," *Advances in the Astronautical Sciences*, Vol. 119, AAS 04-173, Univelt, 2004, pp. 1117-1134.

23. Bowman, B., "The Semiannual Thermospheric Density Variation from 1970 to 2002 Between 200-1100 km," *Advances in the Astronautical Sciences*, Vol. 119, AAS 04-174, Univelt, 2004, pp. 1135-1154.
24. Cefola, P. J., R. J. Proulx, A. I. Nazarenko, and V. S. Yurasov, "Atmospheric Density Correction Using Two Line Element Sets as the Observation Data," *Advances in the Astronautical Sciences*, Vol. 116, AAS 03-626, Univelt, 2003, pp. 1953-1978.
25. Yurasov, V. S., A. I. Nazarenko, P. J. Cefola, and K. T. Alfriend, "Results and Issues of Atmospheric Density Correction," *Journal of the Astronautical Sciences*, Vol. 52, No. 3, July-September 2004, pp. 281-300.
26. Yurasov, V. S., A. I. Nazarenko, K. T. Alfriend, and P. J. Cefola, "Reentry Time Prediction Using Atmospheric Density Corrections," *Journal of Guidance, Control, and Dynamics*, Vol. 31, No. 2, March-April 2008, pp. 282-289.
27. Wilkins, M. P., C. A. Sabol, P. J. Cefola, and K. T. Alfriend, "Improving Dynamic Calibration of the Atmosphere," *Advances in the Astronautical Sciences*, Vol. 127, AAS 07-185, Univelt, 2007, pp. 1257-1272.
28. Wilkins, M. P., C. A. Sabol, P. J. Cefola, and K. T. Alfriend, "Validation and Application of Corrections to the NRLMSISE-00 Atmospheric Density Model," *Advances in the Astronautical Sciences*, Vol. 127, AAS 07-189, Univelt, 2007, pp. 1285-1304.
29. Wilkins, M. P., C. A. Sabol, P. J. Cefola, and K. T. Alfriend, "Practical Challenges in Implementing Atmospheric Density Corrections to the NRLMSISE-00 Model," *Advances in the Astronautical Sciences*, Vol. 124, AAS 06-170, Univelt 2006, pp. 1113-1130.
30. Mance, S. R., C. A. McLaughlin, F. G. Lemoine, D. D. Rowlands, and P. J. Cefola, "GEOSAT Follow-On Precision Orbit Improvement Through Drag Model Update," *Advances in the Astronautical Sciences*, Vol. 134, AAS 09-105, Univelt, 2009, pp. 43-62.
31. Doornbos, E., H. Klinkrad, and P. Visser, "Use of Two-Line Element Data for Thermosphere Neutral Density Model Calibration," *Advances in Space Research*, Vol. 41, 2008, pp. 1115-1122.

32. Konig, R. and K. H. Neumayer, "Thermospheric Events in CHAMP Precise Orbit Determination," *First CHAMP Mission Results for Gravity, Magnetic and Atmospheric Studies*, eds. C. Reigber, H. Luhr, P. Schwintzer, Springer, Berlin, 2003, pp. 112-119.
33. Bruinsma, S. and R. Biancale, "Total Densities Derived from Accelerometer Data," *Journal of Spacecraft and Rockets*, Vol. 40, No. 2, March-April 2003, pp. 230-236.
34. Bruinsma, S., S. D. Tamagnan and R. Biancale, "Atmospheric Densities Derived from CHAMP/STAR Accelerometer Observations," *Planetary and Space Science*, Vol. 52, 2004, pp. 297-312.
35. Rhoden, E. A., J. M. Forbes, and F. A. Marcos, "The Influence of Geomagnetic and Solar Variability on Lower Thermospheric Density," *Journal of Atmospheric and Solar-Terrestrial Physics*, Vol. 62, 2000, pp. 999-1013.
36. Schlegel, K., H. Lühr, J. P. St. Maurice, G. Crowley, and C. Hackert, "Thermospheric Density Structures over the Polar Regions Observed with CHAMP," *Annales Geophysicae*, Vol. 23, 2005, pp. 1659-1672.
37. Forbes, J. M., G. Lu, S. Bruinsma, S. Nerem, and X. Zhang, "Thermospheric Density Variations Due to the 15-24 April 2002 Solar Events from CHAMP/STAR Accelerometer Measurements," *Journal of Geophysical Research*, Vol. 110, 2005, pp. 1-9.
38. Sutton, E. K., R. S. Nerem, and J. M. Forbes, "Global Thermospheric Neutral Density and Wind Response to the Severe 2003 Geomagnetic Storms from CHAMP Accelerometer Data," *Journal of Geophysical Research*, Vol. 110, 2005.
39. Sutton, E. K., J. M. Forbes, R. S. Nerem, and T. N. Woods, "Neutral Density Response to the Solar Flares of October and November, 2003," *Geophysical Research Letters*, Vol. 33, 2006.
40. Bruinsma, S., J. M. Forbes, R. S. Nerem, and X. Zhang, "Thermospheric Density Response to the 20-21 November 2003 Solar and Geomagnetic Storm from CHAMP and GRACE Accelerometer Data," *Journal of Geophysical Research*, Vol. 111, No. AO6303, 2006, pp. 1-14.
41. Bruinsma, S. L. and J. M. Forbes, "Storm-Time Equatorial Density Enhancements Observed by CHAMP and GRACE," *Journal of Spacecraft and Rockets*, Vol. 44, No. 6, 2007, pp. 1154-1159.

42. Sutton, E. K., R. S. Nerem, and J. M. Forbes, "Density and Winds in the Thermosphere Deduced from Accelerometer Data," *Journal of Spacecraft and Rockets*, Vol. 44, No. 6, 2007, pp. 1210-1219.
43. Bruinsma, S. L. and J. M. Forbes, "Medium- to Large-Scale Density Variability as Observed by CHAMP," *Space Weather*, Vol. 6, S08002, doi:10.1029/2008SW000411, 2008.
44. Zhou, Y. L., S. Y. Ma, H. Lühr, C. Xiong, and C. Reigber, "An Empirical Relation to Correct Storm-Time Thermospheric Mass Density Modeled by NRLMSISE-00 with CHAMP Satellite Air Drag Data," *Advances in Space Research*, Vol. 43, 2009, pp. 819-828.
45. Doornbos, E., H. Klinkrad, and P. Visser, "Atmospheric Density Calibration Using Satellite Drag Observations," *Advances in Space Research*, Vol. 36, 2005, pp. 515-521.
46. van den Ijssel, J., P. Visser, and R. Haagmans, "Determination of Non-Conservative Accelerations from Orbit Analysis," *Earth Observation with CHAMP Results from Three Years in Orbit*, eds. C. Reigber, H. Luhr, P. Schwintzer, J. Wickert, Springer, Berlin, 2005, pp. 95-100.
47. van den Ijssel, J. and P. Visser, "Determination of Non-Gravitational Accelerations from GPS Satellite-to-Satellite Tracking of CHAMP," *Advances in Space Research*, Vol. 36, 2005, pp. 418-423.
48. van den Ijssel, J. and P. Visser, "Performance of GPS Accelerometry: CHAMP and GRACE," *Advances in Space Research*, Vol. 39, 2007, pp. 1597-1603.
49. Montenbruck, O., T. van Helleputte, R. Kroes, and E. Gill, "Reduced Dynamic Orbit Determination Using GPS Code and Carrier Measurements," *Aerospace Science and Technology*, Vol. 9, 2005, pp. 261-271.
50. Willis, P., F. Deleflie, F. Barlier, Y. E. Bar-Sever, and L. J. Romans, "Effects of Thermosphere Total Density Perturbations on LEO Orbits During Severe Geomagnetic Conditions (Oct-Nov 2003) Using DORIS and SLR Data," *Advances in Space Research*, Vol. 36, 2005, pp. 522-533.
51. Tapley, B. D., B. E. Schutz, and G. H. Born, *Statistical Orbit Determination*, Elsevier Academic Press, Amsterdam, 2004.

52. McLaughlin, C. A. and B. S. Bieber, "Neutral Density Determined from CHAMP Precision Orbits," *Advances in the Astronautical Sciences*, Vol. 129, AAS 07-260, Univelt, 2008, pp. 167-186.
53. McLaughlin, C. A., A. Hiatt, and B. S. Bieber, "Comparison of Total Density Derived from CHAMP Precision Orbits and CHAMP Accelerometer," *Advances in the Astronautical Sciences*, Vol. 130, AAS 08-177, Univelt, 2008, pp. 1193-1206.
54. McLaughlin, C. A., A. Hiatt, T. Lechtenberg, "Precision Orbit Derived Total Density," *Journal of Spacecraft and Rockets*, Vol. 48, No.1, January-February 2011, pp. 166-174.
55. Hiatt, A., C. A. McLaughlin, and T. Lechtenberg, "Deriving Density Estimates Using CHAMP Precision Orbit Data for Periods of High Solar Activity," *Advances in the Astronautical Sciences*, Vol. 134, AAS 09-104, Univelt, 2009, pp. 23-42.
56. Hiatt, A., "Deriving Atmospheric Density Estimates Using Satellite Precision Orbit Ephemerides," M.S. Thesis, University of Kansas, 2009.
57. Lechtenberg, T., "Derivation and Observability of Upper Atmospheric Density Variations Utilizing Precision Orbit Ephemerides," M.S. Thesis, University of Kansas, 2010.
58. Infoterra GmbH, "TerraSAR-X: First Commercial 1m Radar Satellite," 2010, Last Accessed: April 10, 2010, http://terrasar.de/terrasar-x.html.
59. Fattig, E., C. A. McLaughlin, T. Lechtenberg, "Comparison of Density Estimation for CHAMP and GRACE Satellites," AIAA 2010-7976, *2010 AIAA/AAS Astrodynamics Specialist Conference and Exhibit*, Toronto, ON, CA, August 2010.
60. McLaughlin, C. A., T. Lechtenberg, E. Fattig, "Estimating Density Using Precision Satellite Orbits From Multiple Satellites," Astrodynamics 2010, Vol. 139 of *Advances in the Astronautical Sciences*, 2010, AAS 10-307, pp. 3229-3246
61. Fattig, E., "Comparison of Precision Orbit Derived Density Estimates for CHAMP and GRACE Satellites," M.S. Thesis, University of Kansas, 2011.
62. McLaughlin, C. A., E. Fattig, D. Mysore Krishna, T. Locke, and P. M. Mehta, "Time Periods of Anomalous Density for GRACE and CHAMP," Astrodynamics 2011, Vol. 142 of *Advances in the Astronautical Sciences*, 2011, AAS 11-613, pp. 3299-3310.
63. Arudra, A. K., "Atmospheric Density Estimation Using Satellite Precision Orbit Ephemeride," M.S. Thesis, University of Kansas, 2011.

64. Mysore Krishna, D., and C. A. McLaughlin, "Combining Precision Orbit Derived Density Estimates," *Astrodynamics 2011*, Vol. 142 of *Advances in the Astronautical Sciences*, 2011, AAS 11-475, pp. 499-516.
65. Mysore Krishna, D., "Improving and Expanding Precision Orbit Derived Atmospheric Densities," M.S. Thesis, University of Kansas, 2012.
66. McLaughlin, C. A., A. Hiatt, D. Mysore Krishna, T. Lechtenberg, E. Fattig, and P. M. Mehta, "Precision Orbit Derived Atmospheric Density: Development and Performance," *Advanced Maui Optical and Space Surveillance Technologies Conference*, Maui, HI, September 12-14, 2012.
67. Wright, J. R., "Real-Time Estimation of Local Atmospheric Density," *Advances in the Astronautical Sciences*, Vol. 114, AAS 03-164, Univelt, 2003, pp. 927-950.
68. Wright, J. R. and J. Woodburn, "Simultaneous Real-Time Estimation of Atmospheric Density and Ballistic Coefficient," *Advances in the Astronautical Sciences*, Vol. 119, AAS 04-175, Univelt, 2004, pp. 1155-1184.
69. McLaughlin, C. A., A. Hiatt, E. Fattig and T. Lechtenberg, "Ballistic Coefficient and Density Estimation," *Advances in Astronautical Sciences*, Vol. 134, AAS 09-439, Univelt, 2009, pp. 23-42.
70. Mehta, P. M., and C. A. McLaughlin, "Density and Ballistic Coefficient Estimation Revisited," Astrodynamics 2011, *Advances in the Astronautical Sciences*, Vol. 142, AAS 11-609, 2011, pp. 3247-3264.
71. Torrence, M., "CHAMP," CHAMP Satellite Information, NASA, Last Accessed: July 1, 2012, http://ilrs.gsfc.nasa.gov/satellite_missions/list_of_satellites/cham_general.html.
72. Torrence, M., "GRACE-A, -B," GRACE-A Satellite Information, NASA, Last Accessed: July 1, 2012, http://ilrs.gsfc.nasa.gov/satellite_missions/list_of_satellites/graa_general.html.
73. Pail, R., "Gravity Field Missions", Global Geodetic Observing Sysetm, Last Accessed: July 1, 2012, http://www.ggos-portal.org/lang_en/GGOS-Portal/EN/Topics/SatelliteMissions/GravityField/GravityField.html
74. Anderson, R., G. Born, J. Forbes, "Sensitivity of Orbit Predictions to Density Variability," *Journal of Spacecraft and Rockets*, Vol. 46, No. 6, 2009, pp. 1214-1230.

75. Schaeperkoetter, A., C. McLaughlin, "Effects of Density Variations in the Upper Atmosphere on Satellite Trajectories," *Space Flight Mechanics 2010*, Vol. 136 of *Advances in the Astronautical Sciences*, 2010, AAS 10-223, pp. 1817-1830.
76. McLaughlin, C. A., T. Locke, and D. Mysore Krishna, "Effects of High Frequency Density Variations on Orbit Propagation," *Space Flight Mechanics 2012*, Vol. 143 of *Advances in the Astronautical Sciences*, 2012, AAS 12-176, pp. 1061-1068.
77. Konig, R., S. Zhu, C. Reigber, K. H. Neumayer, H. Meixner, R. Galas, G. Baustert, "CHAMP Rapid Orbit Determination for GPS Atmospheric Limb Sounding," *Advances in Space Research*, Vol. 30, No. 2, 2002, pp. 289-293.
78. Michalak, G., G. Baustert, R. Konig, C. Reigber, "CHAMP Rapid Science Orbit Determination: Status and Future Prospects," *First CHAMP Mission Results for Gravity, Magnetic and Atmospheric Studies*, eds. C. Reigber, H. Luhr, P. Schwintzer, Springer, Berlin, 2003, pp. 98-103
79. Konig, R., G. Michalak, K. H. Neumayer, S. Y. Zhu, H. Meixner, C. Reigber, "Recent Developments in CHAMP Orbit Determination at GFZ," *Earth Observation with CHAMP Results from Three Years in Orbit*, eds. C. Reigber, H. Luhr, P. Schwintzer, J. Wickert, Springer, Berlin, 2005, pp. 65-70.
80. Konig, R., G. Michalak, K. H. Neumayer, S. Zhu, "Remarks on CHAMP Orbit Products," *Observation of the Earth System from Space*, eds. J. Flury, R. Rummel, C. Reigber, M. Rothacher, G. Boedecker, U. Schreiber, Springer, Berlin, 2006, pp. 17-26
81. Wright, J. R., "Optimal Orbit Determination," *Advances in the Astronautical Sciences*, Vol. 112, AAS 02-192, Univelt, 2002, pp. 1123-1134, http://www.agi.com/downloads/support/productSupport/literature/pdfs/whitePapers/optimal_od.pdf
82. Analytical Graphics, Inc., "Orbit Determination Tool Kit Help," *Orbit Determination Tool Kit*, Version 5.1.3.
83. Wright, J. R., "Orbit Determination Tool Kit Theorems and Algorithms," *Analytical Graphics, Inc.*, 2007.
84. Vallado, D. A., R. S. Hujsak, T. M. Johnson, J. H. Seago, and J. W. Woodburn, "Orbit Determination Using ODTK Version 6," *European Space Astronomy Center (ESA/ESAC)*, Madrid, Spain, May 2010.

85. Bowman, B. R., F. A. Marcos, K. Moe, M. M. Moe, "Determination of Drag Coefficient Values for CHAMP and GRACE Satellites Using Orbit Drag Analysis," *Advances in the Astronautical Sciences*, Vol. 129, AAS 07-259, Univelt, 2008, pp. 147-166.
86. Bourke, P., "Cross Correlation," August 1996, Last Accessed: February 20, 2011, http://local.wasp.uwa.edu.au/~pbourke/miscellaneous/correlate/.